

Humidity Effects on Turbofan Performance

in a MRO context

S. van Vuuren



Technische Universiteit Delft

Humidity Effects on Turbofan Performance in a MRO context

by

S. van Vuuren

to obtain the degree of Master of Science
at the Delft University of Technology,
to be defended publicly on the 9th of December 2019 at 14:00 AM.

Student number: 4164059
Project duration: January 14, 2019 – December 9, 2019
Thesis committee: Prof. dr. ir. P. Colonna, TU Delft, chair
Dr. W. P. J. Visser, TU Delft, supervisor
Dr. Ir. A. Apostolidis, Air France-KLM Technology Office
Ir. P. Roling, TU Delft

This thesis is confidential and cannot be made public until December 9, 2024.

An electronic version of this thesis is available at <http://repository.tudelft.nl/>.

Preface

With the completion of my master thesis, I have reached the end of my time as student of the Technical University of Delft. I am glad for the opportunities that presented themselves throughout this period and most certainly will look back to my time as a student with a lot of joy. I am happy that I had the opportunity to perform this thesis at KLM Engineering & Maintenance, which proved to be an inspiring operational environment. During the short year at the Engine Services department, I learned an incredible amount about the MRO aspects regarding turbofan engines as well as the MRO world in general. The possibility to closely inspect the engines I was studying never ceased to motivate me.

This thesis, as it is before you now, would not have been the same without the help of others. First of all I would like to thank my supervisors, starting with Wilfried Visser. His guidance throughout the year, feedback and interesting insights helped me along the way. Rob Duivis I would like to thank for all his support and feedback as well as his seemingly endless fascination about gas turbines and therefore also this research. The inexhaustible practical knowledge Rob has gained throughout his career proved to be extremely helpful on more than one occasion. Asteris Apostolidis I would like to thank for his close involvement and support during the whole year. Our weekly meetings gave rise to many fruitful discussions and ensured the project was always on track.

I also would like to express my gratitude to my direct colleagues Martijn van der Werf, Albert Timmer, Mike Brull and Martijn van Moorselaar. The countless walks to the coffee machine and through the hangars were always vitalizing. Bastiaan Roëll and Tim Rootliep I would like to thank for the many interesting discussions and making the travels back and forth between Delft and KLM a lot more fun. Finally, I would like to thank my friends and family for their support throughout the years, making my time as a student a time I will surely never forget.

*S. van Vuuren
Delft, November 2019*

Executive Summary

It is of fundamental importance that aircraft are safe and reliable when in operation. In order to provide for those needs, timely and specialised maintenance is crucial. Maintenance, Repair and Overhaul (MRO) facilities provide for those needs, of which KLM Engine Services (ES) provides turbofan MRO for both KLM as well as external costumers. With the introduction of the "Power by the Hour" contracts, the risk of a premature engine removal lies with the MRO company. Since the airline industry is becoming increasingly competitive, maintenance timing and effectiveness are becoming of greater importance every year. In order to provide maintenance timely and efficiently, it is of paramount importance to be able to perform accurate turbofan engine condition assessments.

Engine performance diagnostics play a major role in keeping track of turbofan condition and performance as well as the identification of possible errors or faults. One of the key performance indicators used in engine performance diagnostics is the on-wing reported Hot Day Exhaust Gas Temperature Margin (EGTM). The EGTM is an overall indicator of engine health and physical condition. The engine control and reporting systems correct the EGTM for power setting, as well as ambient conditions such as pressure and temperature, in order to provide comparability of the reported EGTM between flights. However, ambient absolute humidity, which also affects the EGTM, is not measured nor corrected for and consequently introduces inaccuracy in the reported EGTM. The objective of this research is to investigate the effect of humidity on turbofan performance, in order to provide corrections for the reported EGTM for ambient humidity variation regarding the General Electric CF6 turbofan engine variants. Test-cell corrections, performance simulations and historical data were investigated and compared in order to assess the effects of humidity on turbofan performance.

In open literature, component performance corrections are proposed assuming full flow similarity. However, when analysing the effects on a complete turbofan, conditions imposing full flow similarity may not be met any more. Due to the components operating in equilibrium and the influence of the control configuration, the flow can change notably.

From the test-cell corrections and simulation results it was found that two aforementioned restrictions heavily influence the overall effect of humidity on turbofan performance. Where literature proposes corrections independent of power setting, the test-cell corrections and simulation suggest variation of sensitivity to humidity. It was found that the test-cell corrections and simulation results where, on average, in good agreement. Globally, the ambient absolute humidity generally varies from 0 to 3.1wt%, indicating that the EGT, under identical take-off conditions, N1-setting and hardware condition, decreases by as much as 12K due to ambient absolute humidity. Without proper correction this wrongfully increases the EGTM with the approximately same magnitude.

Also, the effects on other performance parameters were noticeable. For example, for the N1-controlled CF6-80C2, a decrease of thrust of 0.65% per wt% humidity was found. Resulting in thrust reductions up to 2% in very humid environments, indicating an increase of take-off field length. To maintain equal thrust when ambient humidity varies, the simulation results suggest a fan speed increase of 0.27% per wt% of humidity. The simulation also indicated that humidity possibly obscures the effects of deterioration for compressors, or falsely indicates deterioration for turbines when performing GPA.

Historical take-off performance data were related to historical airport weather data containing humidity measurements. It was found that the historical data compared very well to the test-cell corrections and simulation results, displaying higher reported EGTM for increasing ambient humidity. Three correction methods were proposed, where the best performing correction reduced the standard deviation with 10%. With a theoretical contribution to the standard deviation of 16.5% for the CF6-80E1, it was found that humidity only has a minor contribution to the total scatter present in the reported EGTM.

It is therefore concluded that correcting the EGTM for ambient humidity variations is possible. It is, however, of secondary interest due to the minor role on the scatter of the currently reported EGTM. Nonetheless, this research has shed a light on the effect of humidity on turbofan performance and clarified the impact humidity has on the EGTM as well as other performance parameters. With the trend of the increasing accuracy on the reported EGTM for newer engine types, correcting the EGTM for ambient humidity may prove more beneficial in the near future.

Contents

Preface	i
Executive Summary	ii
List of Figures	vi
List of Tables	viii
Nomenclature	ix
1 Introduction	1
1.1 Context & Problem Statement	1
1.2 Research Objective and Questions	2
1.3 Report Structure	2
2 MRO Practices	4
2.1 Gas Turbine Deterioration and Effect on Performance	4
2.1.1 Effect of deterioration on EGT(M)	4
2.2 Engine Health Management	5
2.2.1 Key performance indicators	6
2.2.2 Fault isolation	6
2.2.3 Work scoping	6
2.2.4 Restoring performance	6
2.2.5 Test-cell acceptance testing	7
2.3 Gas Path Analysis	7
3 General Effects of Humidity on Turbofan Performance	9
3.1 General Definitions of Ambient Humidity	9
3.2 Root Causes of Performance Deviations due to Humidity	10
3.2.1 Effects due to condensation	11
3.2.2 Effect of humidity on the thermodynamic properties of air	11
3.3 Effects of Humidity on (Design Point) Cycle Calculation	14
3.4 Effects of Humidity on Off-Design Performance	15
3.4.1 Effect on performance of turbomachinery	18
3.4.2 Effect on combustor	19
3.4.3 Effect on propulsion	19
3.4.4 Notes on theoretical corrections	19
4 Test-Cell Corrections	22
4.1 Correction Formulae	22
4.1.1 Direct humidity correction	24
4.1.2 Indirect humidity correction	24
4.2 Complete Test-Cell Humidity Correction.	25
4.3 Final Remarks on Test-cell Corrections	27
5 Modelling Humidity Effects	28
5.1 Gas Turbine Simulation Program	28
5.1.1 Component based modelling	28
5.1.2 Design point component performance.	29
5.1.3 Off-Design component performance & component maps	29
5.1.4 Numerical instabilities in compressor and turbine maps	30
5.1.5 Gas model & ambient conditions	30
5.1.6 Corrected parameters in GSP	31

5.1.7	State vector and conservation equations	31
5.1.8	Solution methodology	32
5.1.9	Previous studies performed in GSP	32
5.2	Model Implementation	33
5.2.1	CF6-80C2B1F model.	33
5.3	Model limitations	34
5.3.1	Bleeds, variable bypass valves & variable stator vanes	34
5.3.2	Sensor noise and bias	35
5.3.3	Engine to engine differences.	35
5.3.4	Accuracy of compressor maps.	35
5.4	Modelling other Control Configurations	35
6	Simulation Results Analysis	37
6.1	CF6-80C2 Simulation Results	37
6.1.1	Simulation set-up.	37
6.1.2	Preliminary analysis: effect of customer bleed	37
6.1.3	Effect of humidity: N1-sensitivity.	38
6.1.4	Effect of humidity: T1-sensitivity.	39
6.2	Simulation Results for other Engine Control Configurations	40
6.2.1	N1-control.	41
6.2.2	N1c-control	42
6.2.3	TIT-control	42
6.2.4	IEPR-control	43
6.2.5	FN-control.	43
6.3	Humidity Effects on GPA Capabilities	43
7	Statistical Analysis	46
7.1	Statistical Analysis on Humidity Variation	46
7.1.1	METAR Data	46
7.1.2	Global humidity variation	47
7.1.3	Local humidity variation	47
7.1.4	Atmospheric humidity variation	48
7.2	Monte Carlo Analysis.	51
7.3	Take-Off Snapshot Data	53
7.3.1	Scatter in the reported EGTM	54
7.4	Merged Snapshot and Humidity Data	55
7.4.1	Correlation between the reported EGTM and Absolute Humidity	56
8	Correcting the EGTM for Ambient Humidity	57
8.1	Performed Corrections	57
8.1.1	Correcting EGTM using generic correction	58
8.1.2	Correcting EGTM using the complete test-cell corrections.	58
8.1.3	Correcting EGTM using a hybrid approach	58
8.2	Corrections Results	59
8.2.1	CF6-80C2 correction results	59
8.2.2	CF6-80E1 correction results	60
9	Discussion	65
9.1	Literature and Test-cell Corrections	65
9.2	Test-cell Corrections and Simulations	66
9.3	Historical Data, Simulation results and Test-cell corrections	66
9.3.1	CF6-80C2.	66
9.3.2	CF6-80E1.	66
9.3.3	Explanation of EGTM-Humidity linear regression slope variation	67
9.4	Assessment of Operational Effects	67
10	Conclusions & Recommendations	69
10.1	Conclusions.	69
10.2	Recommendations	70

Bibliography	72
A Thesis Assignment	76
B Gas Properties versus Humidity	78
C Effects of Humidity on Design Point Cycle Calculation	82
D CF6-80C2 and -80E1 Engine Specifications	86
E Simulated Bleed Flows	87
F Corrected and Original EGTM Trend over Time	88

List of Figures

2.1	Visualization of deterioration effects	5
2.2	Relation between deterioration, performance and measurements [22] [modified]	7
3.1	Normalized change in gas properties of ambient air	13
3.2	Turbofan engine station numbering [37] [modified]	14
3.3	Exaggeration of a two-spool Turbofan DP calculation T-S diagram, for both dry and humid air	16
3.4	Similar flow field conditions due to equal velocity direction and ratio	17
3.5	Theoretical corrections of \dot{m} , N , $\Delta h/T$ for turbomachinery	21
3.6	Theoretical corrections of Pressure Ratio and Outlet Temperature in turbomachinery	21
3.7	Theoretical corrections of Thrust and Fuel Flow	21
4.1	Test-cell direct humidity corrections	24
4.2	Comparison of magnitude of both the direct and indirect humidity corrections	25
4.3	Correction slopes versus observed $N1$	26
4.4	Test-Cell corrections for the CF6-80C2B1F, $N1 = 3300$ RPM	27
5.1	Screenshot of component based model interface of GSP, CF6-80C2	29
5.2	Generic Compressor and Turbine map	29
6.1	Test-cell and simulated correction slopes versus observed $N1$	39
6.2	Simulated correction slopes versus T_{t1}	41
7.1	Average Humidity in the year 2018 per Airport, largest values $\Psi \approx 2.0$ wt%, smallest values $\Psi \approx 0.38$ wt%	47
7.2	Maximal Humidity in the year 2018 per Airport, largest values $\Psi \approx 3.1$ wt%, smallest values $\Psi \approx 0.75$ wt%	47
7.3	Boxplot and Probability Density Histogram for complete and long-haul only dataset	48
7.4	Observation of variation of humidity for different airports	49
7.5	Altitude w.r.t. airport of CF6-80C2 on-wing Snapshots	50
7.6	Altitude w.r.t. airport of CF6-80E1 on-ning Snapshots	50
7.7	Absolute humidity histogram and Monte Carlo convergence for Case 1	52
7.8	Monte Carlo analysis results, AMS-CGK	52
7.9	Absolute humidity histogram and Monte Carlo convergence for Case 2	53
7.10	Monte Carlo analysis results, AMS-DEL	54
7.11	Example of reported EGTM versus time, left CF6-80C2, right CF6-80E1	55
7.12	Histogram of $EGTM/\Psi_{abs}$ linear regression slopes	56
8.1	Correction methodology	59
8.2	CF6-80C2: Histogram of $EGTM/\Psi_{abs}$ linear regression slopes after correction	60
8.3	CF6-80E1: Histogram of $EGTM/\Psi_{abs}$ linear regression slopes after correction	61
8.4	CF6-80C2: Corrected and original EGTM scatter plots for two different ESN	62
8.5	CF6-80E1: Corrected and original EGTM scatter plots for two different ESN	63
8.6	CF6-80C2: Visualization of corrected EGTM	63
8.7	CF6-80E1: Visualization of corrected EGTM	63
B.1	Mollier diagram and density for different ambient humidity levels	78
B.2	Specific heats for different ambient humidity levels	79
B.3	Specific heat ratio and Gas constant for different ambient humidity levels	80
B.4	Variation of relative and absolute humidity with altitude	81

C.1	T-S diagrams for the "BIGFAN" Design Point calculation	83
C.2	H-T diagrams for the "BIGFAN" Design Point calculation	84
C.3	P-T diagram of the "BIGFAN" Design Point calculation	85
F.1	CF6-80C2: Corrected and Original EGTM versus time	88
F.2	CF6-80E1: Corrected and Original EGTM versus time	88

List of Tables

3.1	The coefficients for the specific temperature ranges [29]	10
3.2	Deviation of thermodynamic properties due to ambient humidity variation	13
3.3	Parameter groups	16
3.4	Various theoretical correction factors for $\Psi = 2.8[\text{wt}\%]$	20
4.1	Average correction slopes of complete test-cell corrections, expressed in $[\%/\text{wt}\%]$	27
5.1	Modelled air composition for dry and humid conditions (3.0wt%) [7]	31
5.2	On-wing engine measurements, CF6-80C2 and -80E1 [54, 55]	34
6.1	Customer bleed result comparison	38
6.2	Average correction slopes of test-cell corrections and GSP results, expressed as $\%/\text{wt}\%$	39
6.3	Average correction slopes of simulated corrections for varying T_{t1} , expressed as $\%/\text{wt}\%$	40
6.4	Effect of humidity ($\Psi_{abs} \approx 3.1\text{wt}\%$) for several control configurations	45
7.1	Mean and standard deviations Case 1	51
7.2	Mean and standard deviations Case 2	51
7.3	Overview of used on-wing snapshot data	56
8.1	Tabulated average correction results for both CF6-80C2 and CF6-80E1	64
C.1	Tabulated values of T, P, s and h	82
D.1	CF6-80C2 and 80E1 specifications [15, 54, 55]	86
E.1	Bleed flows as defined in the CF6-80C2 model	87

Nomenclature

Roman symbols

Symbol	Description	Unit
A	Area	m^2
a	Altitude w.r.t. sea-level	m
c_p	Isobaric specific heat	J/kgK
c_v	Isochoric specific heat	J/kgK
D	Characteristic length, often diameter	m
EGT	Exhaust Gas Temperature	K
EGTM	Exhaust Gas Temperature Margin	K
EPR	Engine Pressure Ratio	–
F	Force	N
FN	Thrust Force	N
g	Gravitational constant	m/s^2
h	Specific enthalpy	J/kg
I	Moment of Inertia	kgm^2
IEPR	Integrated engine pressure ratio	Pa
L	Temperature Lapse rate	K/m
M	Mass in the control volume	kg
Ma	Mach number	–
\dot{m}	Mass flow	kg/s
N1	Fan rotational speed	RPM
N2	Core rotational speed	RPM
P	Pressure	Pa
PW	Power	J/s
Q	Heat	J
R	Universal gas constant	$J/molK$
\bar{R}	Specific gas constant	J/kgK
SF	Shunt Factor	–
s	Specific entropy	J/kg
T	Temperature	K
TIT	Turbine inlet temperature (T_{t4})	K
TSFC	Thrust Specific Fuel Consumption	kg/Nh
t	Time	s
U	Circumferential velocity	m/s
u	Specific internal energy	J/kg
V	Velocity	m/s
v	Specific volume	m^3/kg

Greek symbols

Symbol	Description	Unit
γ	Specific heat ratio	—
δ	Pressure ratio w.r.t. ISA ambient conditions	—
η	Efficiency	—
θ	Temperature ratio w.r.t. ISA ambient conditions	—
μ	Mean	—
ρ	Density	kg/m^3
σ	Standard deviation	—
Ψ	Humidity	—
ω	Rotational velocity	rps

Subscripts

<i>a</i>	air
<i>ax</i>	axial
<i>abs</i>	absolute
<i>amb</i>	ambient
<i>c</i>	corrected
<i>comp</i>	compressor
<i>cc</i>	combustion chamber
<i>DIV</i>	divergence w.r.t. rolling average
<i>d</i>	dry
<i>dp</i>	dew-point
<i>eq</i>	equilibrium
<i>f</i>	fuel
<i>g</i>	gas
<i>HD</i>	hot day
<i>h</i>	humid
<i>hs</i>	heat sink
<i>i</i>	inlet
<i>in</i>	inlet of component
<i>is</i>	isentropic
<i>isa</i>	international standard atmosphere
<i>m</i>	mechanical
<i>out</i>	outlet of component
<i>ref</i>	reference
<i>rel</i>	relative
<i>rolling</i>	rolling average
<i>SD</i>	standard day
<i>sl</i>	sea-level
<i>t</i>	total
<i>turb</i>	turbine

Acronyms

AF	Air France
AFKLM	Air France - Royal Dutch Airlines
BPR	Bypass Ratio
DOC	Direct Operating Cost
DP	Design Point
ESN	Engine Serial Number
E&M	Engineering and Maintenance
ES	Engine Services
GE	General Electric (Aviation)
GPA	Gas Path Analysis
GSP	Gas turbine Simulation Program
HD	Hot Day ISA conditions
HDEGTM	Hot Day Exhaust Gas Temperature Margin
ISA	International Standard Atmosphere
IQR	Inter Quartile Range
KLM	Royal Dutch Airlines
LHV	Lower Heating Value
LLP	Life Limited Part
MC	Maximum Continuous
METAR	Meteorological Aerodrome Report
MRO	Maintenance, Repair and Overhaul
NLR	Netherlands Aerospace Centre
OD	Off-Design
PDF	Probability Density Function
PR	Pressure ratio
RH	Relative Humidity
SD	Standard Day ISA conditions
TIT	Turbine inlet Temperature
TO	Take-Off
TR	Temperature ratio
TSFC	Thrust Specific Fuel Consumption
VBV	Variable Bypass Valve
VGW	Variable Guide Vane
VSV	Variable Stator Vane
wt%	weight percentage

Introduction

Gas turbines play an indispensable role in modern society. Due to their high power density they are extremely applicable for the aviation industry where significant power is required but weight and size are often kept at a minimum. Like every other machine, gas turbines suffer from deterioration, which negatively affects engine performance [1–3]. It is naturally of crucial importance that the engines are fully functional, perform according to standards and that safe operation can be guaranteed.

The Direct Operating Cost (DOC) of a civil aircraft consist of roughly a quarter of engine DOC. In turn, the DOC of an engine consists for a third of fuel costs and a third of maintenance related costs [2]. Effective maintenance has impact on both areas. While cost effective maintenance can reduce general maintenance costs and provide longer operating engines, it also improves engine performance and fuel economy, therefore having a dual effect on the DOC of an engine.

Aircraft Maintenance, Repair and Overhaul (MRO) facilities are specialised in aircraft and engine MRO, and are responsible for maintaining a healthy fleet. Where in its early days the MRO industry performed mainly scheduled maintenance, the quest for lower MRO costs forced the industry to provide performance based maintenance [1]. For example with the introduction of "Power by the Hour" contracts, the MRO provider receives a fixed maintenance price for a certain amount of flight hours or even a fixed price per flight hour. If an engine is safe and reliable to use for a longer period than expected the MRO generates more profit, if the engine performs shorter than expected the MRO will be subjected to more costs. This moves the risk of an early engine removal from the airline to the MRO company. For the MRO, it is therefore of fundamental importance to be able to accurately assess the condition of the fleet.

Engine performance diagnostics play a major role in keeping track of the gas turbine condition and performance and identification of possible errors or faults. With the already competitive airline industry and the ever increasing price of fuel, quick, efficient and reliable aircraft maintenance, repair and overhaul has become of greater importance over the years. As the total annual global air traffic is expected to increase by as much as 4.4% per year and the global amount of aircraft will possibly be more than doubled by 2037 [4] according to Airbus, the MRO industry is up for a challenge.

1.1. Context & Problem Statement

KLM Engineering & Maintenance (E&M) is such an aircraft MRO facility, of which the 'Engine Services' (ES) department is specialised in turbofan engine MRO. About 200 engines pass through this facility each year. Providing MRO services for the AFKLM fleet as well as for costumers. At the ES department, one of the tools to predict maintenance is performance diagnostics. Engine performance diagnostics are used in order to assess the 'health' of an engine by means of several performance indicators either directly measured in the gas path or calculated using the measured data.

One of the key performance indicators used in engine performance diagnostics is the on-wing reported Hot Day Exhaust Gas Temperature Margin (HDEGTM). As there are different ambient conditions and power settings for every take-off, the recorded EGTM is corrected to a HDEGTM to allow for comparison between consecutive take-offs. For the sake of simplicity HDEGTM is used as EGTM unless stated otherwise. The HDEGTM is calculated by the engine using on-wing measured performance

data such as temperatures and fan speed. The measured parameters and calculated HDEGTM are then reported in an 'on-wing take-off snapshot'.

A low EGTM is an indicator of poor performance and a decision support indicator for performance-related engine removals. The EGTM is subjected to certification limits. It is generally known that the EGTM is affected by ambient conditions such as temperature and is corrected for ambient conditions by the engine's control and reporting systems. Another ambient condition affecting engine performance is humidity. Several studies have been performed in order to research the effect of humidity on engine performance, for example those of [5–11]. All studies show that humidity affects the thermodynamic properties in the engine. On current (civil) aircraft engines ambient humidity is not measured, but instead dry air is assumed. The EGTM is therefore affected by humidity to an uncertain extent. However the total effect of humidity on engine performance is generally small, it becomes increasingly important to accurately monitor engine condition now the airline industry is getting more competitive every year.

1.2. Research Objective and Questions

Within KLM ES the need has arisen to more accurately assess engine condition by means of engine performance diagnostics. There is a strong belief that a correction of the EGTM during take-off, based on real-time airport weather data, can improve the operational decision support and provide a more accurate indication of engine condition. This belief is enforced by the announcement of Rolls-Royce to implement ambient humidity in engine diagnostic systems [12, 13]. Since ambient humidity is not measured on regular civil turbofan engines or aircraft, ambient humidity data will need to be retrieved from an external data source. The main objective of this research is investigating the effects of ambient humidity on turbofan performance, in order to provide corrections for the reported EGTM of the General Electric (GE) CF6 turbofan engines. With the research objective in place, the main research question is stated as follows:

Can engine diagnostics be augmented by correcting on-wing reported EGTM for ambient humidity variations?

The research will be focussed on the CF6 series turbofan engines. This regards the CF6-80C2B1F and CF6-80E1A3. The engines are very comparable in terms of physical characteristics, however the CF6-80E1 is designed for a higher power rating. This higher power rating causes the CF6-80E1 to generally indicate a lower EGTM, making it more susceptible to EGTM related removals and a more accurate representation of the EGTM of greater interest. Test-cell corrections, simulations performed in GSP and historical data will be analysed and compared to provide for an in-depth study. Only an accurate simulation model of the CF6-80C2 is available at KLM ES. Since creating a simulation model can be an MSc. thesis on itself [14–16], it was chosen to investigate the CF6-80C2 as well since a simulation model of the engine is readily available. Due to their physical similarity the effect of humidity on both engines is assumed to be comparable. The test-cell corrections and historical data will conclude if this assumption is valid. In open literature no research is found on the effect of humidity on high bypass ratio ($BPR > 5$) turbofans in operational environments. Also, it will be the first time that historical take-off snapshot data will be related to ambient humidity measurement.

The addition to the body of knowledge of this research is twofold. The in-depth research on the effects of humidity on turbofan engine performance can provide insights for the MRO industry as well as the OEM. For the MRO industry it possibly enhances engine diagnostics. For the OEM, found insights in the humidity effects on turbofan performance possibly result in recommendations to enhance engine control systems by incorporating humidity effects. The effect of humidity on turbofan engine performance seems to be seen as not significant for a long time. However, the competitive market is pressuring OEMs and MROs to accurately predict engine performance & condition and seem to have spiked the interest in humidity effects also at other companies [12, 13]. Using take-off snapshot data combined with humidity data, together with the enhanced modelling software available nowadays, possibly sheds a clearer light on the effect of humidity on turbofan performance and the impact on engine performance diagnostics and engine control.

1.3. Report Structure

The reports is structured as follows, first in Chapter 2 general MRO practices will be presented to shape the context of this research. Second, background information on the root causes of performance

deviation due to humidity is presented in Chapter 3. Third, test-cell corrections as applied in the test-cell facility at KLM E&M will be examined in Chapter 4. Consequently, the simulation model used for the performance simulations is described in Chapter 5 after which the simulation results are presented in Chapter 6. Chapter 7 presents the statistical analysis on global, local and atmospheric humidity variation as well as the process of relating historical snapshot data to ambient humidity data. In Chapter 8, EGTM corrections are proposed and applied to the historical snapshot data to correct for ambient humidity. In Chapter 9 the results of the previous chapters will be discussed together, providing for additional insights while also reflecting on the research methods. Finally, Chapter 10 concludes on the research, answering the main research question and listing recommendations for the industry as well as for further research.

2

MRO Practices

Since this thesis research is performed in cooperation with KLM Engineering & Maintenance and dives deeper into the EGTM, this chapter is introduced to give a short introduction to the MRO practices with relation to the EGTM. This will provide for a better understanding of the importance of the EGTM as a health assessment parameter and the potential benefits in correcting the EGTM with greater accuracy. The focus of this chapter is only on the gas path of the engine. First, engine deterioration will be shortly discussed. Consequently, MRO practices in relation to performance restoration are covered. Last, a short explanation is given on the methodology of Gas Path Analysis (GPA).

2.1. Gas Turbine Deterioration and Effect on Performance

Like every other mechanical machine, gas turbines suffer from deterioration. Engine deterioration can be grouped into three types [17]:

- Recoverable Deterioration: recoverable during operation of the gas turbine.
- Unrecoverable deterioration: only recoverable by overhauling the engine.
- Permanent deterioration: deterioration still present after overhaul.

Without going into detail the most common types of deterioration in the gas path of the gas turbine are fouling, corrosion, erosion and abrasion, particle fusing and mechanical degradation [3, 17]. The deterioration of the components in the gas turbine causes a (negative) shift in performance. The flow path of the gas is often directly affected by the above mentioned degradation mechanisms, for example abrasion causes increasing tip clearance, negatively affecting engine performance. Figure 2.1a shows a simple representation of the T-S diagram of a deteriorated single spool gas turbine. The rotational speeds are kept constant in this example. Both the compressor and turbine have a lower isentropic efficiency due to deterioration. For the compressor this results in a lower pressure ratio and a slightly higher compressor outlet temperature whilst it requires more power. The temperature difference propagates through the engine. Assuming a fixed temperature increase during combustion, this eventually results in a higher turbine inlet temperature. Since the compressor needs more power, the turbine needs to deliver more power, together with the lower compressor delivery pressure this results in a lower turbine outlet pressure. Finally resulting in less net work to use for propulsion or driving another turbine, decreasing the overall efficiency of the gas turbine.

2.1.1. Effect of deterioration on EGT(M)

The EGTM is the margin between a predefined maximum (or red line) EGT and the measured EGT. As discussed later in section 2.2.1, the Hot Day EGTM (HDEGTM) is one of the most important performance parameters. The HDEGTM is the EGTM, assuming hot day ambient conditions (305.2 K for the CF6-C2B1F) on a predefined power setting. Since aircraft operate in different ambient conditions and power setting each flight, the EGT is corrected to an EGT when performing in Hot Day conditions. Also adjustments are applied to account for the difference in operating conditions.

$$\text{HDEGTM} = \text{EGT}_{\text{redline}} - \text{EGT}_{\text{HD}} + \text{EGT}_{\text{adjustments}} \quad (2.1)$$

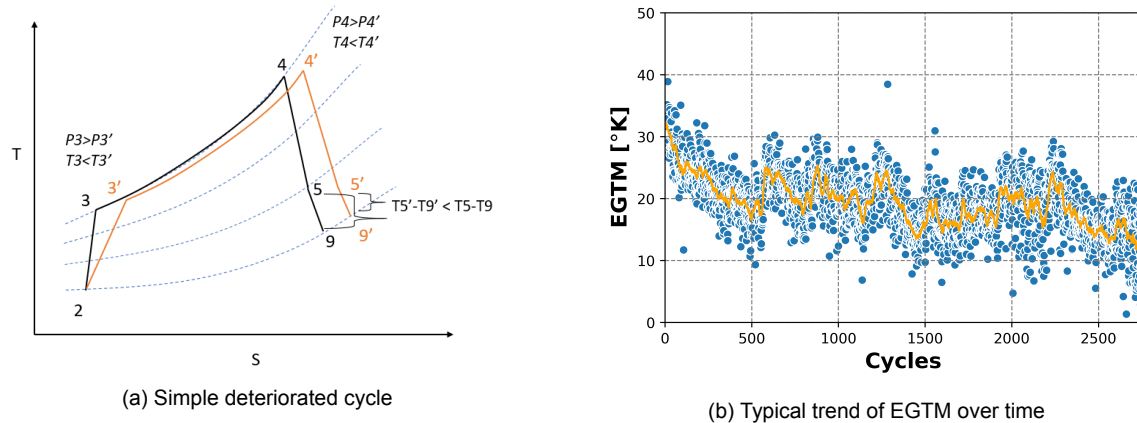


Figure 2.1: Visualization of deterioration effects

"EGTM" will now be used as HDEGTM throughout the whole report unless stated otherwise for the sake of simplicity. Deterioration is clearly visible on the EGTM trend of an engine. While the engine gradually deteriorates due to various reasons, the engine components become less efficient, resulting in an increase in temperatures due to decreased overall thermal efficiency of the engine. Figure 2.1b shows the typical trend of the EGTM of a CF6-80E1 engine for increasing amount of cycles. The effect of a water wash is also visible but will be covered later. It is clear that, however much scatter is present, the EGTM is decreasing over time. Typically, the trend of EGTM reduction of a new or overhauled engine can be split in two parts. The first few cycles the EGTM decreases significantly. This is called the "run-in" effect. It is caused by new seals, shrouds and other newly fitted parts [18] which are "running-in". For example, newly fitted shrouds with abrasable surfaces will deteriorate a lot from abrasion the first few cycles, after which a proper fit is created and the deterioration rate will settle at a lower pace.

What also immediately catches attention in Figure 2.1b is the severe scatter visible in the graph. The Hot Day EGTM is calculated and corrected for ambient conditions, bleed flows, power take-off, power setting and parasitic flows by the OEM. One would expect that, if the corrections and calculations are appropriately performed, the EGTM trend should only vary due to variations in the gas path i.e. degradation and sensor inaccuracy. However, the EGTM varies significantly between consecutive flights (were the degradation effects are thus negligible) to be solely due to inaccurate sensor measurements. The question arises if the Hot Day EGTM as reported by the engine is corrected appropriately. It would not be the first time the OEM is proven wrong in their EGTM correction method as described in the thesis work of Verbist [19].

Since humidity affects the EGT and therefore the EGTM, but no measurements or corrections are applied to take into account humidity. The presumption is made that correcting for humidity will therefore reduce the scatter on the EGTM trend. A too hot EGT significantly facilitates oxidation, corrosion and creep rates in the hot part of the engine. Operating with a negative EGTM can lead to high maintenance costs since many components will be deteriorating exponentially fast due to the high temperatures. It is therefore of crucial importance to keep the EGTM at a sufficient level in terms of safety as well as cost effective operation. Due to the steady gradual decrease in EGTM, EGTM is also used as an indicator of the performance gain of an engine after being overhauled. MROs make agreements in their contracts with the operators where they guarantee a certain EGTM improvement after an overhaul. The EGTM has effectively become a performance indicator of how long the engine can remain on-wing before maintenance actions are required.

2.2. Engine Health Management

The Gas Turbine MRO provider, together with the operator share the responsibility of maintaining safe and reliable engine operation. Naturally, this research focuses on the part of the MRO provider. To get an idea of the responsibilities of the operator one can think of: performing proper take-offs (e.g. with derate etc.), keeping track of basic engine performance parameters, quickly sharing information about incidents occurred during flight and properly storing the aircraft when not in use.

The field of work this research focuses on is the analysis of the aero-thermodynamic gas path of the engine, also known as Gas Path Analysis (GPA). The software Gas turbine Simulation Package (GSP) is used at KLM Engine Services by means of performing GPA on their engines and their costumers'. The GPA methodology is briefly discussed in paragraph 2.3. The software GSP will be more thoroughly discussed in 5.1.

2.2.1. Key performance indicators

When either deciding if an engine needs to be taken off-wing for maintenance, or evaluating the effect of the maintenance actions performed, one has to be able to make an accurate assessment of the performance of the engine. To be able to access the current status of the engine, performance indicators were introduced. The main performance indicators rating the performance of an engine are listed below:

- Hot Day EGTM: The EGT Margin is especially important since it provides a measure of performance restoration. A high margin indicates good performance, while a low margin indicates poor performance.
- Fuel flow: naturally, the fuel economy of the engine is an interesting parameter. Deteriorated engines exhibit decreased fuel economy.
- N2 speed: due to both structural as well as turbomachinery limits, the N2 speed is restricted to certain operating speeds. N1-speed is (often) controlled and therefore not a performance indicator but rather a control input.
- Thrust: a turbofan has to produce a certain amount of thrust w.r.t. certain N1-speeds or fuel flow settings. Note that aircraft or engines are not able to measure thrust when operating on-wing. Thrust is only measured in a test-cell.

The above performance indicators serve as a decision support system in order to decide if (corrective) maintenance actions should be performed. Naturally, other factors influence the decision as well. For example, the expiration of Life Limited Parts (LLP), excessive vibrations or lubrication system analysis finding metal debris.

2.2.2. Fault isolation

Whenever an engine is taken off-wing due to performance deterioration, it is not always immediately clear which component(s) in the engine are the main cause of performance deterioration. Being able to quickly identify the root cause of the performance deterioration is of vital importance for an MRO provider. This is because the MRO provider then knows the time span of the repairs, is able to plan and allocate the required technicians on a specific moment and is able to provide an indication of the costs of the repair. This is of crucial importance for efficiently performing MRO and reducing costs.

There are several methods to find the root cause of performance deterioration such as visual inspection using a borescope or complete disassembly of the engine in order to inspect parts thoroughly. Since these measures are very time consuming and costly and one still cannot always find the root cause, GPA can be a solution. GPA is covered more extensively in section 2.3.

2.2.3. Work scoping

When the failing component(s) is/are found, the corrective maintenance actions can be determined. Together with possible other repairs a work scope is set up for the specific engine. For an MRO provider to be cost efficient, properly set up work scopes are very important. For example, if a LLP will need replacement within the next 50 cycles, and a performance restoration overhaul has already been planned, it would be wise to replace all LLPs of which the life is going to expire soon, as well.

2.2.4. Restoring performance

In paragraph 2.1 the three different classes of deterioration were discussed. The recoverable deterioration can be recovered by means of water washing or abrasive cleaning. Abrasive cleaning is performed by running the engine on the starter motor and feeding it relatively soft abrasive material. The physical

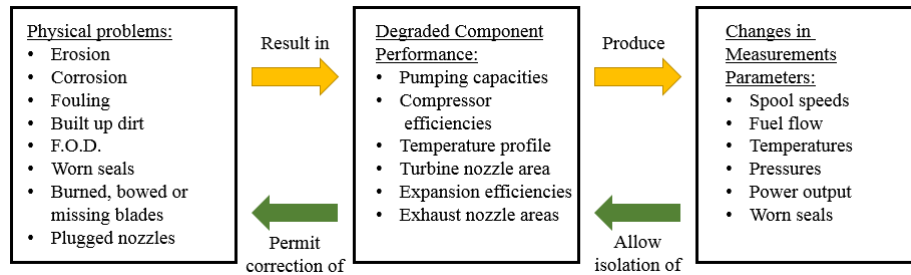


Figure 2.2: Relation between deterioration, performance and measurements [22] [modified]

impact of the material hitting the blades and surfaces in the engine cleans build up deposits of the surfaces. The downside of this method is that it can also damage thin airfoils and block cooling passages. Therefore it is currently not used often any more [20].

A more popular method is water washing. Water, with the possible use of detergent, is ingested by the engine while running on idle. The water cleans the blades and removes build up deposits while it does not damage the blades by means of abrasion. In Figure 2.1b the water washes can be recognized by the smaller upward spikes of the EGTM. The large upward spikes are the effect of an overhaul.

Unrecoverable performance deterioration is recovered off-wing by means of performing repairs to the damaged components or changing the deteriorated parts with new parts. Permanent deterioration, as the name indicates, will be present even after a major performance overhaul.

2.2.5. Test-cell acceptance testing

At KLM ES, after each major overhaul, the overhauled engine's performance will be evaluated in their test-cell facility. The test-cell facility extensively measures gas path parameters when operating at several power settings and converts this data into standard and hot day performance parameters. This is called an "acceptance test". Within the test-cell humidity is measured. When calculating the standard and hot day values of the corrected parameters, the test-cell corrects for humidity. The corrections applied will be further discussed in Chapter 4. The engine is tested at four power settings in order to cover the performance of several important areas of the operating range. The four power settings are listed below:

- Ground Idle
- Flight Idle
- Maximum Continuous (MC)
- Take-Off (TO)

The test-cell has been certified by the OEM to test their specific engines, meaning that the OEM agrees that engines passing the performance acceptance test at the facility are safe and reliable to be used again. Since the test-cell and the engine measure a lot of parameters and both of them output performance indicators, one would expect agreement between the two in some manner. However, it has been noticed that there is a discrepancy between test-cell measurements and on-wing measurements. This discrepancy has been researched, for example by Tonino [21], and is still being researched since no clear conclusion has been found yet.

2.3. Gas Path Analysis

As discussed in section 2.2, one of the practices to assess the condition of a gas turbine is by means of GPA. GPA is used to quickly identify failing components and to reduce the scope the MRO provider should focus on. Urban was the first to introduce gas path analysis in 1975. Urban stated that the degradation mechanics, as discussed in 2.1, resulted in degraded performance. The degraded performance results in its turn in changes in measurement parameters and can be used to identify component faults [22]. Figure 2.2 visualises this process.

Since the introduction of GPA by Urban, several different GPA methodologies have been introduced. Starting with linear models, also introduced by Urban in 1967, non linear models were introduced in

1990 to take into account the non linear behaviour of gas turbines [23]. Solving these non linear systems is done by using conventional optimisation and estimation techniques such as the Newton-Rhapson method and the Kalman filter. To avoid the downsides of these conventional optimisation methods, such as converging to a local minimum or the "smearing" effect of a Kalman filter, genetic algorithms were introduced by Zedda and Singh [24]. Other GPA methodologies used are Neural Networks[25], (Fuzzy) Expert Systems [26] and Fuzzy Logic systems [27]. Each methodology has its benefits and downsides. The main differences between the methods are, among others: empirical/physical, slow/-fast computational speed, low/high model complexity.

Whatever method will be used, the goal of GPA is to assess the degradation status of the gas path components by means of analysing gas path parameters. As pictured in Figure 2.2 the degradation in a component causes a change in gas path parameters which will be measured by the sensors. Using either the mathematical or empirical GPA methodologies, performance deviations, often in terms of component (isentropic) efficiency and mass flow capacity, can be found with respect to a healthy reference engine.

At KLM ES, the Gas turbine Simulation Program (GSP) software is used to perform GPA. The basic principle is that a "take-off performance snapshot" of the engine, which is captured at several moments during flight, is used to assess the health of the engine. The snapshot consists of several measured parameters such as temperatures and pressures, as well as N1- and N2-speed, fuel flow, flight Mach number and ambient conditions (excluding humidity). This data set is used to simulate the engine performance on component level, mainly focussing on the isentropic efficiency and corrected mass flow of the component. These characteristics are then compared to those of a healthy engine, where the deviations found can indicate failing components. Field expertise is important when performing GPA. One should know the limitations of the GPA software and know how to use it. Also, since all the components affect each other, the user should be critical when interpreting the outcome of the GPA analysis. For example, a component which seems to be 'failing' according to GPA due to a lower isentropic efficiency or mass flow, could very well be induced by other failing components up or downstream.

3

General Effects of Humidity on Turbofan Performance

This chapter is dedicated to explaining how humidity affects the thermodynamic properties of the air and consequently the performance of the components and the turbofan engine as a whole.

First, a short description of humidity in general will be given after which the change in thermodynamic properties of the air due to humidity variation will be examined. According to the basic equations used in turbofan performance simulation, the change of thermodynamic properties results in a change of component performance, consequently changing the performance of the complete turbofan. The effects will be described by both performing standard Design Point (DP) calculation as well as reviewing and implementing corrections found in open literature.

3.1. General Definitions of Ambient Humidity

Humidity can be described as the amount of water vapour present in the ambient air. When no water vapour is present in the air the term 'dry air' is used, when water vapour is present in the air this will be denoted as 'humid air'. The assumption of dry air is often used when performing gas turbine calculations and simulations. However, ambient air always contains a certain amount of humidity. Even on the driest places on earth the air contains water vapour [28].

Relative humidity

The most common representation of humidity is as relative humidity. Relative humidity is expressed as the partial pressure of water vapour divided by the equilibrium vapour pressure (saturation pressure) of water over a flat surface of water at a given temperature. It is often expressed as a percentage.

$$\Psi_{rel} = \frac{P_{vapour}}{P_{equilibrium}} \times 100\% \quad (3.1)$$

Relative humidity is used for weather predictions and human comfort. The first since it gives an indication of precipitation, dew or fog. When relative humidity is high, water evaporates more slowly. Since sweating is a method to cool the body, the sweat evaporates slower in humid environments and causes the body to cool off less efficiently. Therefore, a person perceives humid air as being hotter than it actually is. Relative humidity therefore also influences the 'feels like' temperature.

Absolute humidity

The absolute humidity is the mass of water vapour per unit mass of dry air, this is also referred to as the *mixing ratio*. In this research the unit mass is *kg*, therefore the absolute humidity is defined as:

$$\Psi_{abs} = \frac{m_{vapour}}{m_{dry}} \equiv \frac{\rho_{vapour}}{\rho_{dry}} \quad (3.2)$$

It should be noted that the common definition of absolute humidity is in kg/m^3 . A shortcoming of this definition when needing to perform calculations, is that absolute humidity changes when pressure and

temperature change and the volume is not fixed (as for the ambient). Therefore, in engineering and chemistry the absolute humidity is referred to as mass amount of water to mass amount of air as described in equation 3.2. Absolute humidity will be the general definition of humidity in this thesis work. It will be denoted by the weight percentage (*wt%*) of water vapour w.r.t. dry air. When the term humidity is used it will refer to absolute humidity unless stated otherwise.

Specific humidity

Specific humidity differs with absolute humidity in the fact that instead of dividing the mass of water vapour to the mass of dry air, it is divided by the mass of the humid air e.g. the mixture. Specific and absolute humidity are related as denoted in equation 3.4 below.

$$\Psi_{specific} = \frac{m_{vapour}}{m_{a_{humid}}} \quad (3.3) \quad \Psi_{specific} = \frac{\Psi_{abs}}{1 + \Psi_{abs}} \quad (3.4)$$

Dew-Point Temperature

Finally, another well known parameter to assess the amount of water vapour in the air is the dew-point temperature. The dew-point temperature is the temperature to which air, with a specific absolute amount of water vapour, must be cooled to become completely saturated. In other words, the relative humidity increases when the absolute temperature drops towards the dew-point temperature. When the relative humidity is 100% the dew-point temperature is equal to the absolute temperature. The dew-point temperature can be calculated using the *Magnus* equation described by equations 3.6 and 3.5.

$$T_{dp} = \frac{cz}{b - z} \quad (3.5) \quad z = \ln\left(\frac{P_{vapour}}{a}\right) \quad (3.6)$$

Or vice versa, when the dew-point temperature is known, the partial vapour pressure can be calculated accordingly with equation 3.7. It must be noted that in these equations the temperature is denoted in Celsius. The partial pressure of the vapour can be calculated using equation 3.1, given the relative humidity level and the equilibrium pressure. The equilibrium pressure of the water vapour can be calculated, again with the temperature in Celsius, using equation 3.8.

$$P_{vapour} = ae^{\left(\frac{bT_{dp}}{c+T_{dp}}\right)} \quad (3.7) \quad P_{eq} = ae^{\left(\frac{bT}{c+T}\right)} \quad (3.8)$$

Numerous studies have been performed trying to improve the accuracy of the dew-point calculation by finding better approximations of the specific *a, b, c* coefficients. All approximating the dew-point temperature fairly accurate for specific temperature regions. The coefficients derived by Buck [29], give an accurate approximation (max. error = 0.06% at -40°C) for the range -40°C to 50°C. The values of the coefficients are presented in table 3.1.

Table 3.1: The coefficients for the specific temperature ranges [29]

	a	b	c
233 - 273 K	6.1121	17.966	247.15
273 - 323 K	6.1121	17.368	238.88

3.2. Root Causes of Performance Deviations due to Humidity

The humidity of ambient air influences turbopfan performance in two possible ways. First, the water vapour changes the thermodynamic properties c_p, c_v, γ and \bar{R} of the air, resulting in a different operating point compared to dry air operation. Secondly, high relative humidity can cause condensation to occur in the inlet of the engine [6, 30]. Where the first effect is always present since air always contains water vapour, the second one is incidental, i.e. condensation may or may not occur. Since a systematic correction for humidity is researched in this thesis, the incidental effect of condensation is not researched in-depth and left out of discussion.

However to understand how and when condensation phenomena occur and what the effect is on turbopfan performance, could be of added value for this research in general. For example, when performing data analysis, it could be useful to exclude data where condensation may have occurred. Therefore, the next section quickly covers condensation.

3.2.1. Effects due to condensation

When air is accelerated into an inlet, the static temperature can drop beneath the dew-point temperature, causing condensation to occur. The phase change requires a finite dwell time and may not be possible in short intake ducts according to Spencer et al. [31]. The dwell time is dependent on the air-speed and the length of the intake. As mentioned, condensation only occurs when the air is accelerated into the engine. At cruise conditions the aircraft Mach number is higher than the local Mach number at the intake. The air is decelerated in the intake, increasing the static temperature precluding condensation as also mentioned by Blake [32]. Next to the ambient conditions and dwell time, condensation depends on the presence of condensing nuclei [6, 31]. Condensing nuclei are small particles on which the water vapour condenses, with more condensing nuclei in the air water vapour condenses earlier. When condensation does take place, one should be aware of the following consequences according to Bird and Grabe [6]:

- A decrease of compressor efficiency due to surface wetness of the compressor blading. This is also mentioned by Nikolaidis et al. [33] and was found to be more pronounced at lower rotational speeds
- Reduced cycle efficiency due to increase of inlet temperature caused by the release of latent heat in the intake when condensation occurs
- Fouling of the compressor blades due to the deposition of particulate matter
- The pressure instrumentation lines in the intake may be blocked by water droplets

In order to avoid the problem of condensation in test-cell environments boundary values for the ambient conditions can be imposed. Bird and Grabe [6] note the boundaries specified by the manufacturer of the F404 turbofan engine [34] as found below. For the Test-Cell facility at KLM Engineering and Maintenance no boundary values for the ambient conditions are specified.

- $\Psi_{rel} \leq 75\%$
- $\Psi_{abs} \leq 1.428wt\%$
- No moisture visible in the air

Defining if condensation occurs in the inlet of the engine is extremely difficult. This is mainly due to the fact that the condensing nuclei play a big part in condensation phenomena [7]. The author has no access to data about condensing nuclei in the air. Also, determining if the air is accelerated or decelerated at the moment of the snapshot as well as the dwell time may well not be possible with the data available.

Due to the incidental effect and the difficulty predicting inlet condensation, it is chosen that researching condensation is out of the scope of this research. Understanding what effect condensation has on engine performance and being able to possibly exclude data points where condensation may have occurred, e.g. high relative humidity, is kept in mind when performing data analysis.

3.2.2. Effect of humidity on the thermodynamic properties of air

In this section a study is performed on how the thermodynamic properties of air vary with ambient humidity variations. As explained, ambient air always contains water vapour. The saturation pressure of water vapour rises when the ambient temperature rises. This means that with increasing air temperature the air becomes capable of 'carrying' larger amounts of water vapour before condensation occurs. To understand how the thermodynamic properties of the air vary with ambient humidity and temperature, the properties are calculated for a range of ambient temperatures and relative (and absolute) humidity levels.

The ambient temperature is varied in the range of 233K to 323K as is the range for which equation 3.8 is accurate within the error bounds mentioned above and also reflects the range of sea level ambient conditions. The equilibrium pressure is calculated with equation 3.8 for the temperature range as mentioned. The partial vapour pressure is calculated using equation 3.1 for relative humidity levels ranging from 0 – 100%. With the partial vapour pressure the partial dry air pressure can be calculated using equation 3.9, assuming ISA sea level ambient pressure ($p_{amb} = 1013.25\text{kPa}$).

$$P_{amb} = P_{vapour} + P_{dryair} \quad (3.9)$$

$$\bar{c}_p = c_{p_{dryair}} \frac{\rho_{dryair}}{\rho_{tot}} + c_{p_{vapour}} \frac{\rho_{vapour}}{\rho_{tot}} \quad (3.10)$$

However the isobaric and isochoric specific heats vary with temperature, they are chosen as constant values since they vary only slightly in the temperature range mentioned earlier. Also, the specific heats of the mixture are calculated by taking the sum of the specific heats of water and dry air weighted by the ratio of their partial densities w.r.t. the density of the mixture, see equation 3.10. The same equation is also used for c_v and \bar{R} , substituting c_v or \bar{R} for c_p logically. The results are listed in Appendix B and discussed below. The following assumptions apply:

- c_p and c_v are assumed to be constant within the temperature range
- $c_{p_{air}} = 1.0065 \text{ kJ/kgK}$ and $c_{p_{vapour}} = 1.850 \text{ kJ/kgK}$
- $R = 8.314 \text{ J/molK}$ and the molar masses of dry air and vapour (and water) are $M_{air} = 0.028964 \text{ kg/mol}$ and $M_{vapour} = 0.0180 \text{ kg/mol}$ respectively.
- The humid air is assumed to behave like a perfect gas in order to calculate the specific heat at constant volume c_v using: $\bar{R} = c_p - c_v$ and $P = \rho \bar{R} T$

Mollier diagram

Figure B.1a shows lines for constant relative humidity levels versus temperature and absolute humidity, this figure is also known as a Mollier diagram. It is clear that for the same temperature, higher relative humidity levels also indicate higher absolute humidity levels. It also illustrates that air of higher temperature is capable of carrying significantly more water, which is also indicated by the exponential relation between the partial pressure and the temperature.

Variation of ambient air density

Figure B.1b shows the density of air versus the temperature for different relative humidity levels. The expected trend of decreasing density with increasing temperature is clearly visible. Also noticeable is that the density of the humid air decreases with increasing humidity. This is counter-intuitive since one may expect a larger mass in the same volume due to the addition of water. However since the partial density of water vapour is lower than that of air, the larger the volume of water vapour in the air the less volume can be occupied in that same volume by the 'heavier' dry air for the same ambient pressure. Resulting in a decrease in air density when ambient humidity increases. The effects are greater at higher temperatures since the air is able to hold more evaporated water. Nonetheless, the sensitivity of ambient air density to temperature is higher than to ambient humidity.

Variation of specific heats and ratio

Figure B.2a displays the specific heat of the mixture over the temperature range. Again, with increasing temperature, the absolute amount of water the air is able to hold is larger and the effect on the specific heat also increases. The increase is logical since the heat capacity of water vapour is higher than that of air. Thus, more water vapour in the air will result in a higher average heat capacity. Keep in mind that the assumptions mentioned before are applied. The same behaviour has been found for the isochoric heat capacity and is displayed in Figure B.2b.

The variation of the specific heat ratio with increasing temperature for different humidity levels is shown in Figure B.3a. Opposing to the graphs for the specific heats, the specific heat ratio reduces for higher temperature and humidity levels. The percentile change however, is less significant than the percentile change for the specific heats. The decrease of the specific heat ratio is due to the larger increase of isochoric heat with respect to the isobaric heat.

Variation of Specific Gas Constant

Next to the specific heat ratio, the specific gas constant of the air is also affected by ambient humidity variations. The results found for the variation of specific gas constant of the ambient air with varying humidity is depicted in Figure B.3b. An increase in specific gas constant has been found for increasing values of humidity. Whereas for dry air, the specific gas constant naturally stays constant with varying temperature, the increase in temperature increases the capability of the air to carry water. Therefore, the deviation of the specific gas constant with respect to dry air also increases for higher temperatures.

When plotting the specific gas constant and specific heat ratio versus the absolute humidity it becomes visible that the relation can be well approximated as linear. When performing a linear regression for γ versus Ψ_{abs} a correlation score of 0.9991 is found. The same figure has been made for the isobaric and isochoric specific heat and displayed in Figure 3.1b.

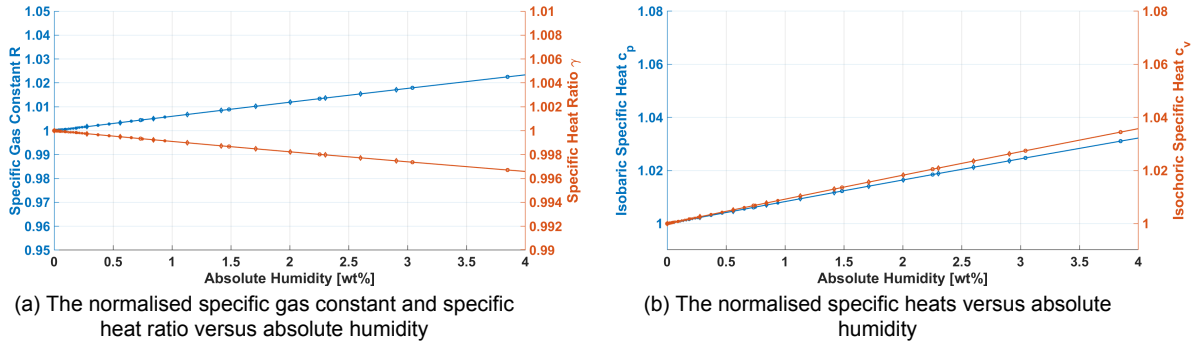


Figure 3.1: Normalized change in gas properties of ambient air

Relation between Relative Humidity and Altitude in ISA conditions

Since the ambient pressure and temperature, within the operating range of the engines, both decrease with increasing altitude, it is also interesting to investigate how altitude relates to humidity. The ISA barometric formula is used to calculate the ambient pressure over the range of 0 to 11km. For ISA conditions, the temperature decreases linearly within 0 to 11km above the surface of the earth with a lapse rate of $6.5K/km$. Relation 3.8 is used once again in order to retrieve the relative humidity levels for different heights using the ISA temperature profile. Figure B.4a shows how the relative humidity levels vary with altitude for ISA conditions. Due to the decreasing temperature on higher altitude, the air is less capable of holding water. The relative humidity therefore increases for the same absolute humidity.

Important to note is that this graph does not display how absolute humidity behaves in the atmosphere, other than displaying that the maximum amount of absolute humidity decreases with altitude. However, it does illustrate that an aircraft operating at lower altitude, for example at take-off, will be significantly more subjected to humid conditions than an aircraft flying at an altitude of 6km, because the root cause of the performance effects are due to the absolute amount of water in the air. The variation of absolute humidity in the atmosphere will be discussed in section 7.1.

Summary on Thermodynamic property variations

As described in the previous paragraphs, humidity alters the thermodynamic properties of the ambient air. To get a better understanding of these deviations, Table 3.2 summarises the deviation of the thermodynamic properties in terms of percentages. Ambient conditions are chosen which represent high ambient humidity, e.g. $T = 308.8K$, $\Psi_{rel} = 80\%$, $\Psi_{abs} = 3.0wt\%$. For the density, a decrease of more than 2% is found. This will possibly also indicate a decrease in mass flow for turbofans performing in humid conditions. Where both c_p and c_v deviate by more than 3%, it becomes clear that the specific heat ratio only changes very slightly in comparison with all the other properties. The gas constant of the mixture increases in the same order as the density decreases. The effect of the change of thermodynamic properties on the performance of the components and the turbofan will be discussed in the next sections.

Table 3.2: Deviation of thermodynamic properties due to ambient humidity variation

Property [units]	Dry Air	Humid Air	Δ w.r.t. dry
$\rho[kg/m^3]$	1.143	1.118	-2.187%
$c_p[kJ/kgK]$	1.0065	1.037	3.030%
$c_v[kJ/kgK]$	0.7195	0.7439	3.391%
$\gamma[-]$	1.399	1.395	-0.2859%
$\bar{R}[J/kgK]$	287	292.1	1.777%

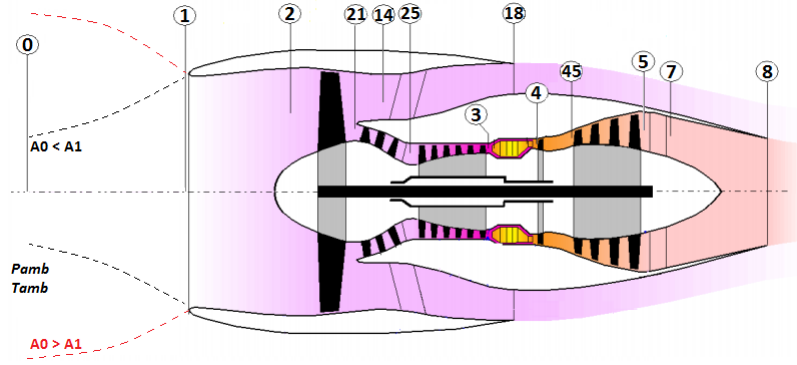


Figure 3.2: Turbofan engine station numbering [37] [modified]

3.3. Effects of Humidity on (Design Point) Cycle Calculation

Before simulating the behaviour of the full turbofan engine it is of added value to research the effect on the components by performing a design point cycle calculation. This will be done just to get a grip on how the design point calculations are affected by the change of thermodynamic properties due to humidity effects. The design point calculation is the starting point when simulating gas turbine performance. The design point calculation determines the size of the components and serves as a reference point for off-design calculations [35]. Some assumptions apply to the cycle calculations below:

- Component efficiencies remain equal with humidity variation
- The gas behaves as an ideal gas

In order to assist the design point calculation for a two-spool turbofan engine, the stations will be numbered as depicted in Figure 3.2. The station numbering applied is conform the ARP-755A station numbering retrieved from Appendix A in [36]. The cycle calculation will be accompanied by the T-S diagram as depicted in Figure 3.3. The entropy change of the air/gas in turbomachinery will be calculated using equation 3.11 as described below.

$$\Delta s = c_p \ln \frac{T_{out}}{T_{in}} - \bar{R} \ln \frac{P_{out}}{P_{in}} \quad (3.11)$$

An adiabatic inlet is assumed where no heat or work is transferred, therefore the stagnation temperature stays constant. Since pressure losses occur due to friction and shock waves [20], η_i is introduced to account for the pressure losses. Equation 3.13 is used for calculation of the total temperature.

$$\frac{P_{t1}}{P_a} = \left[1 + \eta_i \frac{\gamma - 1}{2} Ma^2 \right]^{\frac{\gamma}{\gamma - 1}} \quad (3.12) \quad \frac{T_{t1}}{T_{amb}} = 1 + \frac{\gamma - 1}{2} Ma^2 \quad (3.13)$$

Only when the Mach number is higher than zero the γ term has an effect on the pressure ratio. Since γ decreases when ambient humidity increases the pressure ratio over the inlet decreases. The entropy will increase due to the pressure loss over the inlet as found from equation 3.11. However, for the sake of simplicity and to easily compare the effects on the turbomachinery, the inlet is assumed isentropic. Also, the flow Mach number is set to zero resulting in that the ambient temperature and pressure equal the total pressure and temperature at the fan inlet.

The fan, booster/LPC and HPC all have a designed pressure ratio which is fixed in this design point calculation. Referring to equation 3.14, with a constant isentropic efficiency and design pressure ratio, the temperature ratio will decrease. The entropy change in the components will increase when compared to dry air. This is due to the fact that c_p increases more significantly than \bar{R} and that the decrease of T_{out}/T_{in} is also less significant.

$$\eta_{is,comp} = \frac{\left(\frac{P_{t,out}}{P_{t,in}} \right)^{\frac{\gamma-1}{\gamma}} - 1}{\frac{T_{t,out}}{T_{t,in}} - 1} \quad (3.14) \quad \eta_{is,turb} = \frac{1 - \frac{T_{t,out}}{T_{t,in}}}{1 - \left(\frac{P_{t,out}}{P_{t,in}} \right)^{\frac{\gamma-1}{\gamma}}} \quad (3.15)$$

In this design point cycle calculation the combustion efficiency is also deemed invariant. The fuel flow is a design variable and thus kept constant. Equation 3.16 displays energy balance between the fuel and the temperature rise of the (humid) air and fuel mixture. This relation depicts that the total increase in temperature of the gas will be lower when compared to dry air. This is because c_p is larger for humid air. The change in entropy of the gas will also slightly decrease. This is due to the lower temperature at the exit at the combustor.

$$\dot{m}_g c_p (T_{t4} - T_{t3}) = \eta_{cc} \dot{m}_f LHV \quad (3.16)$$

The turbines are connected to the compressors with shafts. The fan and the booster/LPC are connected to the LPT, the HPC is connected to the HPT. Equation 3.17 considers the power balance between the turbines and the compressor. The mass flow through the turbofan is a design variable and kept constant. There are a lot of changing variables in this equation. Both c_{pa} as well as c_{pg} will increase in approximately the same order when compared to dry air conditions. Since the temperature rise over the compressor has decreased, the temperature drop over the turbine will also decrease in order to maintain validity of equation 3.17. Using equation 3.15 the pressure ratio can be calculated. With a decrease in temperature ratio, the pressure ratio also decreases according to equation 3.15, resulting in a lower turbine outlet pressure. For the LPT exit temperature and pressure the above calculations are repeated, resulting in a lower final exit pressure and temperature. When assuming equal nozzle efficiencies, this will in its turn reduce the thrust in the core nozzle. Due to the lower temperature ratio achieved in the fan, the same can be concluded for the bypass nozzle.

$$\dot{m}_a c_{pa} (T_{t3} - T_{t25}) = \eta_m \dot{m}_g c_{pg} (T_{t45} - T_{t4}) \quad (3.17)$$

The changes in the cycle calculation are visualised in a T-S diagram displayed in Figure 3.3. Note that this visualisation is an exaggeration of reality. Also, a larger initial value of entropy is found for humid air. However to visualise the differences more easily, the entropy at the fan inlet is assumed to be equal. The isobars in a T-S diagram are dependent on the gas properties. The isobars of a gas with lower specific heat ratio will be located slightly lower compared to the isobars of a gas with higher specific heat ratio. When having a fully isentropic process this follows from equation 3.14, since for the same pressure ratio a lower temperature ratio is found. Next to a downward displacement the isobars of humid air also are subjected to a lower slope. This can be shown by substituting the *Gibbs* equation 3.18 in the equation for enthalpy 3.19, resulting in equation 3.20. Where for an isobaric process, and recalling equation 3.21, equation 3.22 results. Since humid air has a higher c_p than dry air the isobars in the T-S diagram of humid air have a lower slope.

$$du = Tds - Pdv \quad (3.18) \quad dh = du + Pdv - vdP \quad (3.19)$$

$$dh = Tds - Pdv \quad (3.20) \quad dh = c_p dT \quad (3.21) \quad \frac{dT}{ds} = \frac{T}{c_p} \quad (3.22)$$

The equations used in this section are also used in GSP. When performing a DP simulation in GSP it runs through the above equations. Since the outcome of some equations are very dependent on the magnitude of the changing parameters with respect to each other, a simple Design Point simulation was ran using the sample project "BIGFAN.mxl" available in GSP. In Appendix C, the method and results are listed.

While this section described how the change of gas properties affects the design point cycle calculation, the following section tries to identify performance changes due to humidity when performing in other operating conditions, i.e. off-design.

3.4. Effects of Humidity on Off-Design Performance

Predicting turbofan component performance when operating off-design is not as straightforward as for the DP calculation, but often involves computer models and simulations in order to iteratively solve several compatibility equations. Modelling gas turbine performance will be discussed more thoroughly in Chapter 5. However, fundamental correction formula's have been derived in literature in order to estimate the performance changes caused by ambient humidity variations such as those of [5, 7, 38]. Understanding the theory behind the performance changes is of fundamental value when analysing simulation results by providing a better understanding of the root cause of the performance changes.

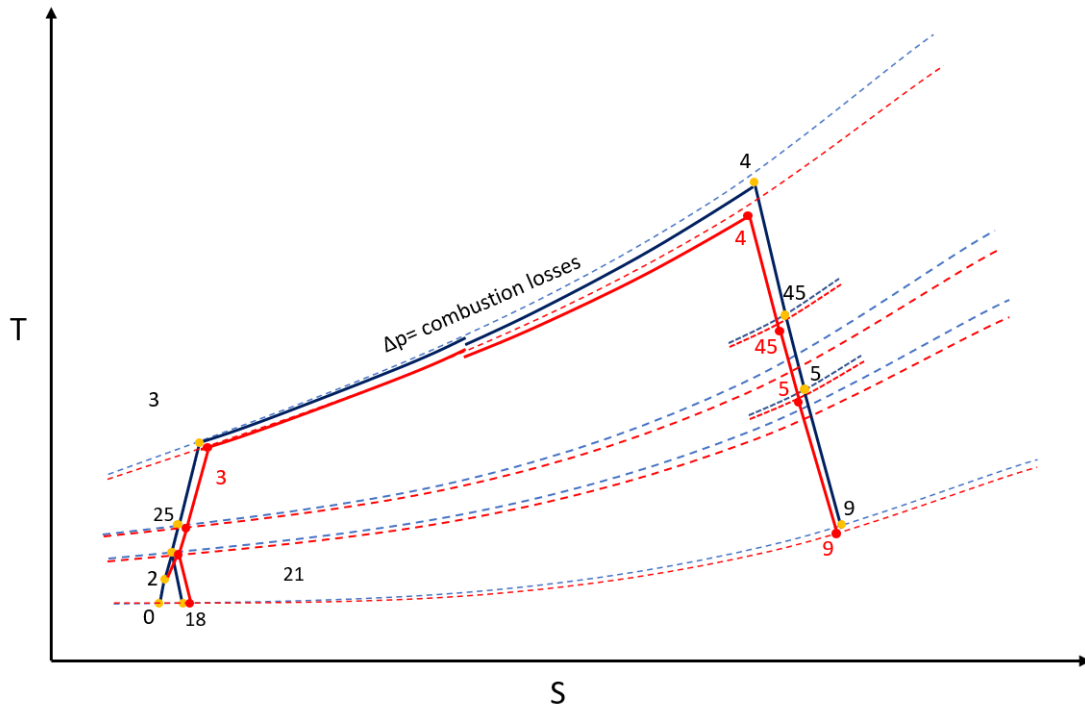


Figure 3.3: Exaggeration of a two-spool Turbofan DP calculation T-S diagram, for both dry and humid air

Therefore this section dives deeper into the corrections as provided in literature which are widely accepted.

When comparing component behaviour quasi-dimensionless or corrected parameters groups are often used. These parameter groups greatly simplify understanding, visualisation and comparing component performance by reducing the amount of variables, grouping them in dimensionless parameters. The most important parameter groups are listed in Table 3.3 and retrieved from [36]. Where θ and δ are defined as in equations 3.23 and 3.24.

$$\theta = \frac{T_{in}}{T_{isa}} \quad (3.23)$$

$$\delta = \frac{P_{in}}{P_{isa}} \quad (3.24)$$

Garwood et al. [7] define correction formulas by approximating full flow similarity (similitude). This follows in the footsteps of the corrections provided by Samuels & Gale [5] and Fishbeyn & Pervyshin [38]. Flow similarity implies that the directions of all velocity vectors are equal for both conditions. For

Table 3.3: Parameter groups

	Dimensionless	Quasi-Dimensionless	Corrected
Pressure ratio	$\frac{P_{t,out}}{P_{t,in}}$	$\frac{P_{t,out}}{P_{t,in}}$	$\frac{P_{t,out}}{P_{t,in}}$
Mass flow	$\frac{\dot{m}\sqrt{RT_{t,in}}}{D^2 P_{t,in}\sqrt{\gamma}}$	$\frac{\dot{m}\sqrt{T_{t,in}}}{P_{t,in}}$	$\frac{\dot{m}\sqrt{\theta}}{\delta}$
Rotational speed	$\frac{ND}{\sqrt{RT_{t,in}\gamma}}$	$\frac{N}{\sqrt{T_{t,in}}}$	$\frac{N}{\sqrt{\theta}}$
Efficiency	η	η	η

two flow fields to be equal the following statements should be met:

1. Geometric similarity
2. Equal V_{ax}/U thus equal $\Delta h/U^2$
3. Reynolds number has negligible effect
4. Prandtl number has negligible effect
5. Equal Mach number
6. Equal specific heat ratio

With the above statements made as assumptions and adding the assumption that the fluid behaves as a perfect gas, Garwood et al.[7] derived the relations as described in equations 3.25, 3.26, 3.28, 3.29 and 3.33. Since the specific heat ratio inherently changes when ambient humidity varies, there is already some arbitrariness in the equations [7].

$$\left(\dot{m} \frac{\sqrt{T_T}}{P_T}\right)_d = \sqrt{\frac{R_h}{R_d}} \sqrt{\frac{\gamma_d}{\gamma_h}} \frac{(1 + \frac{\gamma_h+1}{2} Ma^2)^{\frac{\gamma_h-1}{2(\gamma_h-1)}}}{(1 + \frac{\gamma_d+1}{2} Ma^2)^{\frac{\gamma_d-1}{2(\gamma_d-1)}}} \quad (3.25) \quad \left(\frac{N}{\sqrt{T}}\right)_d = \sqrt{\frac{R_d}{R_h}} \sqrt{\frac{\gamma_d}{\gamma_h}} \frac{1 + \frac{\gamma_h-1}{2} Ma^2}{1 + \frac{\gamma_d-1}{2} Ma^2} \quad (3.26)$$

Since the velocity triangles are assumed to be constant, as depicted in Figure 3.4, the work coefficient is also constant since this is a function of the velocity triangles only as described by equation 3.27. Rewriting the work coefficient in terms of flow Mach number, substituting the relation between static and total temperature finally leads to a correction in terms of work coefficient as described in equation 3.28.

$$\frac{\Delta h}{U_1^2} = \frac{V_{U,1}}{U_1} - \frac{U_2}{U_1} \frac{V_{U,2}}{U_1} \quad (3.27) \quad \left(\frac{\Delta h}{T_T}\right)_d = \frac{R_d}{R_h} \frac{\gamma_d}{\gamma_h} \frac{1 + \frac{\gamma_h-1}{2} Ma^2}{1 + \frac{\gamma_d-1}{2} Ma^2} \quad (3.28)$$

Since the assumption is made that the component efficiencies are independent of humidity variation, one can rewrite equation 3.28 to find the pressure ratio as depicted in equation 3.29 using the isentropic compression relation.

$$\left(\frac{P_{t_{out}}}{P_{t_{in}}}\right)_h = \left[\left(\frac{\frac{P_{t_{out}}}{P_{t_{in}}} \frac{\gamma_d^{-1}}{\gamma_d} - 1}{\frac{R_d \gamma_d c_{p,h}}{R_h \gamma_h c_{p,d}}} \right) \frac{1 + \frac{\gamma_h-1}{2} Ma^2}{1 + \frac{\gamma_d-1}{2} Ma^2} + 1 \right]^{\frac{\gamma_h}{\gamma_h-1}} \quad (3.29)$$

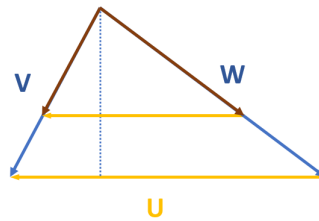


Figure 3.4: Similar flow field conditions due to equal velocity direction and ratio

While the pressure ratio is most interesting for the compressor, for the turbines it is the temperature drop due to its relation with performed work. Maybe the first researchers on the topic of humidity effects on gas turbine performance, Samuels and Gale [5], derived a correction for the turbine outlet temperature. The additional assumption is made that the turbine inlet temperature is invariant with humidity and that sonic velocities are present, thus $Ma = 1.0$. The compressor and turbine efficiencies can be calculated with equations 3.14 and 3.15 respectively. The correction formula is depicted in equation

3.30 as reformulated by Garwood et al. [7]. Following the same chain of thoughts, the compressor outlet temperature correction can also be derived. The assumption is made that the inlet compressor temperature remains unaffected by ambient humidity variation. Equation 3.31 states the correction for compressor outlet temperature. In order to calculate the corrections, the pressure ratios across the turbine and compressor need to be known. Equation 3.29, can be used to calculate these pressure ratio's.

$$\frac{T_{t_{out,d}}}{T_{t_{out,h}}} = \frac{1 - \eta_{turb} \left[1 - \left(\frac{P_{t_{out}}}{P_{t_{in}}} \right)_d^{\frac{\gamma_d - 1}{\gamma_d}} \right]}{1 - \eta_t \left[1 - \left(\frac{P_{t_{out}}}{P_{t_{in}}} \right)_h^{\frac{\gamma_h - 1}{\gamma_h}} \right]} \quad (3.30)$$

$$\frac{T_{t_{out,d}}}{T_{t_{in,h}}} = \frac{1 - \frac{1}{\eta_{comp}} \left[1 - \left(\frac{P_{t_{out}}}{P_{t_{in}}} \right)_d^{\frac{\gamma_d - 1}{\gamma_d}} \right]}{1 - \frac{1}{\eta_c} \left[1 - \left(\frac{P_{t_{out}}}{P_{t_{in}}} \right)_h^{\frac{\gamma_h - 1}{\gamma_h}} \right]} \quad (3.31)$$

3.4.1. Effect on performance of turbomachinery

With the above mentioned equations it is possible to estimate the corrections for the compressor and turbine when operating in humid conditions, keeping all assumptions in mind. The main distinction between the performance of the compressor and the turbine is the assumption of the inlet Mach number. For the compressor $Ma = 0.25$ is chosen, representing inlet Mach number at take-off conditions. For the turbine $Ma = 1.0$ is chosen, since choked flow generally is present at take-off conditions. Note that the effect of Mach number is generally very weak in equations 3.25, 3.26, 3.28 and 3.29, since it only affects the extend in which the specific heat ratio is taken into account which is also generally a weak effect. Since the turbine generally operates at higher temperatures than the compressor, $\gamma_d = 1.3$ is chosen to represent the specific heat ratio for turbine conditions. The ratio $\left(\frac{\gamma_h}{\gamma_d}\right)$ for the compressor is also used for the turbine, resulting in a $\gamma_h = 1.2966$. An isentropic efficiency of $\eta = 0.9$ is chosen for both the compressor and the turbine. Note that in equation 3.29 the pressure ratio in humid conditions is dependent on the dry pressure ratio. In order to calculate the correction factor, equation 3.29 is divided by the dry pressure ratio. The pressure ratio for the compressor and turbine are chosen as $P_{t_{out}}/P_{t_{in}} = 4.0$ and $P_{t_{out}}/P_{t_{in}} = 1/4$ respectively.

The results for mass flow, spool speed and pressure ratio are tabulated in Table 3.4. Please note that all corrections are depicted as corrections from humid to dry air properties. The results show a decrease of corrected mass flow in the order of 1% for both the compressor and turbine when operating in more humid circumstances. For the turbine the effect of Mach number is taken into account more effectively since the Mach number was set as $M = 1.0$. It is apparent that it only has the slightest effect when compared to the compressor correction. The correction for quasi-dimensionless mass flow of the inlet of the turbofan is identical to the correction for the quasi dimensionless compressor mass flow of the compressor. In contrast with the corrected mass flow, the corrected spool speed for both components increases when operating in humid circumstances. The increase is in the order of 0.75%. The specific work increases the most out of the parameters mentioned in the table, with an increase in the order of 1.5% for both the compressor and the turbine. Where the correction of the specific work of the turbine is slightly higher, one can argue that the specific work increase over the turbine has increased due to the increase in c_p when ambient humidity increases.

The pressure ratio of the compressor decreases according to the corrections, however only very slightly. Due to the nature of the equation, an increasing pressure ratio will eventually result in an opposite effect where the pressure ratio increases according to the corrections. For the conditions mentioned above, this happens at $PR \approx 13.4$. Pressure ratios for high pressure compressors in practice reach and surpass such pressure ratios. It is questionable if the sensitivity to humidity changes to have the opposite effect when pressure ratio increases, since the working principle remains equal. It is important to keep in mind that compressor efficiency is deemed invariant with humidity variations and γ and c_p were not varied with increasing pressure ratio, while it also increases temperature ratio.

The turbine pressure ratio increases, since the pressure ratio is defined as $P_{t_{out}}/P_{t_{in}}$. This means that the pressure drop over the turbine decreases. For the temperature ratio a similar trend is observed. The compressor outlet temperature is slightly lower, since the compressor inlet temperature is deemed invariant this also indicates a decrease in temperature ratio. The turbine outlet temperature increases, indicating a decrease in temperature drop and temperature ratio.

3.4.2. Effect on combustor

Next to the turbomachinery in the engine, ambient humidity also affects the performance of the combustor. Due to the change in chemical composition the temperature rise for a given amount of fuel flow will also change. Garwood et al. [7] also state differences in T_4 for different fuel to air ratios. The difference for a fuel to air ratio of 0.03, which is representative of a fuel to air ratio for a large high bypass ratio turbofan engine, is denoted in Table 3.4 and retrieved directly from [7]. A lower combustor outlet temperature is found. This is in line with the expectations since the c_p increases for humid air. Heating the humid air will take more energy and when the fuel flow is kept equal the air will be less heated compared with dry air.

Samuels and Gale [5], formulated a correction formula based on the assumption that the temperature ratio over the combustor remained equal as well as the inlet flow Mach number. This formula is presented in equation 3.32. The correction factor is displayed in Table 3.4. An increase in fuel flow is observed. The opposite chain of thoughts in comparison to the previous paragraph can be followed here. When the temperature ratio remains constant, more fuel will need to be added in order to heat the humid air by the same amount of degrees as that of dry air.

3.4.3. Effect on propulsion

With the turbomachinery and combustor covered, the effect on propulsion is next. Garwood et al. [7] derived a correction equation for (quasi-dimensionless) thrust by assuming the static exit pressure to be equal to the ambient pressure, i.e. the nozzle is not choked. A nozzle efficiency 1.0 is also assumed. The Mach number at the inlet of the nozzle is assumed to be $Ma = 0.6$. The correction as formulated by Garwood et al. is stated in equation 3.33. The correction applied for the humid conditions as stated before is again presented in Table 3.4. A very small decrease in thrust is expected for humid conditions.

$$\frac{\frac{\dot{m}_{f,d}}{\delta\sqrt{\theta}}}{\frac{\dot{m}_{f,h}}{\delta\sqrt{\theta}}} = \sqrt{\frac{R_h\gamma_d c_{p,d}}{R_d\gamma_h c_{p,h}}} \quad (3.32)$$

$$\left(\frac{FN}{AP_T}\right)_d = \frac{\gamma_d (1 + \frac{\gamma_h+1}{2} Ma^2)^{\frac{\gamma_h}{\gamma_d-1}}}{\gamma_h (1 + \frac{\gamma_d+1}{2} Ma^2)^{\frac{\gamma_d}{\gamma_h-1}}} \quad (3.33)$$

3.4.4. Notes on theoretical corrections

The main purpose of a turbofan engine is generating thrust, a change in performance in the turbomachinery and combustor will unquestionably have an effect on the thrust generated by the turbofan. The corrections as formulated in the previous paragraphs are great simplifications based on many assumptions which are only partially valid. Due to the complexity of the components operating in a combined equilibrium, the validity of the assumptions becomes questionable. For example, in the turbine outlet temperature calculation it is assumed that the inlet temperature is equal. However in section 3.4.2 it is explained that for the same amount of fuel flow a different turbine inlet temperature is found. As also noted by [5–7, 38] the effect of humidity on turbofan performance is heavily influenced by the engine's control configuration and re-matching (finding the new equilibrium) due to the change of operating points of the components. In terms of the example of the turbine inlet temperature; only if the turbine inlet temperature is controlled by the engine control system, the last mentioned assumption is valid and the fuel flow will increase. With other control configurations the effects are expected to be different. In order to take all these effects into account simulation models are required.

Chapter 5 describes a simulation model of the CF6-80C2, the turbofan engine of the Boeing-747. However, before diving deeper into modelling and simulation, the test-cell relations for humidity are investigated and compared to the theoretical findings as described in this chapter.

Table 3.4: Various theoretical correction factors for $\Psi = 2.8[\text{wt}\%]$

	Correction
Compressor	
Corrected Mass Flow	1.009
Corrected Spool Speed	0.993
Work coefficient	0.986
Pressure ratio	1.001
Outlet Temperature	1.002
Turbine	
Corrected Mass Flow	1.009
Corrected Spool Speed	0.992
Work coefficient	0.985
Pressure ratio	0.995
Outlet temperature	0.999
Combustor	
ΔT_{rise} ($f_{ar} = 3.0$)[7]	-26K
\dot{m}_f	0.987
Propulsion	
Corrected FN	1.002

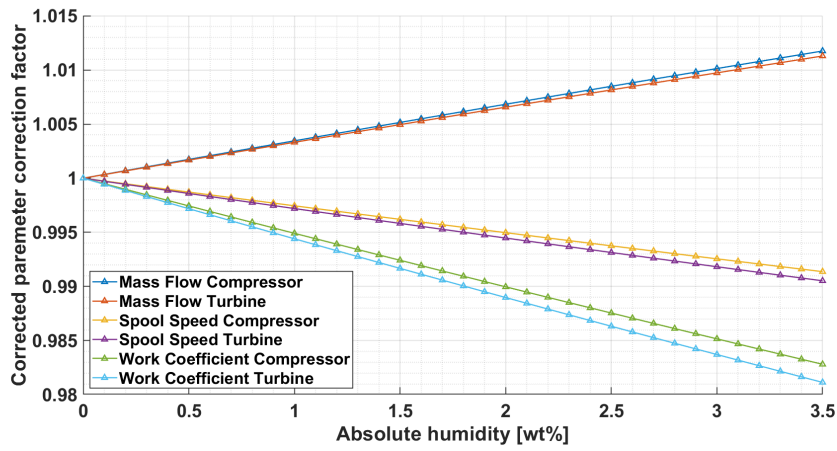


Figure 3.5: Theoretical corrections of \dot{m} , N , $\Delta h/T$ for turbomachinery

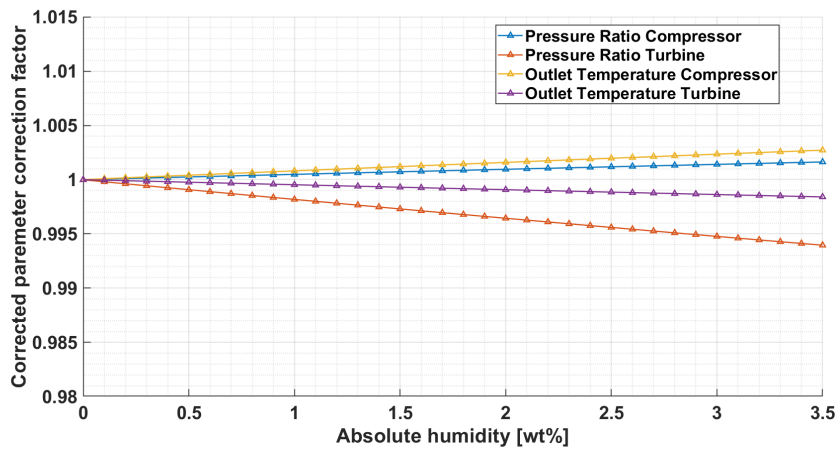


Figure 3.6: Theoretical corrections of Pressure Ratio and Outlet Temperature in turbomachinery

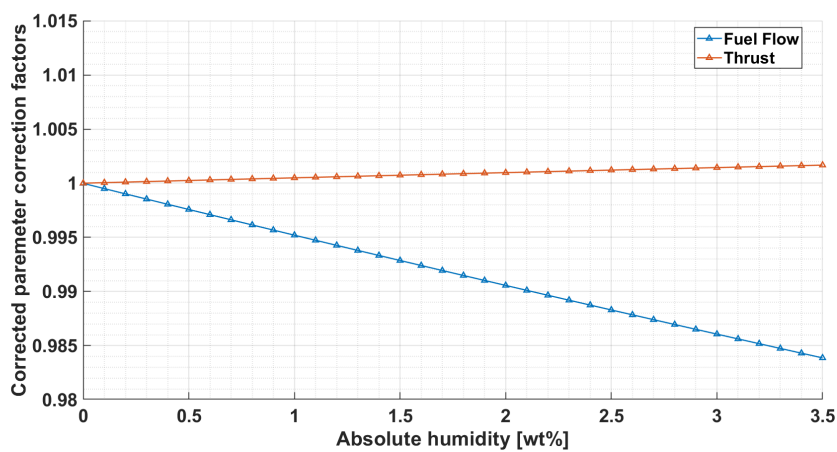
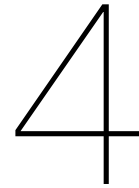


Figure 3.7: Theoretical corrections of Thrust and Fuel Flow



Test-Cell Corrections

At KLM ES, after each major overhaul, engine performance will be evaluated in their test-cell facility. This facility extensively measures gas path parameters when operating at several conditions and converts this data into standard performance parameters to verify if the performance of the engine is according to standards. This process is called an "acceptance test". Within this facility the CF6-80C2A5, CF6-80C2B1F, CF6-80E1A3 and the CFM56-7B are tested. The test-cell is certified by the OEM to test their specific engines in the test-cell. This section describes the test-cell corrections for the CF6-80C2B1F and the CF6-80E1A3 as performed in the test-cell at KLM E&M.

4.1. Correction Formulae

When performing an acceptance test, many parameters are measured. Before discussing the performed correction it must be clear under what operating conditions all acceptance tests are performed. The most important conditions are listed below.

- VBVs are completely closed
- VSVs are in neutral position
- No Customer bleed flows
- Power setting set as close as possible to the test rated fan speed

In order to provide for comparable results, several parameters are corrected to standard and hot day values. The measurements are corrected for ambient conditions, test-cell cowling, facility modifiers and N1K-deviation from the predefined rated test N1K-speed. Note that in this chapter the corrected fan speed, which is usually denoted by $N1_c$, will be denoted by N1K to define test-cell corrected fan speed. Deviation from the predefined rated corrected test speed is called 'throttle push'. For the CF6-80C2 corrections formulae are provided for the fan speed, core speed, fuel flow, exhaust gas temperature, thrust and engine pressure ratio ($\frac{P_{t49}}{P_{t2}}$). For the CF6-80E1 the latter two are not provided.

Humidity and Condensation

For ambient humidity, both the effect of the change in gas properties as well as condensation is taken into account. The humidity correction for the effect of changing gas properties and the effect of condensation are denoted with an H and C respectively.

Throttle push tables

To simplify compatibility, all engines are tested a specific rated corrected fan speeds. However, since it is hard to exactly match the rated corrected fan speed as defined by the OEM, throttle push tables are introduced. The throttle push correction is used for correction if the fan speed does not match the rated corrected fan speed ($N1K_{rated}$). The throttle push correction is found by interpolating for both the rated fan speed as well as measured N1K in the throttle push tables and subtracting the latter from the rated fan speed. This thus adds either a positive or negative delta to the observed corrected

parameter. Throttle push corrections are denoted by a Δ sign prior to the parameter name. The values in the table seem empirically derived. Since the corrections will be eventually used to assess engine performance after overhaul it is expected that the engine(s) used to create the table will be fairly new but have stabilized in terms of performance. Meaning that, for example, the seals are already ran in. This expectation comes from the fact that comparison must be made with a recently overhauled engine. However, it must be stated again the nature of the correction table is unclear to the author. Since N1K, as denoted in equation 4.1, is affected by humidity, humidity has also an indirect effect on the corrected parameters via throttle push adjustments. Both the direct as well as the indirect effect will be discussed in the next section.

Facility Modifier & Test Cowling

In order to take into account test-cell to test-cell differences, a Facility Modifier factor is introduced. This facility modifier correction factor is denoted as the parameter name with FM in the subscript. The cowling of the engine in the test-cell is different w.r.t. the cowling on wing. For example an bell mouth inlet is used in the test-cell. Corrections are available to convert test-cell measurements to on-wing representative measurements. The correction factors with respect to test-cowling are denoted as the parameter name with TC in the subscript.

Theta exponents

Next to these corrections, different θ exponents are found by interpolating for observed fan speed in the 'theta exponent table'. However test-cell documentation is unclear why these exponents change, it is the presumption of the author that they are used to apply appropriate corrections. This presumption follows from the gas turbine parameter corrections applied by Kurzke [39]. Kurzke states that the on Mach number similarity based gas parameter correction methods get complex when effects such as humidity, bleed air or power off-take and variable geometry have to be considered when determining the θ exponents. The OEM is likely to have a lot of experimental data which can be used to tailor these exponents to accurately calculate the corrected parameters. These corrections are denoted with an X prior to the parameter name.

Fan and core speed correction

For the corrected standard day values of the fan + booster/LPC and core speeds equations 4.1 and 4.2 apply.

$$N1K = N1_{obs} \times \frac{1}{\theta}^{XN1} \times H_{N1} \times C_{N1} \quad (4.1)$$

$$N2_{SD} = N2_{obs} \times \frac{1}{\theta}^{XN2} \times H_{N2} \times C_{N2} \times N2_{FM} + N2_{TC} + \Delta N2 \quad (4.2)$$

Thrust correction

The standard day dry thrust is calculated according to equation 4.3.

$$FN_{SD} = FN_{obs} \times \frac{1}{\delta} \times H_{FN} \times FN_{FM} + FN_{TC} + \Delta FN \quad (4.3)$$

EGT(M) correction

The EGT(M) calculation is slightly different since it is also subjected to a shunt factor denoted by SF . The author has rewritten the equations to units of Celsius and Kelvin instead of Fahrenheit and Rankine. The shunt factor is applied within the relative Celsius scale, thus the temperatures need to be converted back and forth.

$$EGT_{SD} = \left([(EGT_{OBS} - 273.15)SF + 273.15] \frac{1}{\theta}^{XT} \times H_{EGT} \times C_{EGT} \times EGT_{FM} + EGT_{TC} + \Delta EGT - 273.15 \right) \frac{1}{SF} + 273.15 \quad (4.4)$$

$$EGT_{HD} = [((EGT_{SD} - 273.15)SF + 273.15)\theta^{XT_{lat}} - 273.15] \frac{1}{SF} + 273.15 \quad (4.5)$$

$$EGTM = EGT_{max} - EGT_{HD} + DEGTM \quad (4.6)$$

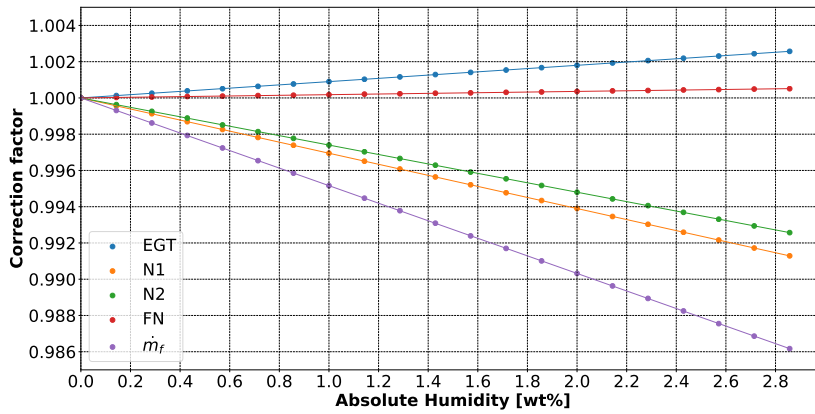


Figure 4.1: Test-cell direct humidity corrections

Fuel Flow correction

The fuel flow is corrected according to 4.7.

$$\dot{m}_{fSD} = \dot{m}_{fobs} \times \frac{1}{\delta} \times \frac{1}{\theta}^{XF} \times H_{mf} \times C_{mf} \times m_{fFM} + m_{fTC} + \Delta\dot{m}_f \quad (4.7)$$

EPR correction

For the EPR equation 4.8 holds, note that the direct humidity correction factor does not appear in this equation.

$$EPR = EPR_{obs} \times EPR_{FM} + EPR_{TC} + \Delta EPR \quad (4.8)$$

4.1.1. Direct humidity correction

The correction factor for humidity is found by interpolating for the observed humidity value in the 'humidity tables'. These test-cell corrections are captured in Figure 4.1. Note that the corrections are applied to correct humid air conditions to dry air conditions. The relations indicate only slight changes and with the effect on fuel flow being the largest. Indicating an increase in fuel flow, thus a negative correction factor, from humid to dry air of $\approx 1.4\%$ w.r.t. dry air for large values of ambient humidity. This is also similar to the correction found assuming flow similarity as listed in table 3.4. The other parameters follow the same trend however differ in correction magnitude. Interesting is to note that the humidity corrections are identical for both engines, this raises the suspicion that the direct effect of humidity is based on flow similarity as described in the previous section since those corrections are engine independent. The method of derivation of these corrections however, is unclear to the author.

4.1.2. Indirect humidity correction

In order to research the test-cell relations more deeply, all the above mentioned calculations were performed over a range of N1. The Facility Modifier factors are discarded from the equations since they are independent of humidity. The correction factors for inlet condensation are also discarded since condensation is not within the scope of this research. Since the test-cell corrections will be used to compare with simulation results and on-wing data, the test-cowling corrections are also discarded. The magnitude of the effect of humidity on the throttle push adjustments is calculated by subtracting the interpolated values of the 'dry' N1K from the interpolated values of the 'humid' N1K, resulting in the sole difference caused by humidity.

Relative contribution to the total correction

The throttle push table does not show linear behaviour. Therefore, the magnitude of the indirect correction depends on N1K. Figures 4.2a and 4.2b display the ratios and direction of both the direct and indirect correction for two power settings. The first power setting was chosen in the middle of the examined N1-range and the second power setting closer to maximal N1-speed. The direction of correction stays the same for the whole operating range. It is visible that the throttle push correction is positive

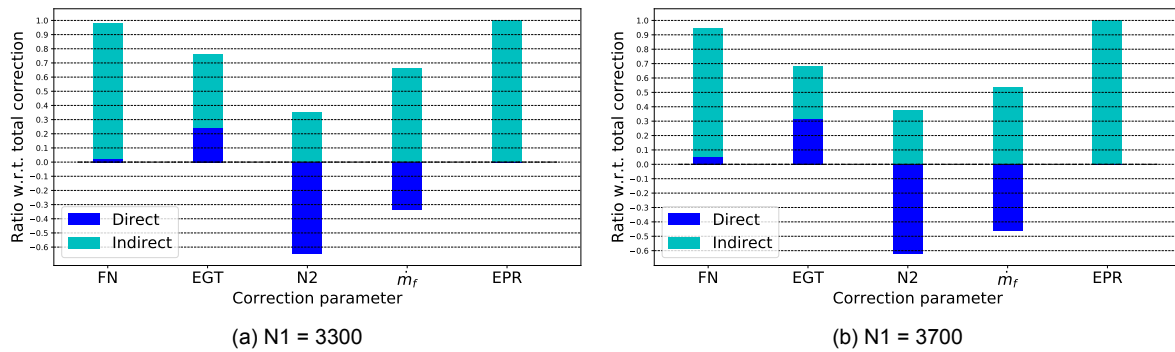


Figure 4.2: Comparison of magnitude of both the direct and indirect humidity corrections

for all parameters. Indicating that the parameters will increase when converted from humid to dry air performance.

While both the direct humidity effect as well as the indirect throttle push corrections are in the same direction for FN and EGT, this cannot be stated for the corrections for N2 and \dot{m}_f . The N2 correction for humidity is downward. However, the indirect correction is upward. This increase however is less than the decrease caused by the direct effect of humidity leaving the overall correction factor negative, indicating that the (corrected) core speed is expected to be lower in dry air compared with humid air. This is also in accordance with the theoretical corrections. The N2 correction is the only correction where the direct effect of humidity is larger than the indirect effect.

Both the FN as the EGT are expected to be higher in dry air than in humid air. This trend is also found in the theoretical equations described in section 3.4. According to the test-cell relations the EPR is also lower for humid air. Theory supports this since humid air causes the pressure ratios in the compressors to drop. Consequently a lower EPR will be observed when performing in humid air.

The fuel flow shows that the overall correction would be positive, indicating that for dry air larger values of (corrected) fuel flow are expected compared to humid air. The fuel flow increases according to the direct humidity correction, which is in accordance with the theoretical corrections. However, the greatest part from the correction is due to the throttle push and in the opposite direction, finally resulting in a decrease in fuel flow when ambient humidity increases. Thus, a N1-controlled engine will reduce its fuel flow in humid area's, yielding a positive correction factor for fuel flow when correcting to dry air. This may well be the effect of the control system operating the engine. The CF6-80C2B1F engine is a FADEC N1-controlled engine. According to the corrections the humid air causes the fan to spin faster compared with dry air, the fan will speed up if no corrective action is performed. In order to decrease the fan speed back to the required value, the engine will reduce the fuel flow.

4.2. Complete Test-Cell Humidity Correction

In order to understand how the complete corrections are affected by N1(K) the corrections were calculated for several fan speeds. For each fan speed the corrections were calculated. Linear regression is used to find the slope of the correction per observed N1K. Assuming linearity is justified since the regression coefficient over the N1 range averages $R \approx 0.9999$ for all parameters. The variation of these slopes with N1 are displayed in Figure 4.3 and are expressed as percentage change of the corrected parameter per wt% absolute humidity. Since no measurements are performed using this approach, the observed values are retrieved from the throttle push table. This is done for the dry corrected fan speed, thus no humidity correction, calculated from the simulated fan speed. Using this approach, the calculated 'observed' values will be a good presentation of values one would actually observe in a representative engine. This may give a slight overestimation since $N1K_{\text{humid}}$ is generally slightly lower than $N1K_{\text{dry}}$ and thus maybe slightly overestimate the dry value. Since the correction slopes are determined in terms of percent normalized deviation per weight percent humidity this causes no error in the calculated slopes.

The theoretical corrections are independent of corrected fan speed. As apparent from the figure, this is not the case for the test-cell corrections. Variable guide vanes, variable stator vanes and active clearance control are all functions of spool speed. The flow field changes with these varying control

systems. Also as explained, the theoretical corrections are applicable for a component and not necessarily for the whole engine. The combination of these variable systems dependent on spool speed in combination with all the components operating in equilibrium together results in different correction slopes for different spool speeds.

Due to the linear interpolation for N1K the slope of correction sometimes shows step increases or decreases instead of smooth behaviour. This is due to the linear interpolations performed for the theta exponents and throttle push corrections. The N1K step size between which is interpolated also differs per table, this causes the jumps not to appear at the same distance. When humidity increases N1K decreases, there are regions of N1 for which the N1K moves towards another N1K interpolation region for increasing values of humidity. The overall correction value will then be a (weighted) average between both the interpolations. This step increases are therefore not discrete but slightly tilted.

The values in the tables are expected to be retrieved from many controlled experiments. If higher order polynomial fitting was performed in between the lines, the graphs will probably result to be more smooth. However, according to the test-cell documentation as provided by the OEM it is the practice to interpolate linearly in between each step. Also, the differences are that small that it is probably accurate enough to use linear interpolation. The trends and magnitude are still easily visible.

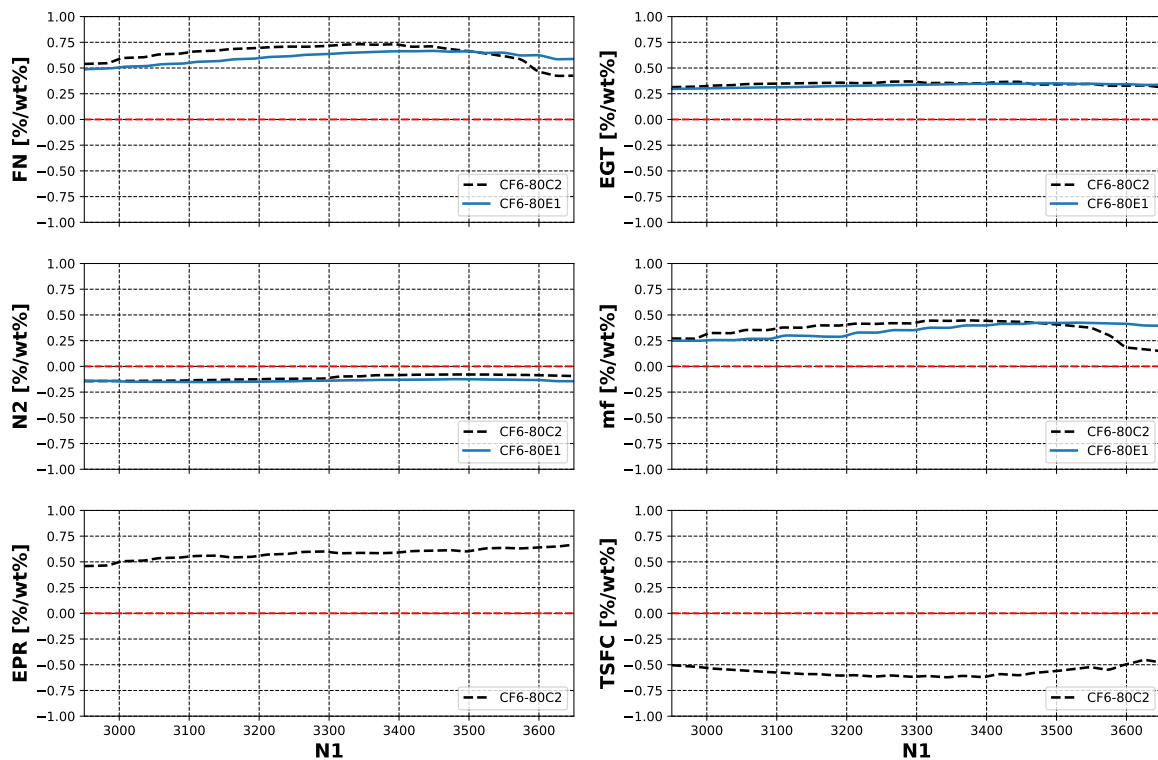


Figure 4.3: Correction slopes versus observed N1

CF6-80C2

All the corrections, except for the fuel flow, are in terms of direction in accordance with the theoretical corrections retrieved from literature. However, in magnitude they differ notably. According to the test-cell documentation the thrust is expected to decrease with more than 2% for an absolute humidity of 2.8wt%. For that same ambient humidity level, the theoretical flow fields similarity corrections only predict a thrust decrease of 0.2%. At higher spool speeds it is noticeable that the correction slopes are of less magnitude. This is due to the fact that in the throttle push tables the sensitivity of the parameters with respect to N1K decreases. In that region the engine seems less sensitive for throttle push corrections. This follows from the fact that the region is close to the maximal operating power. The engine is operating at full force and all variables reach their limits. The sensitivity of these parameters with respect to corrected spool speed starts to flatten, and due to the nature of the N1K correction of humidity, the indirect effect of humidity on those parameters also decreases.

Since the indirect correction for most parameters is the largest in magnitude, this is also very well visible in the overall effect, as can be seen in Figures 4.2a and 4.2b. The Figures show that the indirect correction magnitude with respect to the total correction reduces.

CF6-80E1

All corrections are very similar compared to the CF6-80C2. The EGT and N2 correction trends display the closest similarity. It is noticeable that a shift to the right is visible for FN and the \dot{m}_f . Within the investigated range the CF6-80E1 seems to be less affected by N1K sensitivity decrease for higher power settings. This may be attributed to the fact that the CF6-80E1B1F engine has a higher power rating than the CF6-80C2. For example, the rated fan speed is about 200RPM higher. The throttle push tables however present only corrected fan speeds up until N1K = 3650RPM where the throttle push tables for the CF6-80C2B1F lists corrected fan speeds up to N1K = 3750RPM. It was therefore not possible to calculate corrections for higher (corrected) fan speeds. The power settings for which the sensitivity decreases more notably is possibly not reached and therefore not completely visible in the graphs.

4.3. Final Remarks on Test-cell Corrections

Table 4.1 lists the average corrections for both engines. From the test-cell corrections it has become clear that due to the control configuration the effect of humidity actually varies with power setting. Corrections are found which may not be deemed negligible. For example FN indicates a thrust decrease of approximately 1.2% when ambient absolute humidity is 2wt%. For that absolute humidity an EGT reading of 1200K will need to be corrected in absolute sense with approximate 8.5K. For extreme cases, with ambient absolute humidity of 3.0wt%, this will result in errors of approximately 12.5K. When not corrected for humidity this error will be directly translated to an error of similar magnitude for the EGTm.

The difference between flow similarity theory and eventual corrections applicable for a whole turbofan stresses the importance of taking into account the different components operating in equilibrium as well as the engine control system.

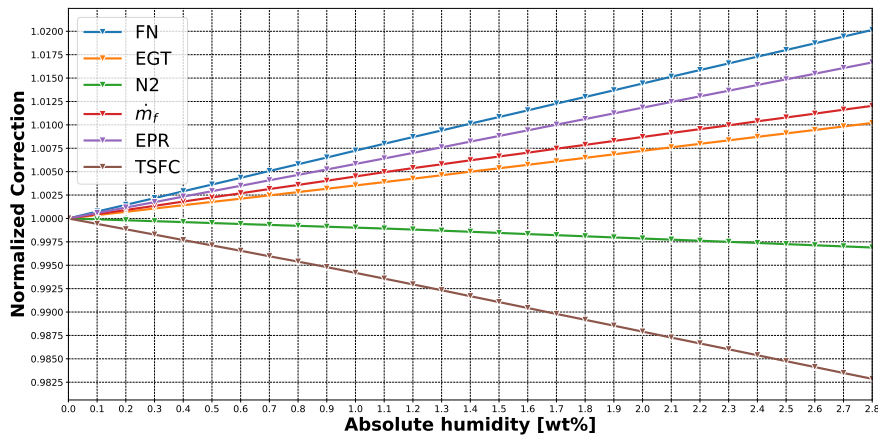


Figure 4.4: Test-Cell corrections for the CF6-80C2B1F, N1 = 3300 RPM

Table 4.1: Average correction slopes of complete test-cell corrections, expressed in [%/wt%]

	FN	EGT	N2	\dot{m}_f	EPR	TSFC
CF6-80C2	0.65	0.35	-0.11	0.37	0.58	-0.57
CF6-80E1	0.60	0.33	-0.14	0.35	-	-

5

Modelling Humidity Effects

This chapter is dedicated to explaining the working principles of the software package GSP, as well as describing the model used for simulation. The working principles of GSP will be explained first, after which the origin of the model used for simulation will be discussed. Finally, the modifications made to simulate the behaviour for other control configurations will be described.

5.1. Gas Turbine Simulation Program

This section is dedicated to researching the modelling capabilities of GSP since this is the proposed program for modelling gas turbine performance during the thesis assignment. This chapter gives an overview of the simulation and solution methodology. Please refer to [35] for an extensive description of GSP and its development.

In order to accommodate the need to be able to predict gas turbine performance, several Gas Turbine Simulation software packages were developed over the past few decades such as: DYNGEN, GasTurb, NPSS, TurboMatch, PROOSIS and GSP. The last is used at the Engine Services Department of KLM Engineering & Maintenance and will therefore be researched in more detail. The development of GSP started in 1986 at the Technical University of Delft where NASA's DYNGEN was used for jet and turbofan simulation but found to have problems with the numerical stability and user interface [40]. This triggered the development of GSP. Through the years GSP has been co-developed together with the Netherlands Aerospace Centre (NLR) and the last is now product owner of the software package.

5.1.1. Component based modelling

GSP is a component based modelling environment, characterised by a user friendly drag and drop interface [41]. Gas path or control components can simply be added by dragging the components into the user interface. When creating software to simulate, for example, gas turbine performance, the developer has the freedom to choose to what dimensional extend the performance will be modelled. Four distinctions are made for components models:

- 0-D component model: models that simulate the behaviour only at a certain point, often at the inlet/outlet of a component, represented as an average value.
- 1-D component model: the average parameters are calculated along a spatial parameter, often along the flow path.
- 2-D component model: the 1-D model augmented with another spatial parameter forming a 2-D plane, flow dynamics can now be taken into account with for example the use of CFD.
- 3-D component model: full dimensional analysis, often used when exact flow behaviour must be predicted, for example when designing a rotor blade using CFD.

All the standard gas path component models in GSP are 0-D. However, there are some extended 1-D component derivatives such as the multi-reactor combustor model and the 1-D thermal recuperator model [35]. Both of these components are not used in this research, thus all model components are

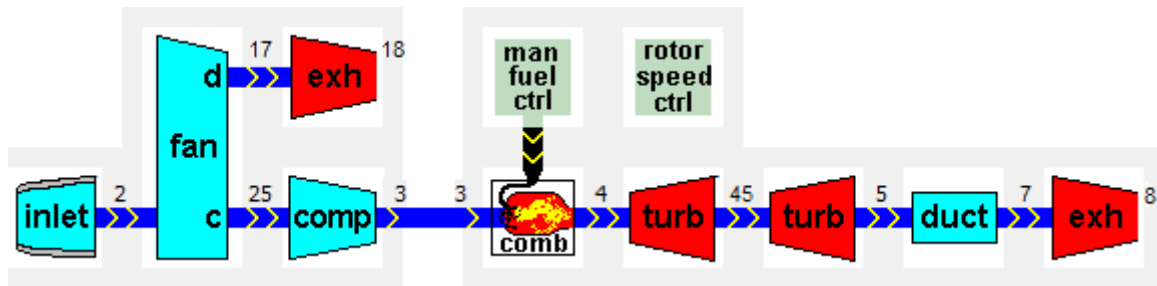


Figure 5.1: Screenshot of component based model interface of GSP, CF6-80C2

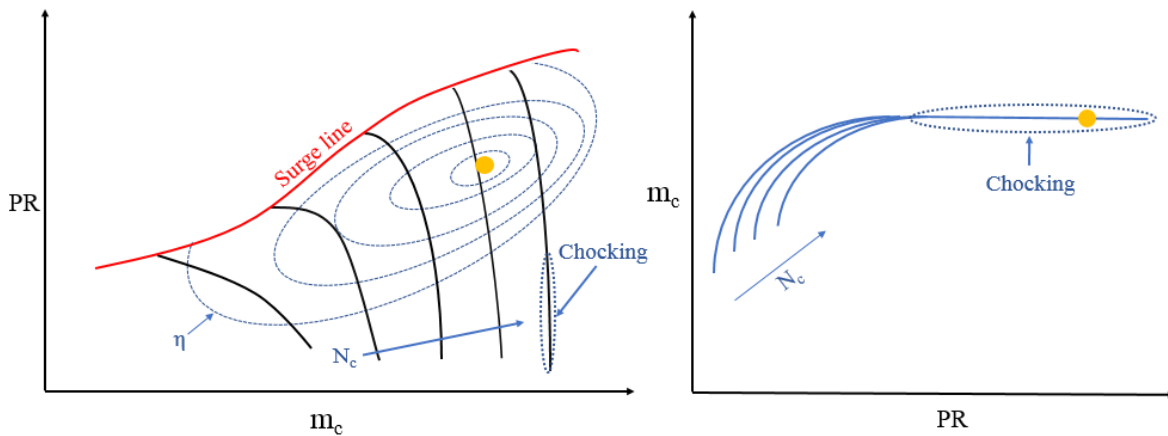


Figure 5.2: Generic Compressor and Turbine map

0-D. An example of an engine model, composed of several components, in GSP is displayed in Figure 5.1.

5.1.2. Design point component performance

When simulating a gas turbine distinction is made between DP performance and off-design performance. This also accounts for all the components in the model of the gas turbine. In GSP, first the DP calculation must be performed before any other OD calculations can be performed since the DP calculation sets the geometry and parameters of the engine. It will then be used as a *reference point* (RP) for any following OD calculations [42]. The DP component characteristics must be inserted in each component model. Examples of DP component characteristics are for example: the mass flow at the inlet, the pressure ratio, rotational speed and isentropic efficiency for compressors, the fuel flow and combustion efficiency for a combustor and the isentropic efficiency and rotational speed for turbines. When all necessary DP values are defined, the complete DP calculation can then be performed as in 3.3.

5.1.3. Off-Design component performance & component maps

When engine performance is simulated at any other operating point other than the DP, the engine is said to be operating off-design (OD). Thus, for OD performance simulation, the operating point generally differs from its design point. For a steady state OD calculation all the time derivatives of the parameters are zero, thus they are time independent. For transient simulation this does not hold. This research focusses on steady state behaviour only since the OEM implies that the on-wing TO snapshot can be assumed to be captured when operating in steady-state conditions.

To be able to simulate OD behaviour of the gas turbine, compressor and turbine maps are fundamental. These maps capture the behaviour of the compressor and the turbine in the whole operating range by making use of corrected parameters. Without the use of accurate compressor and turbine maps performance calculations will not be trustworthy. A generic compressor and turbine map are displayed in Figure 5.2

Compressor maps are significantly more complicated than turbine maps. They are usually depicted

with the (corrected) mass flow on the horizontal axis and the pressure ratio on the vertical axis. The thick black lines that move from upwards of the graph to the bottom and are ordered from left to right are the operating lines at constant (corrected) compressor speed N_c . Note that the lines become increasingly more vertical when the corrected mass flow increases. Also the operating lines all end in the upper region of the graph at a line called the *surge line*. The surge line logically displays when surge occurs in the compressor. If the blades of a compressor stall, resulting in a complete disruption of the airflow, this is referred to as surge. Surge occurs when the adverse pressure gradient on the compressor blades is so high that the flow separates and stall is induced. If the pressure ratio increases while running at the same operating speed, the graph 5.2 shows that the corrected mass flow reduces. If the pressure ratio increases the density also increases, which follows from the perfect gas law. Since $\dot{m} = \rho Av$ and ρ increases, the velocity v of the flow has to decrease significantly. Having the same rotational speed but decreased axial flow velocity, the relative velocity will direct itself in a more vertical manner, increasing the adverse pressure ratio until stall occurs and the whole flow is disrupted. In the regions of higher mass flow the operating lines become vertical. An increase/decrease in pressure ratio does not result in a different mass flow, e.g. the flow is choked.

Compressor maps are unique and are defined by the compressor geometry [43]. Also due to deterioration effects altering the compressor geometry, one could argue that compressor maps are unique for each compressor in use. OEMs have in-depth knowledge about the compressor maps of their engines, however it is often regarded as confidential information and not supplied to third parties. When the component maps are not available it is common practice to use maps available from open literature and 'tune' them using available operating data to match the behaviour of your compressor. Various studies [43–46] have been performed in order to find the best method to create or tune compressor maps. The general finding is that creating component maps is a hard and laborious task. In order to tune compressor and turbine maps more easily Kurzke has developed software packages called *SmoothC* and *SmoothT* [43]. The data used to tune the compressor maps should also be of high accuracy otherwise errors in the data propagate in the component maps [47].

For a turbine map the axis are switched w.r.t. a compressor map. The pressure ratio is now defined as inlet over outlet pressure and not vice versa as the case for the compressor map. Again the black lines indicate constant (corrected) operating rotational speeds. As noted by Walsh, it is found in practice that turbines do not exhibit large variations in non dimensional flow with non dimensional speed, but that they are often restricted by components downstream of it [36]. It is visible that a large region of the turbine map is restricted to the choked condition. The operating DP is often located in the choked region where the (corrected) mass flow has reached a maximum for a certain pressure ratio. Surge does not occur in turbine maps. Turbine maps are less complicated since turbines generally operate under choking conditions [20] and stall is not an issue. Therefore turbine maps often introduce less errors when simulating off-design performance. Keep in mind that the actual mass flow can still increase due to an increase in pressure ratio and thus higher densities, even if the corrected mass flow is restricted.

5.1.4. Numerical instabilities in compressor and turbine maps

As explained in the previous paragraph, the operating point on a component map can be defined by one or more input parameters. However, due to the vertical lines (compressor map) or horizontal lines (turbine map) due to choking conditions, two input parameters may not be sufficient to define the operating point. For example in a compressor, if \dot{m}_c and N_c are inputs, there are multiple pressure ratios and efficiencies possible for the same \dot{m}_c and N_c . Therefore GSP introduces an additional helper input, the 'Beta' polar coordinate [35]. Thereby avoiding converging issues which would be caused by parameters becoming insensitive to changes of others.

5.1.5. Gas model & ambient conditions

The Gas Model of GSP was extended in 1998 with a detailed gas composition model with an algorithm to calculate the equilibrium in the combustion chamber using the equilibrium constants method [48]. The c_p , h and s of the gas are calculated using polynomials dependent on the specie and the temperature of the fluid. It is based on NASA's thermo-chemical gas model CEA as introduced by Gordon and McBride [49, 50]. The polynomial for c_p is denoted in equation 5.1, the polynomials for h and s are constructed likewise. Please note that to find the entropy also the pressure is taken into account and must be subtracted from the outcome of the polynomial as is earlier defined in equation 3.11.

$$\frac{C_p}{R} = \alpha_1 T^{-2} + \alpha_2 T^{-1} + \alpha_3 + \alpha_4 T + \alpha_5 T^2 + \alpha_6 T^3 + \alpha_7 T^4 \quad (5.1)$$

When ambient air humidity is modelled, the c_p of the gas will be a weighted average of both c_p of air and water vapour both calculated by the polynomial using the temperature of the gas mixture. GSP is able to simulate real gas effects and if this setting is applied γ and R are also taken into account when calculating the corrected parameters. Table 5.1 [7] displays both the dry and humid air composition. When humid air is modelled, the fractions of the dry air specie reduce in the same order as the humid air is added. The ratios of all the dry air specie stay constant with respect to each other.

Table 5.1: Modelled air composition for dry and humid conditions (3.0wt%) [7]

	N_2	O_2	H_2O	Ar	CO_2
Dry Air	78.084%	20.948%	-	0.937%	0.032%
Humid air	74.491%	19.984%	4.601%	0.893%	0.03%

Modifying the ambient conditions in GSP is straightforward. GSP allows to input various ambient conditions. Being able to model the ambient conditions as ISA, augmented ISA (ISA+) or a custom variant. Static properties for the ambient pressure and temperature can be selected as well as the flight speed and the amount of ambient humidity. The last can be defined as absolute, volumetric or relative humidity.

5.1.6. Corrected parameters in GSP

As mentioned in the previous paragraph, GSP is able to take into account real gas effects. When selected, GSP corrects the component maps for the changing γ and R . This option is selected by default. GSP therefore calculates the corrected parameters slightly different than is depicted in Table 3.3. The corrected parameters as calculated by GSP are depicted in equation 5.2 and 5.3 [35].

$$\dot{m}_c = \frac{\dot{m}\sqrt{\theta}}{\delta} \sqrt{\frac{\bar{R}}{R_{ref}}} \sqrt{\frac{\gamma}{\gamma_{ref}}} \quad (5.2)$$

$$N_c = \frac{N}{\sqrt{\theta}} \sqrt{\frac{\gamma_{ref}\bar{R}_{ref}}{\gamma\bar{R}}} \quad (5.3)$$

5.1.7. State vector and conservation equations

In GSP, the operating point is numerically represented by the state vector \bar{s} [35]. It is not uncommon that components share the same states, such as mass flow and rotational speed since they can be physically and mechanically connected. States in the state vector are normalised to the *reference point*, which is as discussed, the design point in GSP. This normalisation is done to avoid numerical instability in the Newton-Raphson iteration process [19] described in the following paragraph.

$$\bar{s} = \begin{bmatrix} s_1 \\ s_2 \\ \vdots \\ s_m \end{bmatrix} \quad (5.4)$$

In order to find a valid solution for a certain operating point GSP tries to solve the conservation equations between components. The conservation equations are a function of the states defining the system. The conservation equations GSP uses are the following [35]:

Conservation of mass:

The equations 5.5 below display the conservation of mass equations. Where M_v denotes the total mass in the control volume and V_{comp} the volume of the control volume.

$$\begin{aligned} \frac{\delta M_v}{\delta t} &= \dot{m}_{in} - \dot{m}_{out} \\ M_v &= \rho V_{comp} \\ \frac{\delta M_v}{\delta t} &= \left(\frac{1}{\bar{R}T} \frac{\delta P}{\delta t} - \frac{P}{\bar{R}T^2} \frac{\delta T}{\delta t} \right) V_{comp} \end{aligned} \quad (5.5)$$

Conservation of Energy:

For a drive shaft, with I being the moment spool inertial moment equation 5.7. For heat transfer between a heat sink (hs) and a gas (g) and thermal network components, equation 5.8 holds. Where U_{HT} is the heat transfer coefficient and u denotes the specific internal energy. The subscripts *del* and *abs* denote *delivered* and *absorbed*.

$$\frac{\delta M_v}{\delta t} u + M_v \frac{\delta u}{\delta t} - Q = \dot{m}_{in} h_{in} - \dot{m}_{out} h_{out} + PW_{abs} \quad (5.6)$$

$$I \frac{\delta \omega}{\delta t} = PW_{del} - PW_{abs} \quad (5.7) \quad Q_{hs} = U_{HT} A (T_{hs} - T_g) \quad (5.8)$$

Conservation of momentum:

Finally, the conservation of momentum is defined as below, with v as the axial velocity:

$$\sum \dot{m}_{in} V_{in} + A_{in} P_{s_{in}} + F_x = \dot{m}_{out} V_{out} + A_{out} P_{s_{out}} \quad (5.9)$$

5.1.8. Solution methodology

In order to retrieve a solution for the conservation equations, which in their turn are a function of the states, error equations are introduced. To create a fully determined system the same amount of error equations as there are states must be created. For an OD steady state simulation the solution is found when the error functions are lower than a predefined user value, which for GSP is initially set on 0.001 [51]. Thus for the standard GSP case the solution is converged as:

$$\bar{E}(\bar{S}) < 0.001 \quad (5.10)$$

The solution is found iteratively using the Newton-Rhapson method. For the design point the error equations are linearised by taking the partial derivatives of the states w.r.t. the error functions to set up a Jacobian matrix as in 5.12 [42].

$$\Delta \bar{E} = \mathbf{J} \Delta \bar{S} \quad (5.11) \quad \mathbf{J} = \begin{bmatrix} \frac{\partial E_1}{\partial S_1} & \dots & \frac{\partial E_m}{\partial S_1} \\ \vdots & \ddots & \vdots \\ \frac{\partial E_1}{\partial S_m} & \dots & \frac{\partial E_m}{\partial S_m} \end{bmatrix} \quad (5.12)$$

The small change in the state vector \bar{S} is described by equation 5.13 and inserting this in equation 5.11 yields the function to determine a new equilibrium operating point[42].

$$\bar{S}_{i+1} = \bar{S}_i + \Delta \bar{S}_i \quad (5.13) \quad \bar{S}_{i+1} = \bar{S}_i + \mathbf{J}^{-1} \cdot \Delta \bar{E}_i \quad (5.14)$$

Since this is a multi-variable application the step-size for the state vector is very important. Some states may indicate a large step size, but for others this could result in overshoot creating divergence problems. To account for this a scaling factor f is introduced and added to equation 5.11, resulting in equation 5.15. The scaling factor is predefined at 0.05 [51], controlling that the change per iteration step for a certain state is at maximum 5% of its current state.

$$\bar{S}_{i+1} = \bar{S}_i + f \mathbf{J}^{-1} \cdot \Delta \bar{E}_i \quad (5.15)$$

5.1.9. Previous studies performed in GSP

Several studies have been performed using GSP. These studies differ from implementing GPA applicability in GSP by means of Adaptive Modelling (AM) [52, 53] to modelling specific engine types in GSP such as the CF6-80 family and GENx [15, 16, 19], improving compressor maps using On-Wing data [14, 45] and results of applying GPA with GSP using on-wing data [18, 47].

All studies conclude on the applicability of GSP as a useful tool to simulate engine performance and perform GPA. Other interesting conclusions, limitations and recommendations found in these studies include:

- Without the use of accurate component maps off-design simulation and GPA is very limited [15, 16, 19].
- Bleeds must be taken into account correctly otherwise simulations or GPA cannot be trusted. [15, 47]

- Scatter due to sensor noise and different operating conditions when using On-Wing data increases inaccuracy when: simulating performance, applying GPA or tuning component maps. [16, 18, 47]
- Having fewer measurement sensors decreases GPA and simulation accuracy since additional assumptions must be made [16, 18].
- Research the effect of humidity by combining airport humidity data with TO performance snapshots [14].

5.2. Model Implementation

This section introduces the model used for simulation and discusses the modifications made to account for different control configurations. This chapter only covers aspects of the model which are deemed most important by the author. For a full understanding of the development of the model, please refer to [15] and [19].

5.2.1. CF6-80C2B1F model

The model used to simulate the effects of humidity on turbofan performance, is that of the CF6-80C2B1F turbofan engine as introduced by Den Haan [15] and further improved by Verbist [19]. At the time, KLM ES had chosen to purchase the extended sensor package for all CF6-80C2B1F engines. Other engine types are not equipped with the extended sensor package. For an overview of difference in available sensors of the CF6-80C2 and CF6-80E1 see Table 5.2. As described in the previous section having fewer measurements decreases simulation accuracy. The CF6-80C2B1F model is therefore the most accurate and trustworthy model available, since it is equipped with the most sensors. Also, due to the studies of both Den Haan and Verbist, of which the last author also tuned the compressor maps [45], the model has been improved throughout the years and is believed to provide a good approximation of the engine performance. For some general specifications about the CF6-80C2 see Appendix D.

The design point, or reference point, of the model is constructed using test-cell acceptance test data [15]. These tests are always performed on approximately the same fan speed and a lot of parameters are accurately measured in the test-cell providing for a good measurement set to act as a reference point. The test-cell recordings include (i.a.): all measurements as for the CF6C2 presented in Table 5.2 as well as the ambient relative humidity and turbofan thrust. The design point of the model is defined at a fan speed of 107,47%, corresponding to a physical fan speed of 3525 rpm. On-wing TO snapshots were used to tune the compressor maps [45], to give the most representative behaviour when performing off-design.

It is important to note the missing pressure and temperature measurements between the fan outlet and the booster/LPC. The lack of information causes the components to be modelled as one component. However, since the fan and booster/LPC are connected to the same shaft and consequently share the same rotational speed this will not introduce notable inaccuracy. The power setting is defined by the 'Rotor Speed Control' component.

Next to that, the inlet is modelled as adiabatic and frictionless. This is due to the fact that on-wing, the total temperature and pressure are measured in front of the fan. These total conditions are inserted as ambient static conditions in GSP with a Mach number of zero. With an adiabatic inlet this corresponds with identical total properties at the fan inlet.

For this research it is important that the model captures the performance deviations due to humidity correctly. Both in terms of trend as well as (normalized) correction magnitude. It is not of importance that the model exactly calculates the individual parameters in the gas path corresponding to a certain power setting and operating conditions. As long as the model captures the normalized ratios properly, that is, the deviation caused solely by humidity on the parameters in the gas path.

From the experience obtained from literature and test-cell corrections, linear corrections are expected per fan speed setting. However, test-cell corrections indicated differences in correction magnitude depending on the power setting. As explained earlier, in the GSP model, the compressor maps are of vital importance for accurately predicting off-design performance. Since the compressor maps are tuned using on-wing data to provide for a best-fit and are not of experimental/empirical nature as those of the OEM, inaccuracies in the maps possibly affect the results. Especially since the overall effect of humidity in an absolute sense will be small, the results will be prone to errors. In order to

investigate how the model reacts to different operating conditions, an N1-sensitivity analysis will be performed. This will provide for a comparison with the test-cell results. High ambient absolute humidity is inherently correlated to high ambient temperatures. Ambient temperature affects both the corrected speed as well as the corrected mass flow, thus changing the location of the operating point on the component maps. Therefore, also T1-sensitivity will be analysed by simulating the absolute humidity variation for different ambient temperatures.

Table 5.2: On-wing engine measurements, CF6-80C2 and -80E1 [54, 55]

Parameter	Identification	80C2	80E1
T_{t_2}	Fan inlet temperature	x	x
P_{t_2}	Fan inlet pressure	x	x
$P_{s_{14}}$	Fan duct static pressure	x	
$T_{t_{25}}$	Booster outlet temperature	x	x
$P_{t_{25}}$	Booster outlet pressure	x	
T_{t_3}	HPC discharge temperature	x	x
P_{s_3}	HPC static discharge pressure	x	x
$T_{t_{49}}$	HPT discharge temperature (EGT)	x	x
$P_{t_{49}}$	HPT discharge pressure	x	
T_{t_5}	LPT discharge temperature	x	
N1	Fan/Booster and LPT spool speed	x	x
N2	HPC and HPT spool speed	x	x
\dot{m}_f	Fuel flow	x	x

5.3. Model limitations

As explained in the previous section the model is created using both test-cell data as well as on-wing data. When using on-wing data for gas turbine simulation, new challenges arise compared to using test-cell data. However most of the challenges are already covered or deemed insignificant to this research, it is important to understand where other model inaccuracies originate from.

5.3.1. Bleeds, variable bypass valves & variable stator vanes

When the engine is tested at the test-cell, the customer bleed valves are closed, the Variable Stator Vanes (VSV) are in neutral position and the Variable Bypass Valves (VBV) are closed. However, at the moment the snapshot is captured on-wing it is possible that these settings do not apply. This alters the compressor maps since the (corrected) mass flow changes. The VSVs are in neutral position as in the test-cell at TO since they are used to reduce stall effects on lower operating settings and TO is naturally at a high power setting. The VBVs are also only opened for lower power settings such as when operating on ground, at TO and cruise conditions they are assumed to be closed [15].

The bleeds are of greater importance since they can be opened when commencing TO. Distinction can be made between internal bleed cooling flows which are used to cool the turbines and customer bleed used for cabin pressurisation and air conditioning. Where the internal bleeds expand in the turbines again there is almost no potential power lost in terms of thrust. The latter however does not return to the engine, resulting in an efficiency drop. Flow schedules are not available for both the 80C2 and 80E1, but their maximum values are listed in the Type Certificate Data Sheet (TCDS). Internal cooling bleed flows are not actively controlled and Verbist therefore modelled them as constant mass fractions [19]. Verbist researched the effect of customer bleeds on the accuracy of GPA and found that large customer bleed values are disastrous for GPA [19]. Therefore, the recommendation is made that customer bleed should always be taken into account when performing GPA. Otherwise, the results can not be trusted [19].

The internal bleed and cooling flows simulated in the model are depicted in E.1. Please note that by default the customer bleed is switched off. There are no measurements of flow schedules available for internal cooling flows. The values were generated by iteratively varying the cooling mass flow fractions until the performance data matched the test-cell results [19]. The question arises if customer bleed affects the effect of humidity on performance. Therefore a quick analysis is performed in section 5.1.

5.3.2. Sensor noise and bias

Marinai et al. state that accurate assessment of engine condition is complicated by having relatively few measurements, as well as errors in the measurements such as noise and biases [2]. Sensor bias is the difference between the average value of the sensor and the actual value. Sensor noise is the random variation around the average value of the sensor. It can be modelled with a probability density function. Since several measurements are used, all having their own bias and noise variation, the overall outcome can be affected notably.

Verbist researched the effect of sensor noise on GPA capabilities by simulating different levels of noise on a simulated deteriorated measurement set. The conclusion was that noise can have a notable effect on the GPA results, however due to the availability of multiple sets the results can be averaged. Verbist created 20 sets of simulated deteriorated measurements and even for noise levels of 4% GPA results of GSP approximated the deteriorated components accurately [47]. When researching on-wing data, Verbist found that for the CF6-80C2 the on-wing noise effects were smaller than 1% since the sensor noise analysis just mentioned shows a larger variation than the on-wing measurements [47].

Also mathematically, when data from the same engine (and thus same sensors and bias) is used to perform engine simulations the inaccuracy caused by sensor bias is undone when comparing results since this is a constant difference. Finally, Verbist [19] states sensor accuracies retrieved from the Engine manual. The sensor inaccuracies are relatively small, for example: thermocouples are reported to deviate $\pm 0.5^{\circ}\text{C}$ from the true value for a 2σ spread. This is expected to be generally significantly smaller than the effect humidity has on, for example, the EGT when being subjected to day-to-day ambient humidity variations.

5.3.3. Engine to engine differences

Every engine of the same type will be slightly different in terms of the gas path due to deterioration. These differences are called '*engine to engine*' differences. Even when engines are brand new, differences in EGTM are reported due to these engine to engine differences. If one wants to simulate the performance of an engine more accurately, engine to engine differences can be eliminated by taking the data set of only one engine and tune the standard model to represent that specific engine [19]. With this engine specific model the performance will be simulated and verified against a test set of a to be defined number of consecutive take-offs. Important of this test set is that it must be within a small time-frame in order to be able to neglect deterioration effects developing over time. Since modelling each engine separately takes a large amount of time, it is chosen to work with the standard model available.

Also, it is assumed that the differences in sensitivity w.r.t. to ambient humidity variations between the engine models will be small and that the gain in accuracy will not be proportional to the added workload. Since deteriorations alters the compressor maps, it will also ultimately affect the sensitivity of the turbofan to humidity variations. After consulting Verbist it becomes clear that the engine used to tune the maps represented an average engine in terms of performance. Therefore the assumption is made that the deterioration effects, inherently present in the tuned component maps, are of average magnitude. This will cause the model to simulate the 'average' sensitivity to humidity. In practice better or worse performing engines having slight differences with respect to the average.

5.3.4. Accuracy of compressor maps

The fact cannot be stressed enough that the components maps are fundamental when simulating turbofan performance. Since on-wing data was used to tune the compressor maps, and take-off is generally performed with maximal allowable derate, most of the tuning process is performed for lower fan speeds. Simply due to the fact that the engines are not operating often on the rated fan speed as tested on in the test-cell. This may cause discrepancies when simulating higher fan speeds. The N1-sensitivity analysis will shed a light on these possible discrepancies.

5.4. Modelling other Control Configurations

As stated earlier in Chapter 3 the effect of humidity on the performance of the turbofan is also dependent on the control configuration. Four other control configurations are researched in order to retrieve a broader view on the effects of humidity.

N_c-control

In order to identify the difference between an N1- and N1_c-controlled engine. The N1_c-control configuration corrects to standard day N1 using appropriate corrections for ambient temperature as well as γ and R . The N1_c-control simulated thus takes into account humidity effects. N1_c-control can easily be selected in the 'Rotor Speed Control' component.

TIT-control

One could argue that the N1-control configuration is both an indirect control of thrust as well as TIT. It is of importance that the Turbine Inlet Temperature does not exceed certain threshold temperatures, since due to overheating the engine deterioration pace will increase exponentially as explained earlier. In order to simulate TIT-control, the N1-control component is discarded. The TIT can be directly controlled as a parameter using the manual fuel flow control component.

IEPR-control

Rolls-Royce uses the Integrated Engine Pressure Ratio (IEPR) as a control parameter for at least the RB-211 [20] and possibly other engines as well. The IEPR can be expressed as the weighted average of the bypass and the core nozzle pressures by corresponding outlet area. Since it is Rolls-Royce that announced to incorporate humidity since it makes an engine appear to need maintenance earlier than is necessary by affecting the turbine gas temperatures [13], it is interesting to see which effects occur for IEPR-controlled engines and identify possible differences between N1 and IEPR effects.

In order to simulate engine control for constant IEPR the Equation schedule Control component is used, discarding the 'Rotor Speed Control' component. With the Equation schedule Control component the model keeps equation 5.16 constant for ambient humidity variation.

$$\text{IEPR} = \frac{P_{t_{18}} \times A_{bypass} + P_{t_8} \times A_{core}}{A_{bypass} + A_{core}} \quad (5.16)$$

FN-control

Finally, FN-control will be simulated. Although direct accurate FN control is currently not possible nor implemented in the aviation industry, it is interesting to see how humidity will effect the engine when constant thrust is required. This will give an indication on how engine manufactures should correct their control system in order to maintain equal thrust while controlling another parameter. In order to control the FN, the "thrust control" component replaces the 'Rotor Speed Control' component.

6

Simulation Results Analysis

In this chapter the simulation results will be discussed. First, the simulation results for the N1-controlled CF6-80C2 turbofan engine over a range of power settings and ambient temperatures will be presented. Those results will also be compared to those of the test-cell documentation. Second, the results for different operating control configurations will be discussed. Finally, a short analysis of the potential effects of humidity on GPA will be discussed.

6.1. CF6-80C2 Simulation Results

Since only a model of the CF6-80C2 was available as mentioned earlier, no simulation results are shown for the CF6-80E1. First, the simulation set-up is described after which a small study on the effect of customer bleed is presented. Consequently, the N1- and $T_{(t)1}$ -sensitivity results will be discussed.

6.1.1. Simulation set-up

The simulations are performed using the case control component. The case control component is used to vary ambient humidity from 0 to 100% relative humidity, with a step size of 10%. The simulations are performed at an ambient temperature of 305.35K. This is the Hot Day flat rated temperature as used in the Test-Cell corrections to convert to Hot Day conditions. At this temperature, 100% relative humidity corresponds with an absolute humidity of 3.1wt%. The pressure is set at ISA conditions of 1013.25kPa. Consecutively, these simulations are performed for fan speeds ranging from 90 to 110%. This corresponds to physical speeds ranging from $\approx 2950 - 3600RPM$. This range is chosen since it represents physical fan speeds during take-off and is also the range in which the model is validated. Deviating too much from this operating range will reduce the simulation accuracy. Since the effect of humidity in absolute sense will be small, the iteration accuracy is set from $\bar{E}(\bar{S}) = 10^{-3}$ to 10^{-5} for all simulations, in order to minimize the effect of numerical errors. The option to simulate real gas effects is selected.

6.1.2. Preliminary analysis: effect of customer bleed

As mentioned in the previous chapter properly taking into account customer bleed is of crucial importance when performing performance simulations or GPA. The question is if it also obscures the effect of ambient humidity on turbofan performance. In order to research the effect on the GSP model, the first simulation was performed without customer bleed and the second simulation was performed with customer bleed flow. Both simulations will run with dry ambient settings according to those described in the next section on a power setting of N1 = 100%. From the on-wing database a maximum reported customer bleed of ($\dot{m}_{cb} \approx 4kg/s$) is found and used in the simulation where customer bleed is present.

The results for several performance parameters are presented in Table 6.1 as a percentage deviation according to the equations 6.1, where X is the performance parameter in question. While the actual parameters differ in the order of several percent, it has only a slight influence on the sensitivity to humidity. All parameters display a slight increase of sensitivity. Since the deviations are in the order

of hundreds of a percent, the deviations will not significantly affect the results.

$$\delta_X = \left(\frac{X_{dry}}{X_{hum}} \times 100\% \right)_{bleed} - \left(\frac{X_{dry}}{X_{hum}} \times 100\% \right)_{nobleed} \quad (6.1)$$

$$\Delta_X = \frac{X_{bleed}}{X_{nobleed}} \times 100\%$$

Table 6.1: Customer bleed result comparison

	N2	EGT	\dot{m}_f	FN
δ_X	0.023%	0.046%	0.064%	0.000%
Δ_X	0.7%	2.17%	3.09%	-0.38%

6.1.3. Effect of humidity: N1-sensitivity

The results of the simulations are presented in 6.1. It concerns the parameters also corrected in the test-cell corrections. In order to assure comparability with the test-cell corrections, all parameters are corrected to SD values. The correction slopes are derived by means of performing a linear regression on the relation between humidity and the normalized performance parameter (X_n). This is also visualized in equation 6.2, where X is the parameter in question. Note that $X_{humid}(\Psi_{abs} = 0) = X_{dry}$. The corrections found in Figure 6.1 can therefore be read as correction factors to multiply with the humid air performance *to correct to dry air performance*. The TSFC for the GSP simulations is calculated using the actual thrust, whereas for the test-cell corrections the minimum thrust as certified by the OEM is used. The two are therefore not directly comparable.

$$X_n = \frac{X_{dry}}{X_{humid}(\Psi_{abs})} \quad (6.2)$$

All the corrections are in the same direction as they were for the test-cell corrections found in the previous chapter. That is, when operating in dry air instead of humid air; FN increases, EGT increases, N2 decreases, \dot{m}_f increases, EPR increases and TSFC decreases. Thus, in terms of fuel efficiency an engine performs worse in humid air. Just as in the test-cell corrections, variation of correction slope is visible over the operating range of the engine. However, the variation is less pronounced than for the test-cell corrections. The slightly parabolic curve as is found for the test-cell corrections is not visible in the GSP simulations. Also, for all parameters, except for FN, an unnatural sudden step increase occurs around $N1 = 3450RPM$. Where, for reasons explained earlier, the test-cell corrections are not smooth, the step increase found in the GSP simulations is of greater magnitude. The step increase is found when moving to the design operating point of the model, this DP power setting is indicated with a vertical red line. As explained, the design point is created using a test-cell report at an operating speed of 107,46%. Then on-wing data is used to tune the compressor maps when performing off-design. It is customary to perform a de-rated take-off when possible, thereby decreasing fuel consumption and engine deterioration. Therefore, in practice, most take-offs are performed de-rated and full rated take-offs are very rare. This causes the data used for map tuning to be generally consisting of lower fan speeds. Consequently, this causes the maps to be mainly tuned for lower regions of fan speed and not for higher fan speeds such as the design point. The DP of the model therefore only represents one engine at one moment (the specific engine in the test-cell), while the off-design map tuning is performed using 93 consecutive [19] snapshots of one engine.

The engine used to create the DP is not the same engine as used for the map tuning process. As explained in 5.1.3, due to deterioration effects, every component maps is unique. Using two different engines for the DP modelling process and the map tuning process will therefore inevitably result in model inaccuracies, especially since the tuning process was focussed on the lower operating range, leaving the maps at the DP unaltered. Due to this method of model creation it is assumed that the model is more accurate in the region where the maps are tuned. For FN, also a step increase is found, however of lower magnitude. This step increase is located at around $N1 = 3300RPM$. The major part of the thrust ($\approx 80\%$) is generated in the bypass duct of the engine. Since this step increase is only apparent for the thrust (and therefore inversely for the TSFC) it is assumed that the step increase is due to irregularities in the fan duct map. It should be noted that due to the step increase the results with the

test-cell corrections are more comparable until the design point rating is reached and both corrections diverge.

Table 6.2 displays the average correction slopes of the parameters both for the GSP as well as for the test-cell results. It is found that, on average, the test-cell corrections and GSP simulations agree very well. Please note that the absolute discrepancy between the test-cell and GSP results increases for larger values of ambient humidity. For an engine operating with an EGT of 1100K, the correction would imply an increase of 3.85K per weight percent ambient humidity. For very humid conditions (e.g. 3wt%), this will result in a discrepancy of 11.5K. Since the EGT_M is often in the order of several tens of degrees Kelvin, especially for older more deteriorated engines, the simulations indicate that humidity can have a significant effect on the EGT_M.

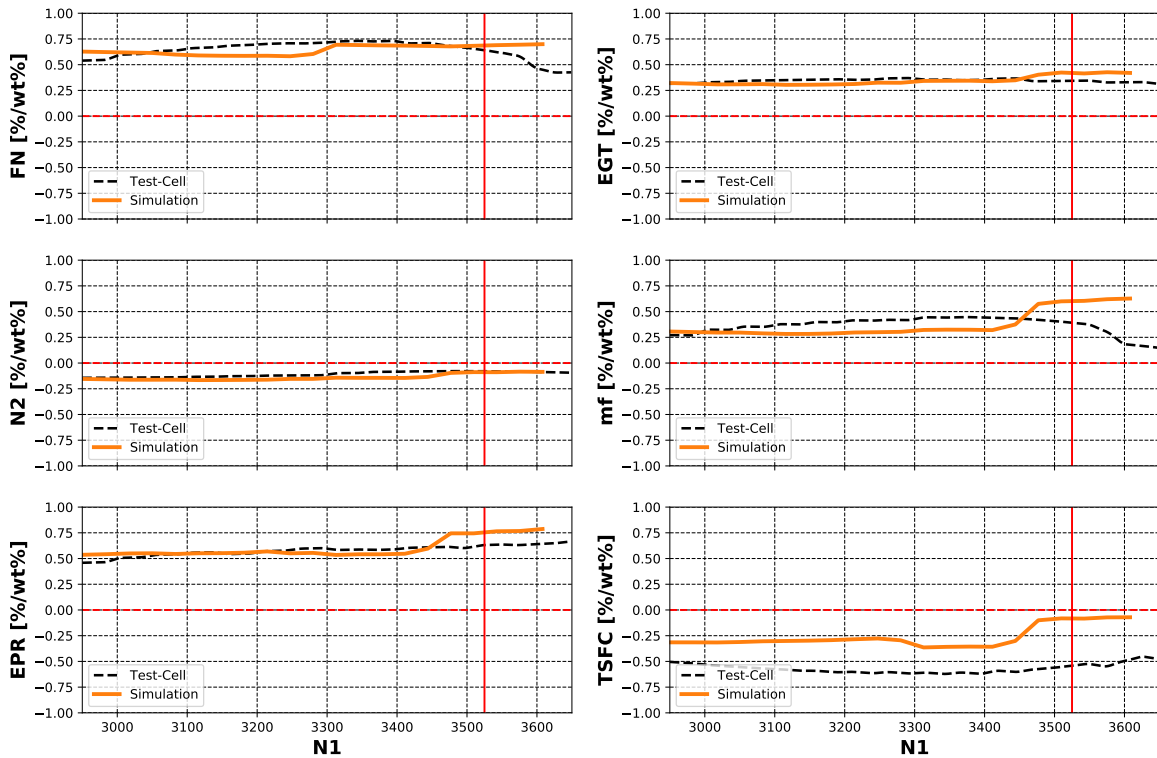


Figure 6.1: Test-cell and simulated correction slopes versus observed N1

Table 6.2: Average correction slopes of test-cell corrections and GSP results, expressed as %/wt%

	FN	EGT	N2	\dot{m}_f	EPR
Test-cell	0.65	0.35	-0.11	0.37	0.58
GSP	0.64	0.35	-0.13	0.38	0.60

6.1.4. Effect of humidity: T1-sensitivity

In GSP, when simulating the effect of larger amounts of ambient humidity, one is inherently bound to the consequence that high(er) ambient temperatures will need to be simulated as well. Since the operating point on the component maps are defined by corrected parameter groups, altering the outside air temperature will naturally also change the location of the operating point. However small the effect of humidity is, it may cause the operating point to move to less validated areas and indicating a trend which may not be a good representation of the true effect of humidity. The question thus arises if the behaviour of the model for higher temperatures may be assumed representable and how the behaviour changes with varying T_{t1} . Therefore a study is performed investigating the effect of changing outside air temperature. Since in the previous section the conclusion is drawn that the simulated effect of humidity varies with power setting, the simulations are performed for three power settings: N1 = 93%

(2952RPM), $N1 = 100\%$ (3280RPM), $N1 = 107.47\%$ (DP = 3525RPM).

Figure 6.2 displays the simulation results for varying ambient temperature. Also, the averages for each parameter per power setting are displayed in Table 6.3. The flat rated temperature as mentioned earlier is indicated with a red vertical line. When solely looking at the effect of T_{t1} , for $N1 = 93\%$ and $N1 = 100\%$ there are no significant effects visible. The only noticeable change is found for FN and therefore TSFC. The fuel flow sensitivity for the two lower simulated power settings does not vary significantly and is close to equality. Where for $N1 = 100\%$ the thrust sensitivity to humidity is generally higher, especially for lower temperature, when increasing the temperature to the flat rated temperature the correction starts to overlap with the sensitivity slope of $N1 = 93\%$. Referring to Figure 6.1 it must be noted that for FN the sensitivity at the DP rating has closer similarity with the test-cell correction than the other mentioned power settings.

This cannot be noted for the trends of EGT, there the two power settings (especially the lowest) show greater compatibility. Where according to the test-cell corrections the sensitivity of EGT to ambient humidity slightly increases with increasing power setting, this is also the case for the simulations. However, the simulations seem to overestimate the sensitivity for higher power settings, where the test-cell corrections seem to decrease sensitivity. The nature of why the test-cell corrections show a decreasing trend in the test-cell corrections has already been explained.

For the two lower power settings the trends for $N2$, \dot{m}_f and EPR show great similarity. This similarity is not found for $N1 = 107.47\%$. While the $N2$ sensitivity magnitude and trend are comparable, a step increase is found for the other parameters when increasing T_{t1} from 288K to 293K. Physically, the sensitivity of the parameters to ambient humidity is expected to change gradually when modifying the operating conditions. This step increase is therefore probably caused by not smoothed irregularities on the compressor maps. It seems that in order to maintain equal fan speed, the model suddenly demands more power for slight variations of the corrected parameters. This causes the fuel flow sensitivity to be higher as well as the EPR, TSFC, FN and EGT. The EGT however, shows the smallest step increase, since the results of $N1 = 93\%$ and $N1 = 100\%$ are very similar. The results strengthen the assumption that the compressor maps are generally more accurate for lower $N1$ -speeds due to the aforementioned tuning process performed by Verbist [45].

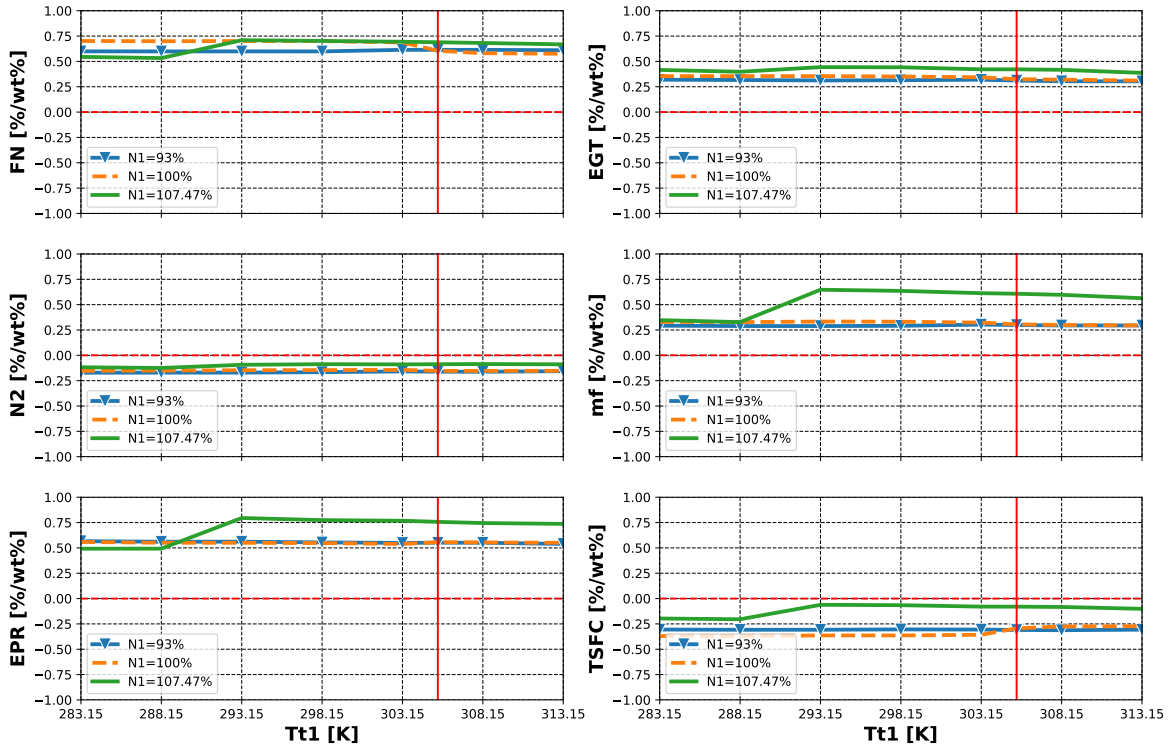
It is a time consuming effort to simulate the effects for both T_{t1} and $N1$ because a series of simulations will need to be performed for each T_{t1} - and $N1$ -setting. To display the simulated sensitivity of the parameters to humidity for both power setting and ambient temperature in one figure, a surface plot would be perfect. This is possible with the API unit as developed by the TU Delft. At the time this research was conducted this extension was not available to the author. Therefore it was chosen only to simulate the effects for three $N1$ -settings when varying T_{t1} .

Table 6.3: Average correction slopes of simulated corrections for varying T_{t1} , expressed as %/wt%

$N1$	FN	EGT	$N2$	\dot{m}_f	EPR	TSFC
93%	0.61	0.31	-0.16	0.29	0.55	-0.31
100%	0.66	0.34	-0.15	0.32	0.55	-0.33
107.47%	0.65	0.42	-0.10	0.54	0.70	-0.11

6.2. Simulation Results for other Engine Control Configurations

As explained in the previous section the effect of humidity differs over the operating range. Since it is assumed that the model accuracy is higher for lower fan speeds than the design point, a power setting of $N1 = 100\%$ (e.g. $N1 = 3280RPM$) is chosen. It is also not of interest how the model simulates the other control configurations over the operating range, since only the direction and a fair estimation of correction magnitude are of interest. Due to the comparability of the results in the previous section with the test-cell corrections, it is assumed that the model is able to provide for those interests when simulating other control configurations. For all simulations, the humidity is varied from 0-100% relative humidity. As explained, when increasing humidity the operating point on the component maps will slightly change, resulting in different N_c , TIT and IEPR per ambient humidity value. In order to keep the operating points for the different control configuration simulations as close as possible, the power settings for IEPR, TIT and N_c are chosen as averages of those parameters in the $N1$ -control

Figure 6.2: Simulated correction slopes versus T_{t1}

simulation. The same ambient conditions are applied as for the N1-sensitivity simulation mentioned in the previous section. The results of all simulations are listed in Table 6.4. The results are depicted as percent deviation with respect to their dry value. The table lists general performance parameters as well as turbine temperatures, turbine output power, temperature ratios, compression ratios, turbine efficiency changes due to movement of the operating point over the component maps, and finally deviations in calculated isentropic component efficiency assuming dry air conditions. The last will be further discussed in section 6.3. The change in efficiency due to movement of the operating point over the component maps is only displayed to assist with explaining the simulation results.

6.2.1. N1-control

However some effects for N1-control have already been discussed, this paragraph presents a broader view of the internal effects in the engine. The general effects already discussed in the previous section are naturally also found in Table 6.4, e.g. when operating in humid air a lower FN, lower \dot{m}_f , lower EPR, higher N2, lower EGT and higher TSFC are found when compared to dry air. Due to the lower density of humid air, for the same fan speed, less mass flow flows through the engine and consequently thrust decreases. Fuel flow also decreases since the fan spins more easily through the less dense air. However, the thrust decreases more significantly resulting in poorer TSFC.

Where the fan speed is controlled by the engine control configuration, this is not the case for the core speed and an increase in core speed is found. The corrected fan speed, as according to equation 5.3, decreases. This is the direct result of the increasing specific gas constant \bar{R} . This effect is inversely found for N1 for an N1_c-control configuration as will be discussed in the next paragraph.

Looking at the turbine temperatures, lower temperatures are found. The greatest effect is found for the TIT, as also visible from the table, this can be explained by the reducing temperature ratios in both the compressors. Together with the lower temperature rise in the combustion chamber as discussed in section 3.4.2, this leads to a significantly lower TIT.

The lower temperature and pressure ratios can be explained by the decreased turbine power output of both the HPT and LPT. Remembering that c_p is higher for humid air, together with a decrease in available compressor power as provided by the turbines, this will inevitably result in a lower temperature and pressure ratio over both compressors. The difference in temperature and pressure ratio decrease

between the turbines may be attributed to the fact that the HPT operating points seems to move to a more efficient region whereas the movement of the operating point of the LPT hardly changes the efficiency.

Regarding the pressure ratios in the compressors, lower compression ratios are found, especially for the LPC spool. The HPC hardly seems affected. The difference in compressor ratio decrease may be attributed to the fact that the LPC is the controlled spool. Thereby being affected by the sole effect of humidity decreasing pressure ratio according to flow similarity alone as well as the fan speed being kept constant. The N2 spool is able to increase in speed and the conditions in the LPC may therefore give a better representation of flow similarity. Please note that for flow similarity alone the effect on compressor pressure ratio is generally very small as displayed in Table 3.4.

Bare in mind that the aforementioned table regards corrections to correct from humid to dry air properties, and that the percentage deviations as listed in Table 6.4 are deviations for humid air w.r.t. dry air and thus can be seen as the inverse.

6.2.2. N1c-control

As found from the corrections in literature, $N1_c$ decreases for humid air, resulting in a increase of N1 for a $N1_c$ -controlled engine. Where the N1-controlled engine is subjected to a significant thrust decrease when humidity increases, the thrust for a $N1_c$ -controlled engine is almost unaffected. This can also be concluded for the EPR. Arguing that N1-control is used as a measure of thrust, $N1_c$ -control including humidity measurements may be a good alternative especially since the control configuration only has to be adjusted slightly.

As for the N1-controlled engine, TSFC will still increase due to an increase in fuel flow. Due to the larger increase in fuel flow also the core speed increases more compared to N1-control. Also due to the fuel flow increase in the combustor, increased power generation is found for both turbines. The reduction in both temperature ratio and pressure ratio is therefore less significant. For the HPC a slight increase in pressure ratio is found.

Whereas for the N1-control simulation the LPT isentropic efficiency hardly changed, for the $N1_c$ -control the change is relatively of larger magnitude. This affects the temperature ratio but mostly the pressure ratio since the pressure ratio is a lot more sensitive for turbine efficiency changes. Comparing the pressure and temperature ratio deviations with respect to N1-control this is very well visible since the pressure ratio changed more significantly compared to the temperature ratio for a relatively small efficiency change. Please, bare in mind that the efficiency change is caused by the movement of the operating point on the component map. Summarizing, the $N1_c$ -control responds better in terms of thrust when ambient humidity varies. However, at the cost of increased fuel flow and decreased fuel efficiency.

6.2.3. TIT-control

The poorer fuel efficiency, as expected from section 6.2.1, is extremely well visible for the TIT-control simulations. With the compressors delivering lower outlet pressures and temperatures for the same physical fan speed as explained earlier, maintaining the same TIT request a notable amount of additional power from the turbines and consequently a noticeable rise in fuel flow. A fuel flow increase of approximately 5% is found. This is especially interesting for industrial gas turbines. Whereas for turbofan engines thrust is the main performance parameter, and if deemed necessary for operation, the TIT margin or EGTM is temporarily exceeded, industrial gas turbines are often controlled for constant TIT never exceeding the temperature margins. Also notice that to maintain the same TIT the mass flow needs to exceed the dry air mass flow. Indicating once again that humidity decreases the overall efficiency of the system. TIT control is also the only configuration where the turbine temperatures are found to be increasing. Naturally, this can be attributed to the decrease in temperature drop in the turbines in humid air.

Assuming the TIT is controlled via measuring the EGT, the following can be noticed. Whereas for the $N1_{(c)}$ -controlled configuration humidity causes the EGTM to drop, for a TIT-control configuration it actually has the opposite effect. E.g. for identical measured EGT in dry as well as humid air, the operator may increase the power setting for humid air to maintain equal TIT, whereas for $N1_{(c)}$ -control the operator must be cautious since for drier air the turbine temperatures may start to exceed the red line temperature. Just as the change in pressure and temperature ratio in the LPT for the $N1_c$ -control configuration, the operation point of the LPT in the TIT-control simulation moves to a region with higher

efficiency. The change in efficiency is larger than for the previously mentioned control configuration, even resulting in an increase of pressure and temperature ratio instead of decrease. The direction of the moving operating point is a direct result of the engine control configuration and ambient condition variations.

6.2.4. IEPR-control

Accordingly to the right of existence of IEPR-control, the IEPR-controlled engine displays to be the best measure of thrust. FN hardly varies with the changing ambient humidity conditions. The effects on the IEPR-controlled engine are very comparable to the $N1_c$ -controlled engine.

It is interesting to note that the EGT for an IEPR-controlled engine is also higher in dry air, as is for a $N1_{(c)}$ -controlled engine. With a lower EGT due to humidity and no correctional actions performed, the EGTM will (falsely) be higher. The announcement that Rolls Royce starts incorporating airport humidity data for engine diagnostic purposes to improve on-wing time lead initially to the assumption that the EGTM was corrected for humidity. This assumption originated from the fact that the EGTM is one of the most important performance parameters. However, with the simulation pointing out that the humidity corrected EGTM will always be lower than uncorrected EGTM, this is believed not to be the driver for the improvement of on-wing time. Potential benefits that can be identified consulting the performed simulations are stated below.

- A better approximation of the EGTM will result in a more accurate planning for maintenance and water washes, which will result in lower costs and safer operation and, on the long-term, possibly improve on-wing time.
- An increase in fuel flow is measured when controlling IEPR. Thus, the fuel efficiency has decreased. This reduced fuel efficiency can be falsely interpreted as deterioration, predicting the engine needs maintenance earlier than necessary.
- As further discussed in 6.3, decreasing temperature drops will be measured in the turbines when ambient humidity increases. With the dry air γ assumption this results in lower isentropic efficiency according to equation 3.15. This can then be falsely interpreted as deterioration, resulting in premature maintenance actions.

6.2.5. FN-control

As expected the results are very comparable to the IEPR-results since IEPR is an accurate indicator of thrust. Since for IEPR-control the simulation results still show a slight thrust decrease, for FN-control an increase in fuel flow is found compared to IEPR-control. It becomes apparent that for an N1-controlled engine, to maintain equal thrust, a fan speed correction of $\frac{0.83\%N1}{3.1wt\%} \approx 0.27\%N1/wt\%$ should be applied. Comparing the fuel flow for both control configurations, this will result in a fuel flow increase of roughly 2%. One can therefore argue that not taking into account humidity for a N1-controlled engine results in a too low throttle setting, increasing take-off field length. It is expected that the OEM has implemented safety margins to account for such effects, however it can be concluded that high ambient humidity reduces these safety margins. Since the test-cell corrections indicate a slightly larger correction for thrust at the power setting used in the simulation as depicted in Figure 6.1, the actual correction may even be greater than the implemented correction.

6.3. Humidity Effects on GPA Capabilities

Compressor and turbine efficiency can be assessed using the measured temperature and pressure ratios and calculating the isentropic efficiency according to equations 3.14 and 3.15. Since humidity changes the specific heat ratio γ , not taking into account humidity will result in an error w.r.t. the calculated efficiency assuming humid air. In order to investigate the magnitude of the error, the deviation caused by humidity in the isentropic efficiency calculation is calculated with the dry air assumption for both the humidity affected pressure and temperature ratio. The isentropic efficiency is then normalized compared to the dry air and unaffected pressure and temperature ratio. This is visualized with equation 6.3.

As stated earlier, humidity causes the operating point to move on the component map possibly altering isentropic efficiency. The isentropic efficiency change is also reported in Table 6.4. This movement

must be accounted and corrected for in order to visualize the sole difference of wrongfully assuming dry air. This is done by subtracting the normalized efficiency deviation expressed as $\mu_{\delta_{maps}}$ from μ_{δ_n} as expressed by equation 6.4. The isentropic efficiency difference between dry and humid air assumption will be denoted by $\Delta\mu$ and is calculated as in equation 6.4.

$$\mu_{\delta_n} = \frac{\mu(\gamma_{dry}, PR_{humid}, TR_{humid})}{\mu(\gamma_{dry}, PR_{dry}, TR_{dry})} \quad (6.3) \quad \Delta\mu = \mu_{\delta_n} - \mu_{\delta_{maps}} \quad (6.4)$$

For all the control configurations mentioned in the previous section $\Delta\mu$ is calculated and listed at the bottom of table 6.4. In terms of GPA the results are not promising. Fairly large deviations are found for the LPC isentropic efficiency assessment, with even larger differences for the HPC. On average, when performing gas path analysis on compressors operating in humid air, the efficiency will be overestimated by 1%. This is an error of significant magnitude in GPA context and may obscure the effect of deterioration. Especially for the HPC this is unfavourable since it is a component generally subjected to significant deterioration due to the high temperatures and ingestion of salts, sands etc. The results found are comparable with those of Garwood et al. [7] indicating that for increasing pressure ratio the effect becomes greater, explaining the increased efficiency overestimation for the HPC.

Where assuming dry air for the compressor leads to an overestimation of efficiency, for the turbine it is the exact opposite. Both the HPT as the LPT indicate isentropic efficiency reductions of approximately 1%. This may lead to the false conclusion that the turbines are deteriorating. This is also comparable to the results of Garwood et al. indicating lower isentropic efficiencies when assuming dry air, which increase towards 0 for increasing pressure ratios. Where the pressure ratios of the LPC and HPC are 1.5 and 13 respectively, the LPT and HPT are both more similar and close to 5, therefore the turbine show less discrepancy in isentropic efficiency error when comparing to the compressors.

Where in the test-cell humidity is measured and everything is corrected for accordingly, it can be concluded that using on-wing data for GPA analysis without humidity measurements will be subjected to significant uncertainty. Not correcting for humidity when calculating the isentropic efficiency may therefore either obscure the effects of deterioration of compressors or falsely indicate deterioration of turbines.

Table 6.4: Effect of humidity ($\Psi_{abs} \approx 3.1wt\%$) for several control configurations

	N1	N1 _c	TIT	IEPR	FN
General Parameters					
N1	0.00%	0.76%	2.23%	0.81%	0.83%
N1 _c	-0.76%	0.00%	1.46%	0.05%	0.06%
\dot{m}	-1.77%	-0.95%	0.71%	-0.90%	-0.88%
FN	-1.86%	-0.14%	3.36%	-0.04%	0.00%
\dot{m}_f	-0.94%	1.05%	4.99%	1.17%	1.22%
TSFC	0.93%	1.19%	1.58%	1.21%	1.22%
EPR	-1.69%	-0.05%	3.11%	0.05%	0.09%
N2	0.47%	0.75%	1.30%	0.75%	0.78%
Turbine Temperatures					
T_{t4} (TIT)	-1.33%	-0.89%	0.00%	-0.86%	-0.85%
T_{t49} (EGT)	-1.00%	-0.53%	0.41%	-0.50%	-0.49%
T_{t5}	-0.53%	-0.23%	0.38%	-0.21%	-0.21%
Turbine Power					
PW_{HPT}	-1.50%	0.39%	4.09%	0.51%	0.55%
PW_{LPT}	-1.84%	0.60%	5.38%	0.75%	0.80%
Pressure Ratios					
$PR_{fan+LPC}$	-1.81%	-0.28%	2.51%	-0.18%	-0.14%
$PR_{d_{fan+LPC}}$	-0.69%	-0.05%	1.25%	-0.01%	0.00%
PR_{HPC}	-0.01%	0.01%	0.45%	0.10%	0.10%
PR_{HPT}	-0.13%	-0.13%	-0.12%	-0.13%	-0.13%
PR_{LPT}	-0.93%	-0.03%	1.67%	0.02%	0.04%
Temperature Ratios					
TR_{LPC}	-0.74%	-0.26%	0.60%	-0.23%	-0.22%
$TR_{d_{LPC}}$	-0.29%	-0.12%	0.20%	-0.11%	-0.11%
TR_{HPC}	-0.57%	-0.58%	-0.57%	-0.58%	-0.58%
TR_{HPT}	-0.33%	-0.36%	-0.41%	-0.36%	-0.36%
TR_{LPT}	-0.48%	-0.30%	0.03%	-0.29%	-0.28%
Isentropic efficiency					
$\eta_{fan+LPC_c}$	0.05%	0.01%	-0.07%	0.01%	0.01%
$\eta_{fan+LPC_d}$	-0.17%	0.03%	0.62%	0.04%	0.04%
η_{HPC}	-0.01%	0.01%	0.04%	0.01%	0.01%
η_{HPT}	0.18%	0.21%	0.25%	0.21%	0.21%
η_{LPT}	0.01%	0.05%	0.12%	0.05%	0.05%
Δ Isentropic efficiency					
$\Delta\eta_{fan+LPC_c}$	0.83%	0.84%	0.85%	0.84%	0.84%
$\Delta\eta_{fan+LPC_d}$	0.79%	0.79%	0.80%	0.79%	0.79%
$\Delta\eta_{HPC}$	1.07%	1.15%	1.29%	1.15%	1.15%
$\Delta\eta_{HPT}$	-0.78%	-0.86%	-1.00%	-0.86%	-0.86%
$\Delta\eta_{LPT}$	-0.73%	-0.81%	-0.97%	-0.81%	-0.82%

7

Statistical Analysis

In this chapter the statistical analysis will be covered. First global, local and atmospheric ambient humidity variation will be researched. Second, the take-off snapshot data used for the analysis will be discussed. Finally, the process of merging on-wing snapshot data with corresponding humidity data will be discussed and the merged data will be analysed.

7.1. Statistical Analysis on Humidity Variation

This section is dedicated to describing the weather data used for this research and analysing the data.

7.1.1. METAR Data

The humidity data has been retrieved from Meteorological Aerodrome Reports (METAR). The METAR are broadcast half hourly or hourly, and contain information regarding the current weather and is broadcast by airport weather observation stations. Over the course of several years, KLM has created a database containing METAR data of all commercial airports worldwide. METAR is an abbreviation of Meteorological Aerodrome Report.

METAR EHAM 260725Z 21008KT 9999 FEW010 11/09 Q1011 NOSIG=

The METAR gives information in the consecutive order: indication of the type of report, airport ICAO, date and time, wind details, visibility, cloudiness, temperature and dew-point, sea level atmospheric pressure, change in weather indicator. The underlined parts of the code are of interest for this research, which will be discussed shortly in consecutive order again. First, it must be sure the data is a METAR. Second, the airport of interest must be known. Third, the date and time of the measurements are needed to be able to relate to a specific take-off snapshot. Fourth, obviously the temperature and dew-point (both rounded to whole degrees) are of interest. Last, the pressure (in millibars rounded to four digits) is needed to calculate the absolute humidity using relations described in paragraph 3.1. Please note that this pressure is defined as the ambient pressure at sea level. In order to calculate the pressure at the airport, the altitude of the airport (a) with respect to sea level is required. Naturally, for flight operations, airport altitude data is very important and therefore was easily retrieved. The actual airport pressure is calculated using equation 7.1 with the ISA standard lapse rate K .

$$P = P_{sl} \left[\frac{T_{isa,sl} - L \times a_{airport}}{T_{isa,sl}} \right]^{\frac{-g}{R_{air}L}} \quad (7.1)$$

With the ambient temperature, pressure and dew-point temperature known, the absolute humidity can be calculated. Equation 3.7 is used to calculate the partial vapour pressure. Using equation 3.9 the partial dry air pressure is calculated and consequently, using the ideal gas law, the partial densities of the vapour and air are calculated. Relation 3.2 is then used to calculate the absolute humidity.

7.1.2. Global humidity variation

In order to investigate the global humidity variation, airports were selected where the CFM56-7B, CF6-80C2, CF6-80E1 and GEnx-1B engines of AFKLM operate. The reason for including engines next to the GE CF6 series is to be able to research a large dataset of airports. The METAR data of these airports was retrieved and the corresponding humidity data was calculated. In order to get a grip on the distribution of airports in the data set, Figures 7.1 and 7.2 give an indication of the average and maximum ambient humidity per airport. From Figure 7.1 it is visible that in general airports located near the equator and close to the coast have climates with high average ambient humidity. This is not surprising since temperatures are generally high and thus increase the capability of air to carry larger amounts of water. Also, these airports are less exposed to seasonal climate changes, which results in high average humidities. However, not the airports closest to the equator are subjected to the maximal encountered humidity values.

From Figure 7.2 it becomes clear that the highest values are encountered near the Gulf of Oman and the Persian Gulf. This area is subjected to great heat during the summer (thus the air is able to 'hold' large amounts of water) and is also more subjected to seasonal changes. Also, on days when the wind direction is from inland towards the sea, very dry air is carried from the desert. The average absolute humidity of those airports is therefore lower.

Figure 7.3a displays a boxplot of the complete humidity data set. The whiskers reach to $Q3 + 1.5 \cdot IQR$ and minus $Q1 - 1.5 \cdot IQR$. The mean of the data set is located around $0.9 \text{ wt}\%$, with the lower quartile border on $\approx 0.5 \text{ wt}\%$ and the upper quartile on $\approx 1.5 \text{ wt}\%$. As is visible in Figures 7.1 and 7.2, a significant amount of the airports in the dataset are located in Europe. Therefore they are located in similar climate conditions and thus similar (moderate) ambient humidity conditions. This is also very well visible in Figure 7.3b due to the two peaks. The average of the data set is depicted with a black line and is located on $\approx 1 \text{ wt}\%$. The CFM engines are used on the Boeing 737 and used for short-haul flights across Europe, therefore this dataset contains a lot of airports located in Europe. The humidity distribution when excluding the Boeing 737 related airports is depicted in Figure 7.3c and 7.3d. It becomes apparent that the long haul flights of AFKLM regularly operate in humid environments. The short haul flights are subjected to lower humidity variation.

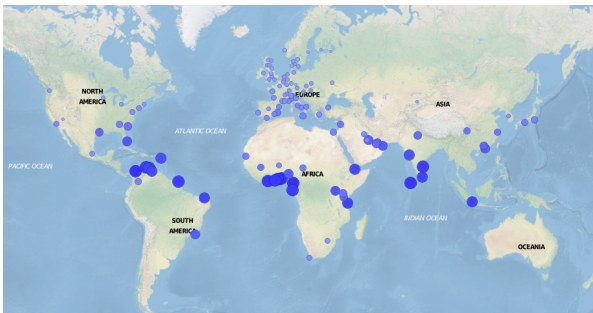


Figure 7.1: Average Humidity in the year 2018 per Airport, largest values $\Psi \approx 2.0 \text{ wt}\%$, smallest values $\Psi \approx 0.38 \text{ wt}\%$

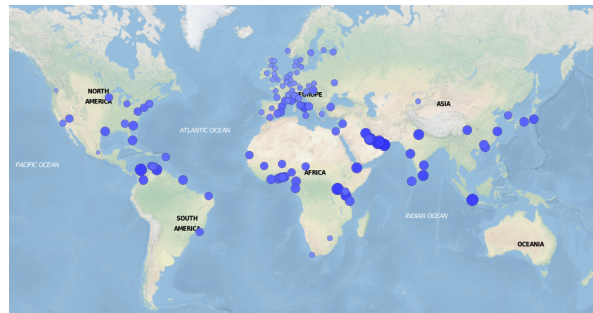


Figure 7.2: Maximal Humidity in the year 2018 per Airport, largest values $\Psi \approx 3.1 \text{ wt}\%$, smallest values $\Psi \approx 0.75 \text{ wt}\%$

7.1.3. Local humidity variation

In order to get a better understanding of the seasonal variation on a local scale, box plots have been generated for certain airports for each month of the year 2018. The assumption is made that the year to year variation is not significant and researching other years would yield similar results. The box plots have identical whisker size to those defined in the previous paragraph. For air to be very humid two conditions must be met. First, the air must be relatively hot. Second, there must be large amounts of water available that can evaporate into the air. Amsterdam Airport is subjected to a moderate sea climate which is very well visible in the humidity distribution in the course of a year. It is characterised by dry winters and summers with moderate temperatures (e.g. 295K). New Delhi also shows this seasonal distribution but has a monsoon influenced land climate. It is subjected to extremely hot temperatures in the summer (e.g. 310K), which is accompanied by a rainy season in the months July-September. This makes up for extremely humid circumstances and causes a big step increase in absolute humidity

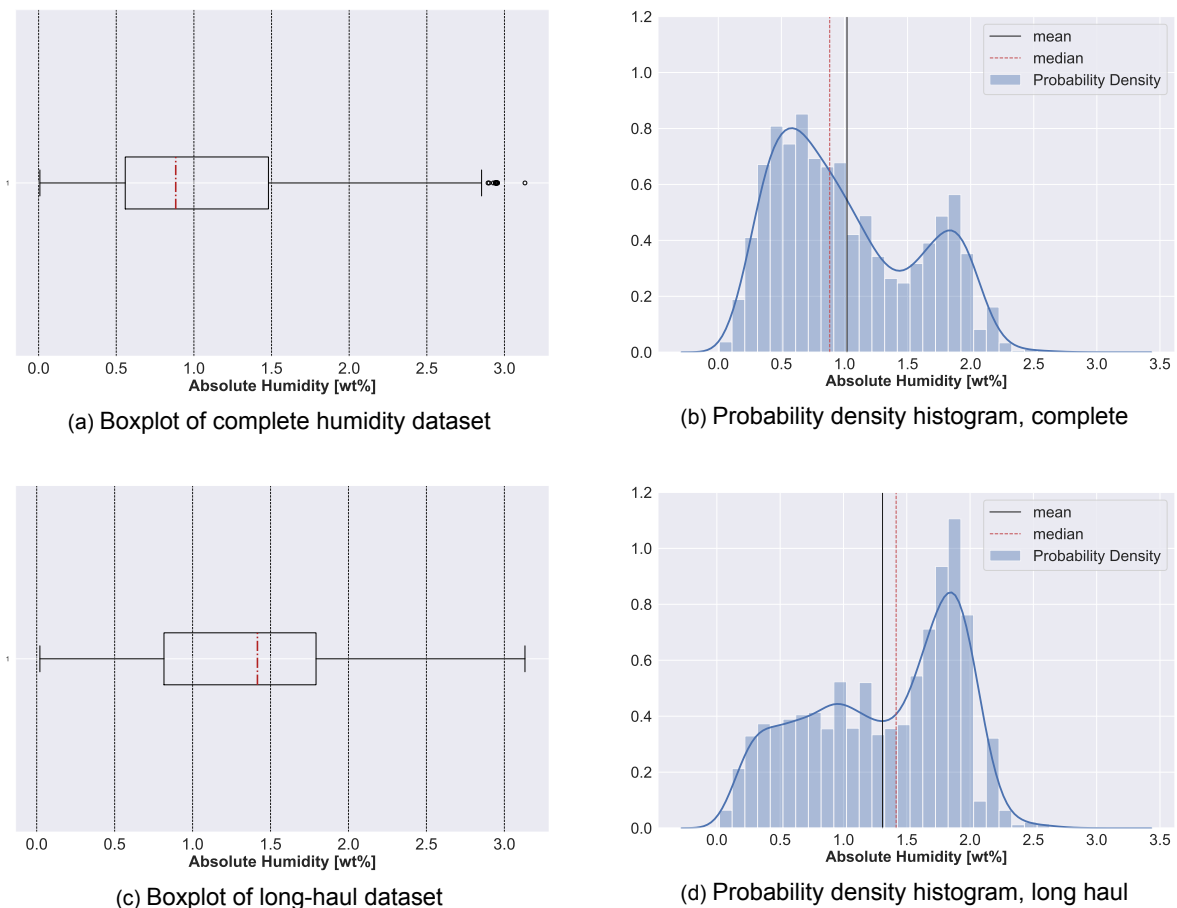


Figure 7.3: Boxplot and Probability Density Histogram for complete and long-haul only dataset

for those months. In the other months ambient humidity is moderate. New York has a comparable climate to Amsterdam. New York however, is known to be hotter in the summer, making up for higher absolute humidity values since it is also closer to the coast. Finally, Jakarta Airport is subjected to a more tropical climate. It is not very seasonally dependent due to its close proximity to the equator and is generally subjected to hot temperatures throughout the year. The tropical monsoon lasts from October until May, with a drier period from June to September. This is also visible in the box plots. However, there is always enough water to evaporate in the direct environment of Jakarta and together with the high temperatures make up for a high average of absolute humidity.

The fact must be stressed that data points defined as outliers in the boxplots are not necessarily points that can be discarded. Since each month contains about 730 data points, there are occasions when the ambient humidity is either very low or very high for a few hours. These points can be examined and if found that the temperature and humidity follow a logical physical trend for the conclusion can be drawn that the data are valid. Also, data points have been found where the temperature increases with $10K$ in one hour and decreases with the same amount the hour after, or vice versa. Of course, those data points can then be discarded as they would be likely be caused by measurement error.

7.1.4. Atmospheric humidity variation

The on-wing snapshots are captured between approximately 40 to 50 after commencing full take-off power. Within this time frame, it is possible that the aircraft have gained altitude. Figures 7.5 and 7.6 show the distribution of the reported flight altitudes of both the CF6-80C2 and -80E1. The histograms are constructed using all reported take-off data over the course of January 2013 to December 2018 and therefore contain a huge amount of data. Since the snapshot reported altitude is actually a measure of pressure altitude assuming ISA conditions, the snapshot reported altitude is calculated to the pressure at aircraft altitude. From the METAR data the temperature at sea level is calculated and with the

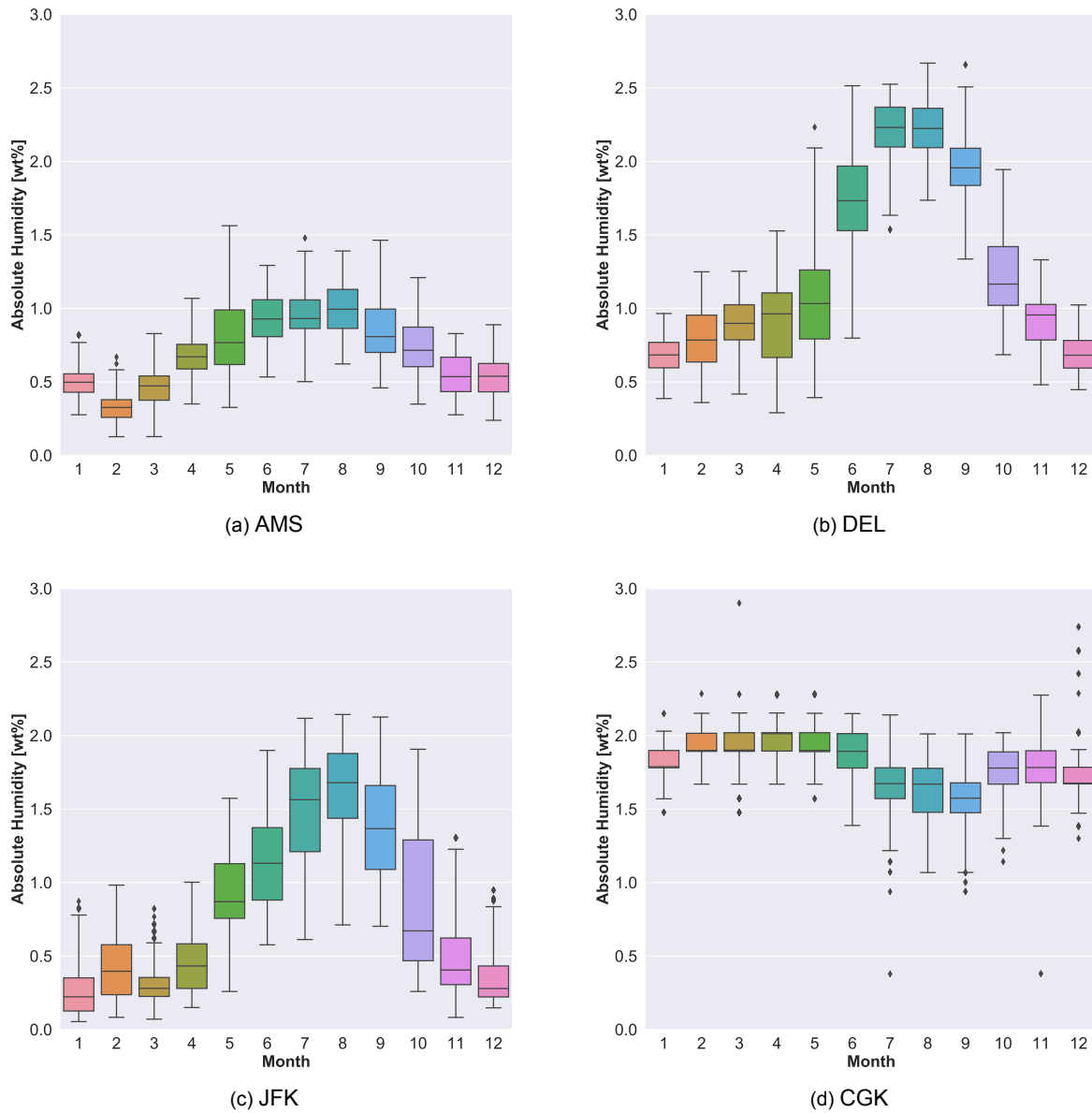


Figure 7.4: Observation of variation of humidity for different airports

pressure adjusted to mean sea level as already reported by the METAR data, the altitude w.r.t. sea level (assuming ISA lapse rate) is calculated. The airport altitude is then subtracted from the aircraft altitude to find the altitude of the aircraft w.r.t. the airport.

Figures 7.5 and 7.6 display the calculated altitudes of the aircraft with respect to the airport. It becomes clear that the snapshots are mostly captured when the aircraft is still on, or near, the ground. There are also snapshots captured when the aircraft has gained some altitude, the altitude increase however is generally marginal. In Figure 7.5, the aircraft reporting higher altitudes are found at airports which are located on high geographical altitude, namely Johannes Burg Tambo JNB (1.680m), Bogota El Dorado BOG (2.548m), Mexico City Benito Juárez MEX (2.238m) and Nairobi Jomo Kenyatta NBO (1.624m). These are also the airports with the highest geographical location in the dataset. Possible discrepancies between the actual atmospheric conditions and ISA conditions are magnified for these altitudes, resulting in possible mismatches. Due to the same problem, there are also some altitudes found to be negative. The additional assumption will therefore be made that aircraft with negative altitude w.r.t. the airport are located on airport altitude and thus can directly use the reported ambient humidity. The fifth highest located airport in the dataset of the CF6-80C2 is Chicago O'Hare (KORD), and is with an altitude of 204m significantly lower than the top four. The data points of that airport, and

airports with lower geographical location, are found in the lower region of the histogram.

The general altitude difference between airport and aircraft being clear, the question arises if the humidity at snapshot altitude is similar to the humidity at the airport. Literature is therefore reflected on the distribution of humidity with altitude. For the CF6-80E1, airport altitudes as reported in the CF6-80C2 dataset are not found. It generally operates on geographically lower located airports.

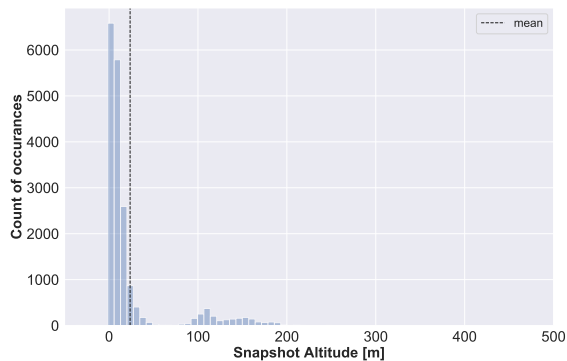


Figure 7.5: Altitude w.r.t. airport of CF6-80C2 on-wing Snapshots

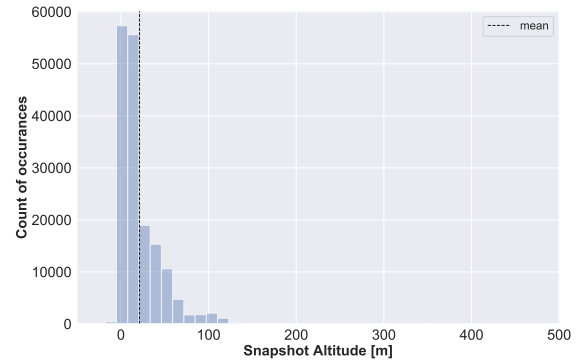


Figure 7.6: Altitude w.r.t. airport of CF6-80E1 on-wing Snapshots

From literature, the general conclusion can be made that humidity variation with altitude is highly variable, but generally decreases in an exponential manner [56–59]. The variation of humidity with altitude is found to be dependent on a lot of factors. There are some approximations, often of empirical basis, for the variation of humidity with altitude. When approximations are made they are often only reasonably valid for certain global areas, such as high/mid/low latitude with seasonal changes such as winter/summer [57] or dry/wet season [60]. Yamamoto [56], as retrieved from [61], proposed an equation to calculate a constant k_w which can be interpreted as the water vapour lapse rate, using the sea level ambient temperature and temperature lapse rate. The equation is reported to result in inaccuracies of 12% up to 6km [56]. Since the paper is written in Japanese and no translation is available, uncertainty exist about the area of validation and how the inaccuracy is distributed. The International Telecommunication Union - Radiocommunication (ITU-R) [57] proposed several reference atmospheres, dependent on latitudinal location and season. Those reference atmospheres are displayed in Figure B.4b. The fact that the variation of humidity with respect to altitude is highly variable, is also well portrayed by measurements from a radiosondes as researched by Culf [59]. The relations are often applicable for ranges up to 11km above sea level.

Since all approximations agree that absolute humidity tends to decrease with increasing altitude, not taking this into account will generally lead to an overestimation of the absolute humidity at aircraft altitude. A general correction for altitude is therefore applied to the absolute humidity measurements to present the absolute humidity level. As Figures 7.5 and 7.6 indicate, at maximum only the first few hundred meters are of interest with the lion's share of the data points in the first 100 meters. The relations for partial vapour pressure proposed are approximations. In turn, those relations can easily be approximated as linear for the range of interest of this research. Due to the exponential nature of the approximations, the steepest decrease is found for humid environments. Since the absolute humidity variation is found to be extremely variable, defining several humidity distributions according to season and longitudinal position will be a significant amount of work. Since most snapshots are captured within the first hundred meters, the humidity variation will be close to negligible. It is only important that the snapshots captured at higher altitudes, do not overestimate the ambient humidity. The accuracy gain when modelling several different absolute humidity variations globally and seasonally does not outweigh the amount of modelling work. Especially when put to perspective with the average reported altitude of the snapshots being close to the airport altitude. The decision has been made to define one global constant lapse rate for absolute humidity with altitude.

The lapse rate of humidity versus altitude is calculated by taking the average of the slopes of several proposed environments of [57]. The found lapse rate is depicted in equation 7.2. In order to be on the safe side when approximating the amount of humidity at a certain altitude, the (weaker) high and mid latitude for winter approximations are discarded. Those environments are also of less interest since they are subjected to low ambient humidity and will therefore not cause large performance discrepan-

cies. The average is thus taken from the four lines on the right side of Figure B.4b. As noted earlier, the fact must be stressed that the humidity correction for most data points will be negligible due to the generally small altitude difference and that the correction is only of value in order to prevent overestimation of ambient absolute humidity for higher altitudes.

$$c_{\Psi} = -0.28 \left[\frac{\text{wt}\%}{\text{km}} \right] \quad (7.2)$$

7.2. Monte Carlo Analysis

With the local monthly humidity variation analysed in section 7.1.3, it is possible to perform a Monte Carlo analysis to investigate the performance deviation due to these humidity variations. Using GSP, a Monte Carlo analysis is performed for two separate cases. For both cases the performance deviation is researched for two consecutive take-offs (e.g. no deterioration), for identical operating conditions. Thus, exactly the same take-off, with the engine having the same physical condition, is being simulated where only the ambient humidity varies according to a normal distribution. The first case is Amsterdam - Jakarta, and the second case is Amsterdam - New Delhi. See Figures 7.7a and 7.9a for their respective absolute humidity histograms. Please note that the line plot in Figures 7.8 and 7.10 is a kernel density estimation, not the normal distribution in question. The kernel density estimation is only displayed in order to visualize normality and assists with explaining the solution approach. Since the difference between two consecutive take-offs is researched, the normal difference distribution of the two airports in question is calculated. For subtraction of two independent normal distributions equations 7.3 and 7.4 can be applied to calculate the normal difference distribution.

$$\mu = \mu_2 - \mu_1 \quad (7.3) \quad \sigma = \sqrt{\sigma_1^2 + \sigma_2^2} \quad (7.4)$$

For both cases, the mean absolute humidity difference, as well as the combined standard deviation are reported in Tables 7.1 and 7.2 respectively. With these μ and σ values, the GSP Monte Carlo analysis is performed. For both cases a series of 3000 normally distributed humidity data points are created and a simulation is performed for each data point with a power setting of $N1 = 100\%$. In order to avoid condensation to be simulated, T_{t1} is set as the flat rated temperature mentioned earlier. The performance deviations are found by subtracting the results from a 'reference' performance simulation from the results with simulated humidity. The reference simulation is performed under the exact same operating conditions, except that the air is modelled as dry. This is also depicted by equation 7.5 with X as any simulated parameter. With the difference in μ and combined σ , subtracting the reference simulation from the Monte Carlo results will yield the same distribution as when subtracting the two individually normal distributions.

$$X_{\Delta} = X_{MonteCarlo} - X_{dryair} \quad (7.5)$$

Airport	μ	σ
AMS	0.32	0.09
CKG	1.94	0.09
<i>Combined</i>	1.61	0.13

Table 7.1: Mean and standard deviations
Case 1

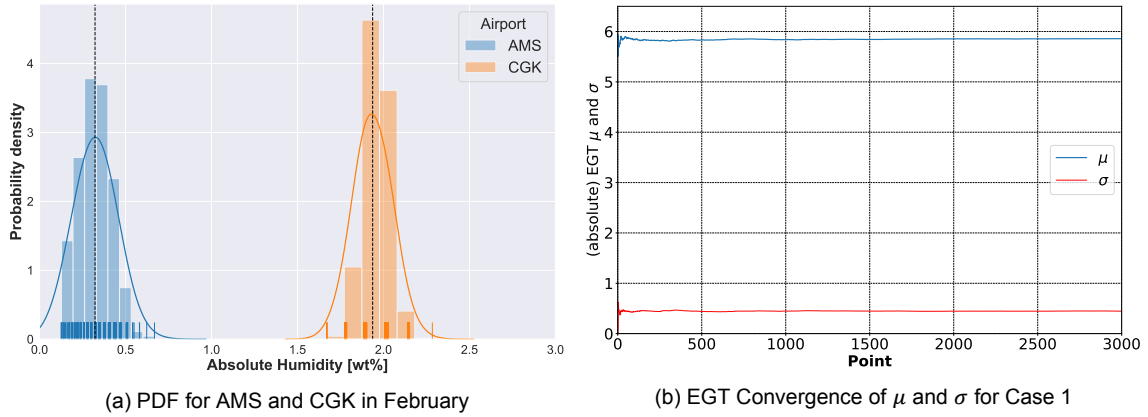
Airport	μ	σ
AMS	0.99	0.17
CKG	2.22	0.16
<i>Combined</i>	1.23	0.24

Table 7.2: Mean and standard deviations
Case 2

Case 1: Amsterdam - Jakarta

In February, Amsterdam is subjected to a generally cold and dry atmosphere. Resulting in low absolute humidity values with low variance. Jakarta on the other hand is subjected to a rainy season in February, with generally high average temperature resulting in a high average absolute humidity, also with little variance. This is also visible in both Figures 7.4 and 7.7a. The results of the Monte Carlo simulation are depicted in Figure 7.8. The vertical red dashed lines represent the mean. The solution is found to be converged as all the parameters converged to their mean values. By illustration, figure 7.7b displays the convergence history of the EGT. All the displayed performance parameters are reported in percentage deviation except for the EGT. The EGT is reported as the variation of the absolute difference in Kelvin, since for the EGT the absolute difference will be of interest. The mean EGT

discrepancy is $-5.8K$, with $\sigma = 0.45K$. The distribution varies in total from approximately $4.5K$ to $7K$. The result implies that aircraft performing an identical take-off in February in Amsterdam and Jakarta will on average have a discrepancy in EGT of $\approx 6K$. When the OEM does not account for humidity variation when correcting their on-wing measured EGT to EGT_M the discrepancy in EGT_M will be somewhat of the same magnitude. In an operational point of view, the EGT_M discrepancy is significant. Referring back to Figure 6.1 the simulation corresponds well with the test-cell results for the implemented power setting, only slightly underestimating the influence of humidity. When arguing that the test-cell corrections are more accurate since they are probably of experimental nature, the discrepancy between reported EGT(M) may even be more significant than presented in Figure 7.8. The same conclusion can be drawn for the thrust. According to the Monte Carlo simulation, an average decrease in thrust of $\approx 1\%$ is found.



(a) PDF for AMS and CGK in February (b) EGT Convergence of μ and σ for Case 1
 Figure 7.7: Absolute humidity histogram and Monte Carlo convergence for Case 1

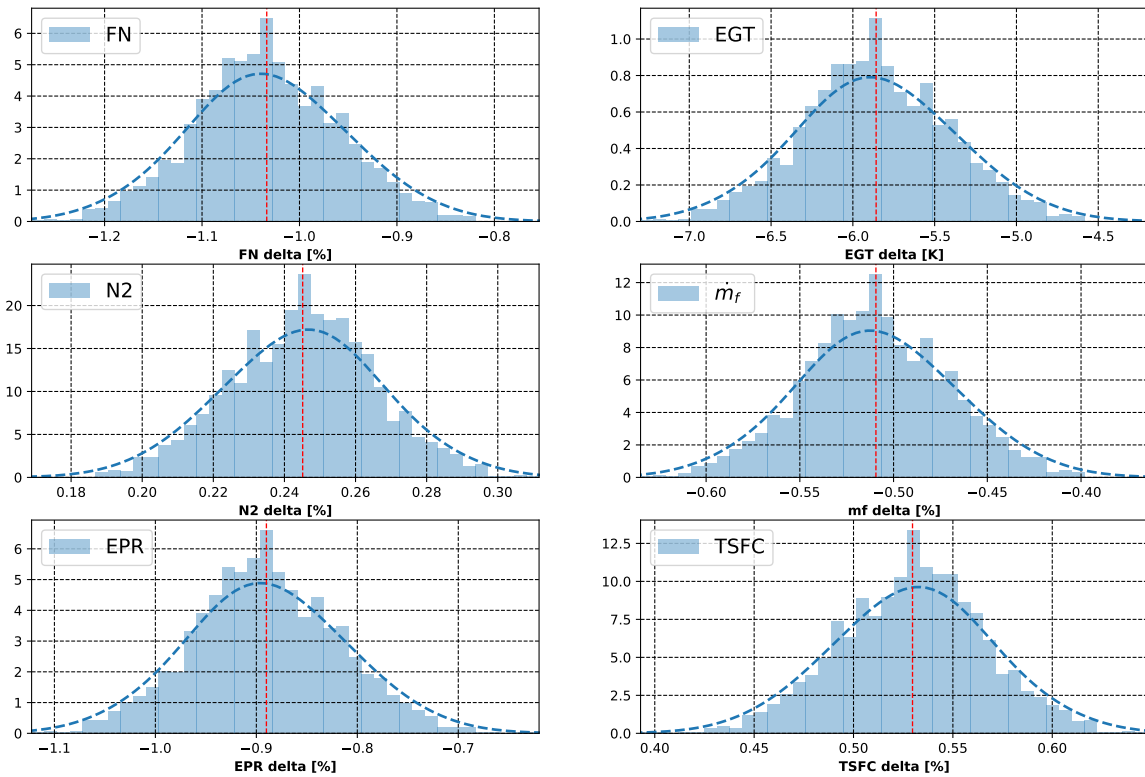


Figure 7.8: Monte Carlo analysis results, AMS-CGK

Case 2: Amsterdam - New Delhi

The second case, Amsterdam - New Delhi, represents an engine encountering two areas with a significant difference in ambient humidity as well as large standard deviations. This should account for higher variance of the parameters than reported for the previous case. In summer, Amsterdam is subjected to moderately high temperatures resulting in moderate ambient humidity values. New Delhi is subjected to extremely high temperatures and high ambient average absolute humidity. Again, this is also visible in both Figures 7.4 and 7.7a. The mean difference in ambient humidity is lower due to the higher average humidity in Amsterdam in the summer. However, the variance for both is more significant w.r.t. Case 1. Figure 7.10 displays the results of the Monte Carlo Analysis. Again, the solution has easily converged as visible from Figure 7.9b. The mean discrepancy is with $-4.6K$ less than for Case 1. The standard deviation is, as expected, more significant with $\sigma = 0.85K$. This makes up for a relatively large range ($\approx 5K$) of EGT(M). Assuming a properly corrected EGT(M) for all other conditions, the found standard deviation can be interpreted as a measure of scatter for on-wing reported EGT(M) for consecutive flights from Amsterdam to New-Delhi and vice-versa.

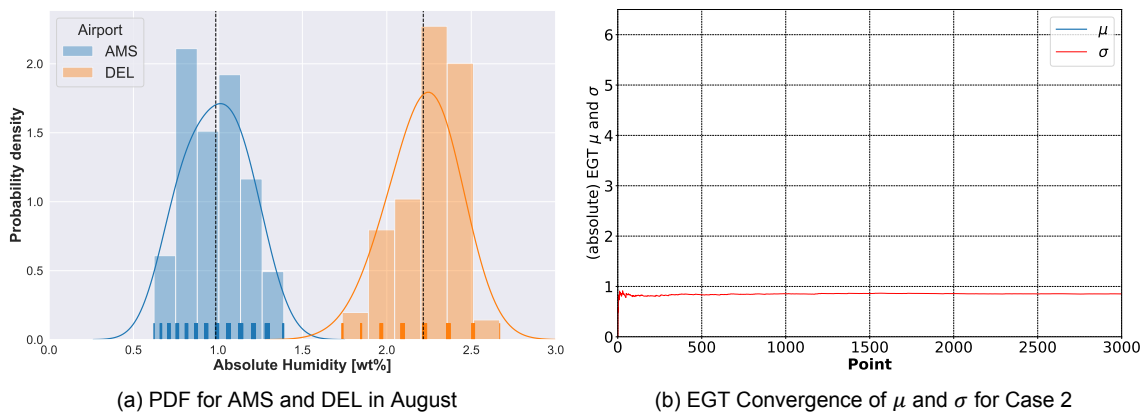


Figure 7.9: Absolute humidity histogram and Monte Carlo convergence for Case 2

7.3. Take-Off Snapshot Data

This section is dedicated to reviewing the on-wing snapshot data which are used for analysis. The on-wing snapshots are captured between approximately 40 to 50 seconds after commencing full take-off speed. The parameters captured in this snapshot differ per engine type and are presented in Table 5.2. The variables are actually averaged over a period of 10 seconds. The OEM states that during this period the engine is performing quasi steady-state. Next to those variables, also the EGT(M) is reported. The method of calculation of the on-wing reported EGT(M) is confidential and unknown to the author. However, after consulting the OEM it becomes clear that dry air conditions are assumed when calculating the on-wing reported EGT(M). After consulting CF6 type engineers, on-wing data engineers and the OEM, the following observations can be summarised about the conditions for which the take-off snapshots are captured.

- VBVs often completely closed during take-off
- VSVs often in neutral position during take-off
- Quasi steady-state assumption, parameters averaged for 10 seconds, starting 40s after commencing full TO power
- Customer bleed may be on or off
- Dry air assumption when calculating EGT(M)

The first two observations are also met in the test-cell. This increases the comparability with the test-cell results. The third observation is a source of inaccuracy. The parameters will not all have reached their steady state value. Parameters such as $N1$ and $T1$ can be assumed to be constant within this time deviation, however other internal parameters such as EGT will still slightly vary. However, since

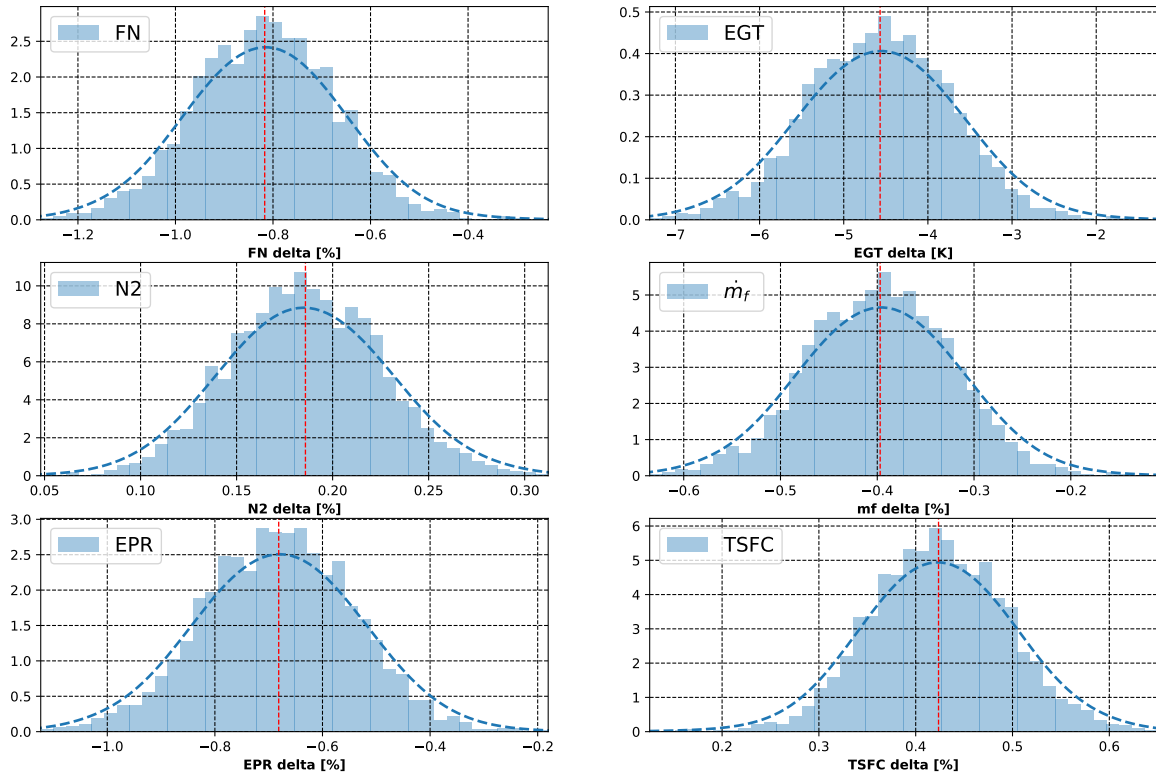


Figure 7.10: Monte Carlo analysis results, AMS-DEL

all parameters are averaged, the relative error is also averaged and since all snapshots are subjected to the same averaging procedure this still ensures comparability between snapshots. The customer bleed may be switched on or off, and when it is on the bleed mass flow may also vary. The preliminary analysis in GSP about customer bleed in section 6.1.2 shows it may affect the sensitivity to humidity of certain parameters. The effects however are very slight and were deemed not to cause large discrepancies. The last observation indicates that the reported EGTM will always be higher when flying in humid areas. Repeated for clarity, the increase in EGTM is caused by decreasing EGT for increasing ambient humidity. When not appropriately correcting for humidity and assuming the in humid conditions measured EGT to be representative of the dry EGT, the margin improves. Consequently, appropriately correcting for humidity will result in a higher EGT and a reduction of EGTM.

7.3.1. Scatter in the reported EGTM

The reported EGTM is subjected to a significant amount of scatter. Figure 7.11 displays the on-wing reported EGTM versus time for both the CF6-80C2 (left) and CF6-80E1 (right). Both engines are chosen since they represent average engines in terms of EGTM with respect to the dataset. It is clearly visible that the CF6-80E1 engine is closer to exceeding the EGTM, due to the higher power rating compared to the CF6-80C2. Deterioration degrades the EGTM and water washes and overhaul improve the EGTM over the lifetime of the engine. When assessing the scatter or standard deviation standardly present on the EGTM, one can minimize the effect of the aforementioned phenomena by calculating the rolling average and subtracting the reported EGTM from the rolling average. The size of the window of the rolling average is set to 21 data points. This should be an adequate window to minimize deterioration effects within the window, but large enough to present a representative average of the point. In Figure 7.11 the rolling average is depicted as the orange line.

$$EGTM_{div} = EGTM_{reported} - EGTM_{rolling} \quad (7.6)$$

On average, for the CF6-80C2, a standard deviation is found of $\sigma_{EGTM_{DIV}} = 6.4K$. For very humid environments (e.g. $\Psi_{abs} = 3.0wt\%$) the effect of humidity on EGT can be approached as $0.35\%/wt\% * 3wt\% \approx 1\%$ of the original EGT reading. For a representative EGT = 1200K, the deviation caused

by humidity is thus 12K, bare in mind that this is an extreme case. Since all reported EGTM are affected by humidity the absolute difference in absolute humidity will therefore be generally lower as will the difference in EGTM. Referring back to the Monte Carlo simulations and Figures 7.8 and 7.10, it can immediately be concluded that the scatter present in the data is of higher variance (or standard deviation) than possibly caused by the effect of humidity. The average absolute humidity encountered during take-off is approximately 1wt%. Arguing from the average absolute humidity, deviation of the EGTM due to ambient absolute humidity variation will, in an absolute sense, be either 1wt% drier or 2wt% more humid. This can roughly be translated to a -3.8 to $+7.6$ degrees Kelvin with respect to the moving average. Referring to the bandwidth visible in Figure 7.11, the conclusion is drawn that the reported EGTM is not appropriately corrected for other phenomena next to humidity since the bandwidth is larger than possibly caused by humidity.

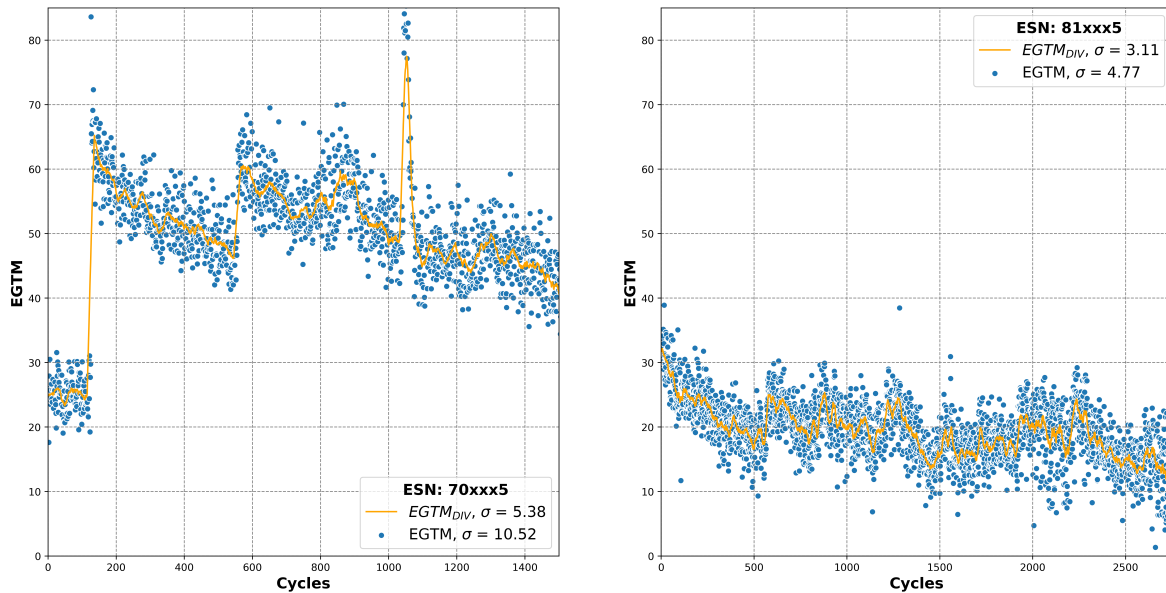


Figure 7.11: Example of reported EGTM versus time, left CF6-80C2, right CF6-80E1

7.4. Merged Snapshot and Humidity Data

With both the humidity data and on-wing snapshot data available, the two data bases were merged. Initially, the departure station was coupled to the corresponding airport humidity file. Next, the timestamp of the on-wing snapshot was matched within a tolerance of 60 minutes with the timestamp of the specific METAR. The humidity data of the corresponding METAR was then added to the on-wing snapshot data. Before the merging process was initialized, the on-wing data was cleaned for corrupted data points. This generally consisted of removing points which missed fundamental data such as the EGTM, removing points reporting Mach numbers below 0 or above 1, removing points which reported not physical ambient pressures or reported altitudes above 3km. Unfortunately, it was found that many of the CF6-80C2 on-wing data missed departure station information. Making those data points useless in terms of humidity research. Consequently, they were discarded from the dataset. Also, not all departure stations reported in the on-wing data could be merged with METAR data. This was due to the fact that for some departure stations no METAR data was available. Finally, all humidity data was corrected for the aircraft altitude with respect to the airport by means of the correction described in section 7.1.4. Table 7.3 lists the counts of removed data points for both the CF6-80C2 and CF6-80E1. It is clear that in terms of data availability, the CF6-80C2 has poor results. Less than 10% of the initial dataset is left after cleaning and merging. The newer CF6-80E1 engine is less restricted by empty readings or corrupted data and has a larger dataset.

Besides the performed corrections mentioned above, an additional EGTM correction was performed. While this research was conducted, Roëll [62] performed research to identify the sources of discrepancy between reported on-wing EGTM and test-cell EGTM. Roëll concluded that for some

specific time frames, the EGTM was wrongfully corrected for customer bleed flow (CF6-80C2) and nacelle- and wing-anti-ice (CF6-80E1). Please refer to the thesis of Roëll [62] for further information on the correction procedure. This correction procedure was also applied on the data used in this research.

Table 7.3: Overview of used on-wing snapshot data

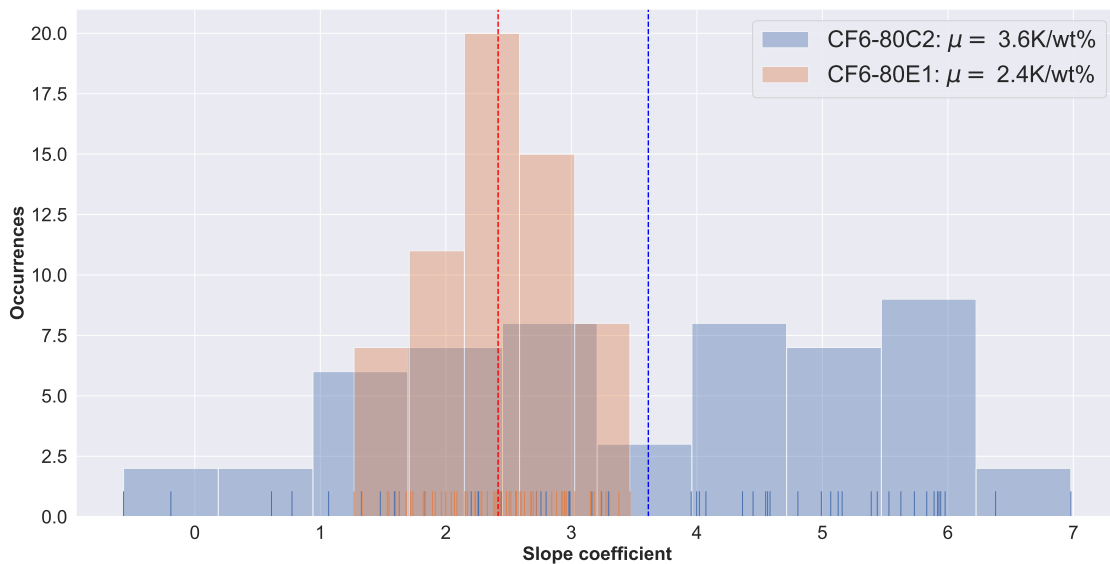
	CF6-80C2	CF6-80E1
Period	2013-2019	2013-2019
Snapshots	141.365	241.880
Corrupted data points	1759	58
Empty Dep. Stat.	113.022	126
Count of useable point	18.790	170.550
Count of ESN	54	61

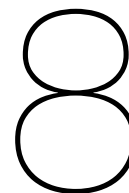
7.4.1. Correlation between the reported EGTM and Absolute Humidity

In order to investigate the correlation between the reported EGTM and absolute humidity, the linear regression slope coefficients were determined for each ESN for the relation between $EGTM_{DIV}$ and absolute humidity. The CF6-80C2 data contains 54 engines, containing approximately 330 data points per engine. As shown in the previous section, for the CF6-80E1 more data were available. The data set contains 61 engines, containing on average approximately 1500 data points.

Figure 7.12 displays the distribution of the linear regression slope coefficients. Naturally, due to the significant scatter, the regression scores were very poor. However, some confidence can be retrieved from the amount of engines examined. It becomes clear that there is significant spread visible for the CF6-80C2. However, most of the regression coefficients show a positive slope. This is in line with the expectation that the reported EGTM, if not corrected for humidity, will be higher for increasing ambient humidity. Also, for the CF6-80C2 the mean regression coefficient is with $3.6K/wt\% \approx 0.33\%/wt\%$ very close to the correction coefficients found in the test-cell corrections and GSP simulations.

This is not the case for the CF6-80E1, indicating on average a lower regression coefficient. The spread around this average is smaller than found for the CF6-80C2. With the test-cell corrections indicating corrections for both the CF6-80C2 and CF6-80E1, the difference found is notable. Especially since the CF6-80E1 data set is larger and statistically speaking would be more accurate.

Figure 7.12: Histogram of $EGTM/\Psi_{abs}$ linear regression slopes



Correcting the EGT_M for Ambient Humidity

This chapter describes several corrections of EGT_M for ambient humidity variation. First, the correction methodology will be explained, after which the results will be discussed.

8.1. Performed Corrections

As concluded from the previous chapters, it is found that the reported EGT_M is slightly higher for larger values of ambient humidity. Also, it is found that significant scatter is present for the reported EGT_M. Nonetheless, an attempt is made to correct the EGT_M for ambient humidity variation. For KLM E&M, it is of added value if the correction is simple to implement in their current diagnostic systems, therefore a correction which is easily applicable to all engines is preferable. A few general correction methods are proposed and the results of the corrections reported.

- Correcting EGT_M using a generic correction of 0.35%EGT/*wt%* (CF6-80C2) and 0.33%EGT/*wt%* (CF6-80E1) as reported in Table 6.2
- Correcting EGT_M using the test-cell corrections
- Correcting EGT_M using a hybrid approach

A simple representation of the correction methodology is displayed in Figure 8.1. Just as the method of calculation of EGT_{M, DIV}, the rolling average is calculated for the corrected EGT_M and the discrepancy between the corrected and rolling average is calculated. Some additional comments must be made to clarify the corrections.

Theta exponents

To convert EGT_{HD} to EGT_{SD} and observed EGT to EGT_{SD}, θ and θ_{flat} exponents must be retrieved. Since those are a function of either the observed fan speed (θ) or the flat rated corrected speed (θ_{flat}), both are not affected by humidity corrections. It is therefore assumed that the engine control system retrieves the θ values similarly to the test-cell corrections. Therefore, in all implemented corrections the test-cell θ and θ_{flat} are used when converting from or to HD and SD.

Shunt Factor

The reported EGT is shunted. Before applying corrections it must always be converted to its non shunted variant with the shunt factor *SF*. The Shunt Factor (SF) is a constant factor for the CF6-80C2. For the CF6-80CE1 it is a function of non-shunted EGT.

N1 modifier

A parameter which was of no influence in the test-cell corrections as described in section 4, but which is of influence when correcting on-wing data, is the N1 modifier. Every engine will perform (slightly)

different with respect to other engines due to engine-to-engine differences discussed earlier. In order to match the thrust between engines operating on the same aircraft, a N1 modifier is implemented. The N1 modifier is calculated after each overhaul and constant for all consecutive flights until the next overhaul. This modifier is based on the thrust margin as calculated in the test-cell. An engine performing better (e.g. higher thrust margin) will be subjected to a negative N1 modifier, since for lower N1 speed the required thrust margin will already be met. For the CF6-80C2 there are only negative N1 modifiers (e.g. only positive thrust margins). The CF6-80E1 also has positive N1 modifiers, thus N1 modifiers for engine with a lower thrust margin than average.

The reported snapshot fan speed is both in terms of corrected as well as indicated fan speed. The indicated fan speed is a conversion of the actual fan speed in combination with the N1 modifier. Only for the CF6-80E1 corrections between $N1_i$ and $N1_{obs}$ are available to the author. Therefore, the $N1_i$ is assumed to be equal to $N1_{obs}$ for the CF6-80C2. For the CF6-80E1 the correction is applied.

Next to correcting $N1_i$ for N1 modifier, the modifier also effects the EGTM. A positive delta, $\Delta EGTM$, is added to the EGTM for engines with negative N1 modifiers, and vice versa for engines with positive N1 modifiers. Please see equation 4.6 for illustration. These deltas are tabulated in test-cell documentation and may add up to 11K for the CF6-80C2. Since these N1 modifiers are known variables as reported by the take-off snapshot, it is assumed that on-wing these modifiers are used for corrections. Therefore, corrections concerning N1 modifier are also applied to all EGTM corrections described below.

'Black-box' on-wing corrections

As explained earlier, the calculation procedure of the reported EGTM is unknown to the author. Possibly several adjustments are made for bleeds, power off-take etc. and corrected for by the engine control system. One can image the on-wing performed corrections to adjust to EGT_{SD} as a 'black box', which will be unaltered. Unfortunately, the major part of the scatter is probably mainly due to the corrections performed in the 'black box' and thus will still be present after correction.

8.1.1. Correcting EGTM using generic correction

This correction is the simplest of the three. The reported shunted EGT is calculated to its non-shunted variant. Using equation 8.1 the delta to be added to the EGT is calculated. Since EGT_{SD} is shunted, the delta is shunted and added to the standard day EGT after which it is corrected to its standard day value. Successively, the 'black box' on-wing corrections are added. The complete standard day EGT is then recalculated to $EGTM_{GEN}$ using the inverse methodology when calculating standard day EGT from EGTM.

$$EGT_{\Delta GEN} = \frac{0.35\% * \Psi_{abs}}{100\%} \times EGT_{nonshunted} \quad (8.1)$$

8.1.2. Correcting EGTM using the complete test-cell corrections

Next, complete test-cell corrections are applied to calculate $EGTM_{TC}$. The reported EGTM is left out of the calculations and the correction is solely based on the EGT, Ψ_{abs} , T_{t1} and $N1_i$ corrections. The corrections for the CF6-80E1 are very similar to those described for the CF6-80C2, except for a variable shunt and some more thorough N1 modifier adjustments and N1K calculations. The corrections are performed accordingly to the corrections described in section 4. This implies that a 'throttle push' delta is calculated between the rated corrected fan speed and the actual corrected fan speed. This approach discards the EGTM corrections which may be applied for operations only performed on-wing and not in the test-cell.

8.1.3. Correcting EGTM using a hybrid approach

Finally, a hybrid approach is proposed to calculate $EGTM_{hybrid}$. This approach originated from the fact that for the CF6-80C2, the generic correction was found not to affect the scatter and the test-cell approach underestimated the correction but decreased the scatter, as will become clear in the next section. The hybrid correction is a combinational approach of the test-cell humidity corrections combined with the on-wing 'black-box' corrections. The humidity corrections are identical to those performed in the test-cell, except that the 'throttle push' delta is calculated as the difference between the dry corrected fan speed and humid corrected fan speed. The 'throttle push' correction of the corrected fan speed not matching the rated corrected fan speed is part of the 'black-box' correction.

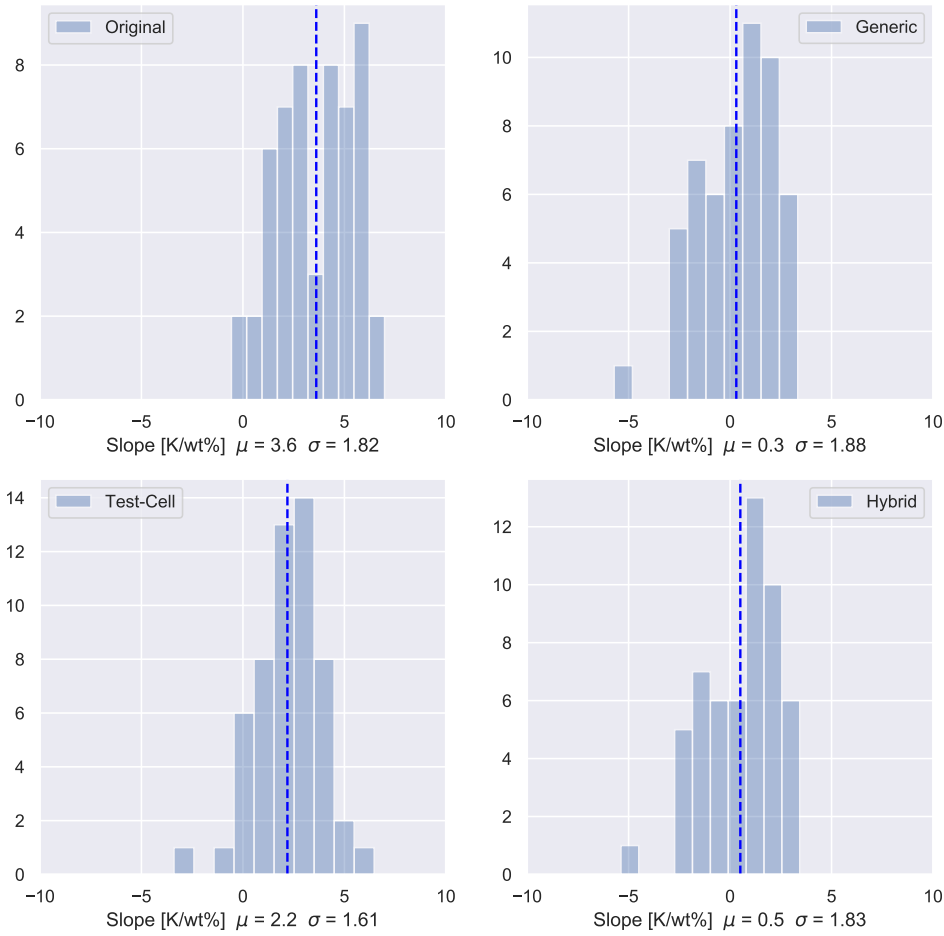


Figure 8.2: CF6-80C2: Histogram of $EGTM/\Psi_{abs}$ linear regression slopes after correction

correction results in terms of linear regression slope, is also found to be subjected to larger scatter. It is found that the scatter increases when the EGTM regresses towards 0. Preliminary conclusions on the performed EGTM corrections for the CF6-80C2 are summarized below.

- On average, the generic and hybrid corrections correct the reported EGTM most appropriately.
- No significant scatter reductions are found after correcting the data
- One of the origins of the scatter is ambient humidity. However, its relative contribution to the overall scatter is limited. The average correction (always downward) will be several degrees Kelvin, with maximum corrections up to 12K for the most extreme cases. With the total bandwidth of the scatter being approximately 20K, scatter due to humidity will only play a minor role.
- When using the complete test-cell corrections, it is interesting to note that the correction on itself does not result in a corrected linear regression slope of zero. Since this does happen for the hybrid correction where the sole test-cell humidity corrections are applied, the test-cell throttle push EGT delta seems to underestimate the overall effect of humidity.

8.2.2. CF6-80E1 correction results

Figure 8.3 displays the correction results for the CF6-80E1. Due to the discrepancy in reported regression slope for $EGTM_{DIV}$ and ambient humidity between the CF6-80C2 and CF6-80E1, the generic and hybrid corrections overcompensate when correcting the data. For the hybrid correction a slight decrease in scatter is observed of approximately 10%. The test-cell corrections show the poorest results, indicating both an increase in regression slope and scatter.

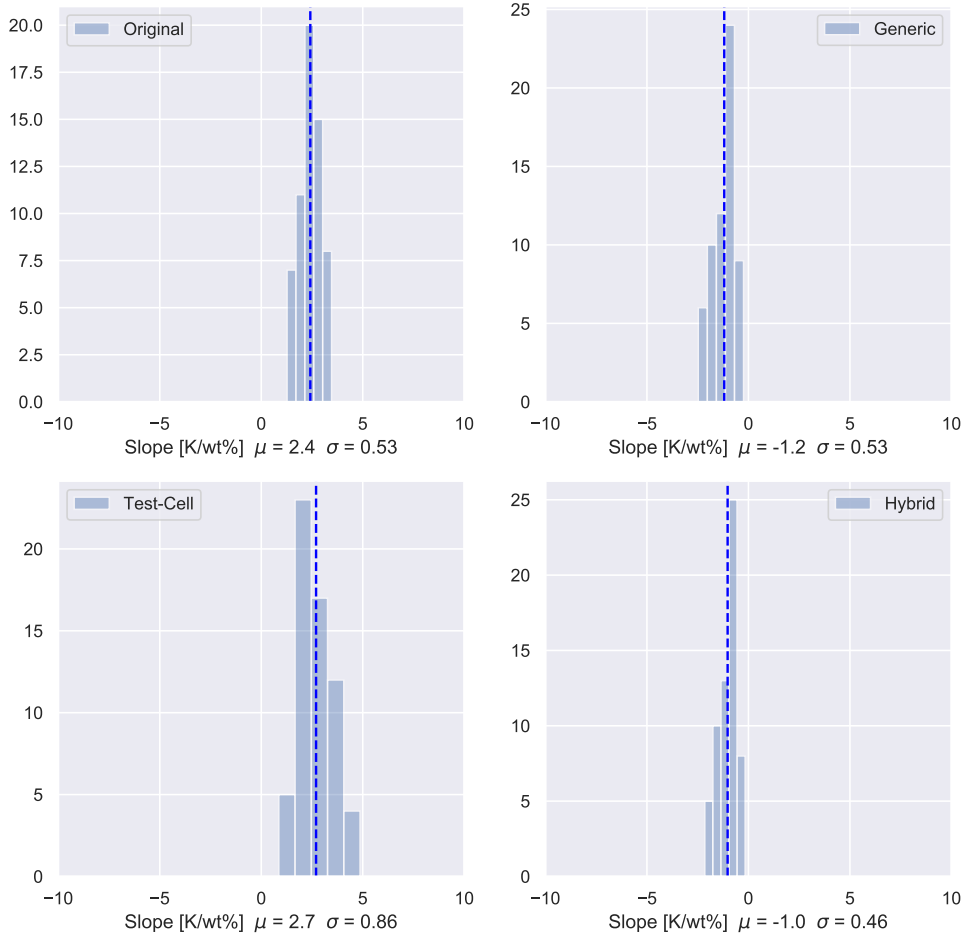


Figure 8.3: CF6-80E1: Histogram of $EGTM/\Psi_{abs}$ linear regression slopes after correction

Figure 8.5 displays the correction results of two engines. The left engine displays engine '80xxx8', where the correction lead to a regression slope coefficient of approximately zero for the hybrid and generic corrections. Whereas the right graphs displays engine '80xxx0' an engine indicating an overestimation in correction slope. It is visible that the corrections for humidity values lower than the average encountered humidity ($\approx 1\%$) move the points upward, larger values of ambient humidity move the points downward. It is also visible that the test-cell correction displays many outliers.

Figure 8.7 displays the original and hybrid corrected $EGTM$ versus the cycle count. Again, it is clearly visible that the humidity correction will decrease the overall $EGTM$. For the engine '80xxx0' it is visible that an overhaul was performed just before 500 cycles. This will negatively affect the $EGTM_{rolling}$ for the data points around the performed overhaul, negatively affecting $EGTM_{DIV}$. In general more scatter is visible for engine '80xxx0'.

The origin of the poor results can be explained by referring to the research performed by Röell [62]. Röell concluded that the origin of the lower regression slope found for the CF6-80E1 in Figure 7.12 results from an incorrect T_{t2} correction as performed on the on-wing reported $EGTM$. The presumption was that this masked the effect of absolute humidity. Röell therefore optimized the θ exponents for each ESN to provide for appropriate $EGTM$ correction regarding T_{t2} . For further explanation of the optimization and correction procedure please refer to [62]. After this correction was applied an average $EGTM_{DIV}$ to absolute humidity regression slope was found of $3.4K/wt\%$ for standard day conditions, which agrees very well with the test-cell corrections for the CF6-80E1 as found in Table 4.1. Preliminary conclusions on the performed $EGTM$ corrections for the CF6-80E1 are summarized below.

- Using the current data, on average, the generic and hybrid corrections overestimate the $EGTM$ correction.

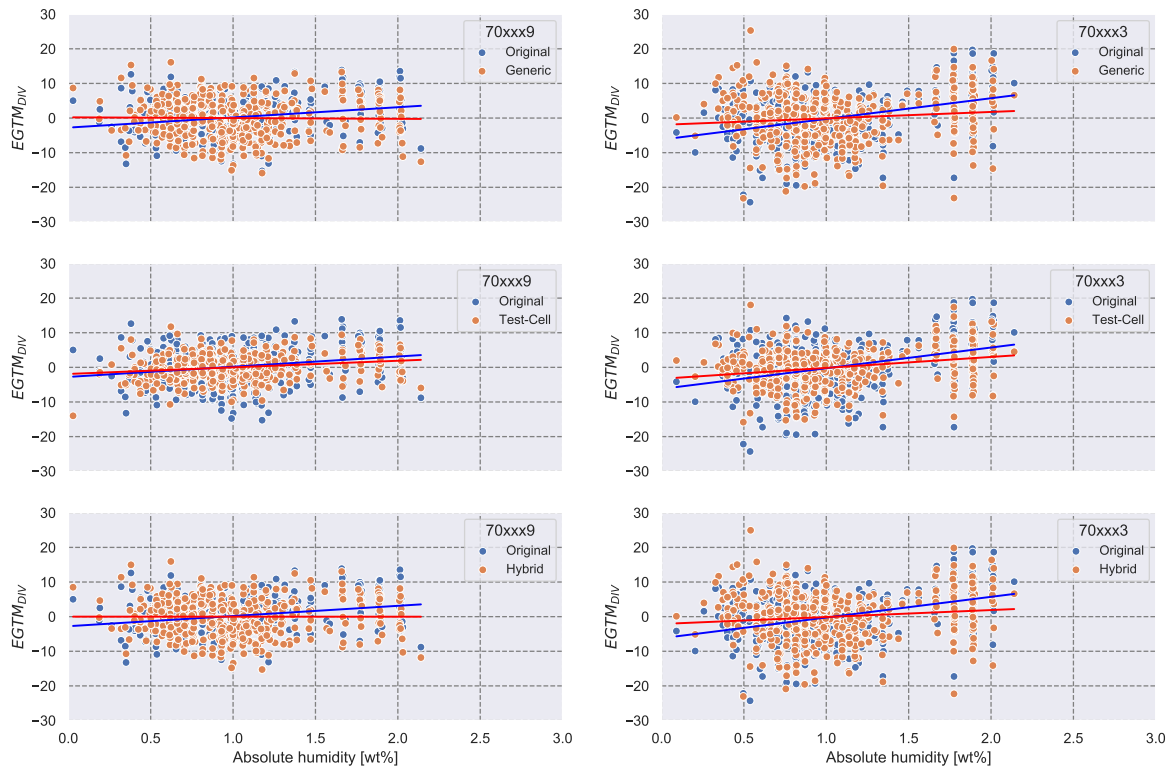


Figure 8.4: CF6-80C2: Corrected and original EGTM scatter plots for two different ESN

- A decrease in standard deviation is found for both the previously mentioned corrections of which the reduction for hybrid correction is the most pronounced.
- With an overall smaller standard deviation of the CF6-80E1 compared to the CF6-80C2, the effect of humidity is more pronounced, already indicating a decrease in standard deviation without using appropriate EGTM data as corrected by Röell [62].
- When using the complete test-cell corrections no reduction in either regression slope nor scatter is observed. It is therefore concluded that the reported $N1(i)$ and EGT generally do not agree with the throttle push table as provided by the test-cell corrections.

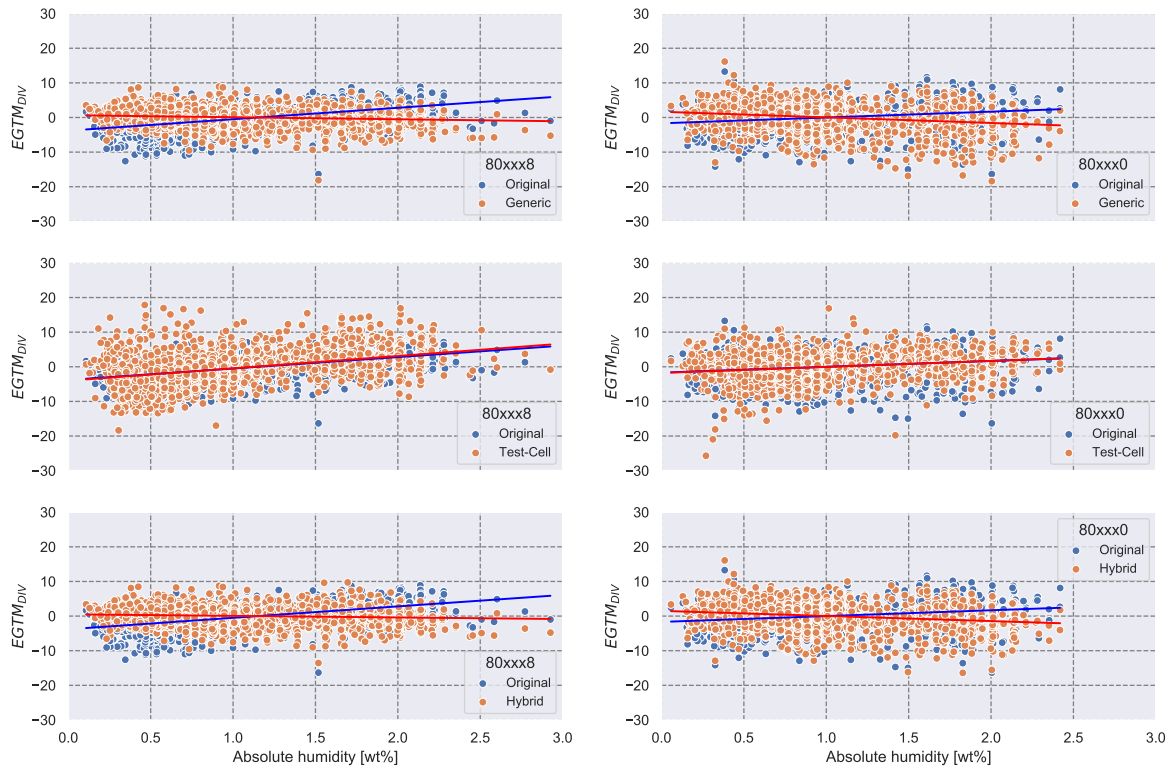


Figure 8.5: CF6-80E1: Corrected and original EGTm scatter plots for two different ESN

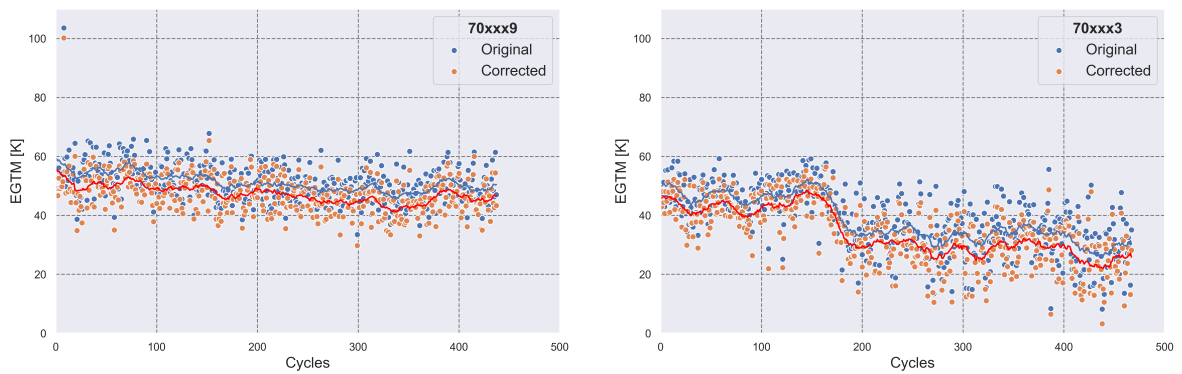


Figure 8.6: CF6-80C2: Visualization of corrected EGTm

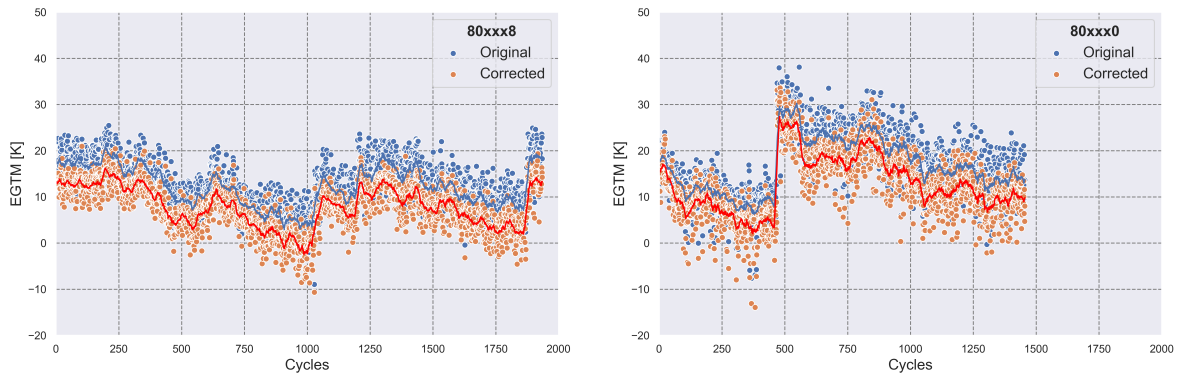


Figure 8.7: CF6-80E1: Visualization of corrected EGTm

Table 8.1: Tabulated average correction results for both CF6-80C2 and CF6-80E1

	CF6-80C2	CF-80E1
Ψ_{abs}		
μ	0.98 wt%	1.07 wt%
σ	0.41 wt%	0.55 wt%
$EGTM_{\mu}$		
Original	42.4 K	11.4 K
Generic	38.5 K	6.9 K
Test Cell	58.0 K	11.7 K
Hybrid	38.6 K	7.2 K
$EGTM_{DIV\sigma}$		
Original	6.4 K	3.8 K
Generic	6.6 K	3.6 K
Test-Cell	4.8 K	4.6 K
Hybrid	6.5 K	3.4 K

9

Discussion

With the test-cell corrections, simulation results and historical data examined and EGTM corrections performed, this chapter provides a discussion of the aforementioned approaches combined.

9.1. Literature and Test-cell Corrections

In literature, component corrections are proposed assuming full flow similarity (similitude) [6, 7, 38]. The assumption of flow similarity imposes, out of others, the following conditions: equal Mach number, equal $\frac{V_{ax}}{U}$ and equal specific heat ratio. With the specific heat ratio being affected by humidity, the last condition is inherently not met and imposes some arbitrariness to the corrections as stated by Garwood et al. [7]. However, since the effect of humidity on the specific heat ratio is generally small, the corrections are assumed to be representative. It was stated by the aforementioned researchers that when analysing the effects on a complete turbofan, conditions imposing flow similarity may not be met any more, due to the components operating in a combined equilibrium and the influence of the control configuration. It was found from the test-cell corrections that this actually makes all the difference.

The direct correction as described in Chapter 4 may be seen as a sort of flow similarity correction for the complete engine, without influence of the control system. Except for the fuel flow, the corrections already showed a discrepancy with those found in literature for single components assuming flow similarity. This may be attributed to the fact that when the turbofan is operating without control system and retrieves constant fuel flow the assumptions mentioned in Chapter 3 are generally met. Both the compressors and turbines however, affect each other by operating in a combined equilibrium, therefore increasing the complexity of the problem deviating from flow similarity. This will however stay an educated guess since the true nature of the direct and indirect humidity correction as found in the test-cell documentation are not known to the author.

The indirect correction may be seen as the effect of the control system. The density of humid air is lower and the fan will spin faster with the same power input. Since the control system implies constant N1, the fuel flow reduces and the equilibrium of the engine changes. It will therefore impose deltas on the corrected parameters. As mentioned in Chapter 4, in the throttle push tables these deltas can be found in terms of standard day corrected deltas, by interpolating for the difference due to humidity between $N1K_{dry}$ and $N1K_{humid}$. The indirect test-cell corrections were found to be generally of greater magnitude compared to the direct humidity corrections, indicating that analysing engine performance without taking into account the control system leads to inaccurate results for N1-controlled engines.

It was also found that the test-cell corrections imply that the sensitivity of the engine to humidity is dependent on power setting. The nature of this sensitivity is due to the interpolation from the throttle push table. When an engine depicts higher sensitivity to N1K between two specific N1K values, the sensitivity of the engine to humidity will also be higher. The origin of the throttle push tables is to correct the actual corrected fan speed to the rated corrected fan speed as reported by the test-cell documentation, and not to correct for humidity only. Since the overall correction for throttle push generally concerns large corrections, and the effect of humidity is generally small, it imposes questions on the applicability of the throttle push tables as a measure of (indirect) humidity effects.

9.2. Test-cell Corrections and Simulations

Confidence is gained by the, on average, great similarity between the simulation results and test-cell corrections. Where the simulations show a slight increase in sensitivity for higher power settings, this is also depicted by the test-cell corrections. The simulations however, seem to overshoot the corrections for higher power settings. The great step increases found are regarded as unphysical since sensitivity to humidity is assumed to vary slowly. Finding the sensitivity of, for example, the fuel flow increasing with approximately 100% when increasing the ambient temperature with 5 degrees Kelvin, can be attributed to non-smoothness or not insufficiently tuned parts of the compressor maps.

The results for different control configurations visualize the differences of the effect caused by the implemented control configuration, while having the same physical engine and operating conditions. It was found that *TIT*-controlled engines are affected the most by ambient humidity variation and display a fuel flow increase of about 5% for extreme humid operating conditions. With the main purpose of a turbofan engine generating thrust, it was found as expected, that the IEPR control configuration shows the lowest sensitivity to humidity in terms of thrust. $N1_c$ -control comes second with only a negligible thrust decrease. For the general $N1$ -control configuration it was found that $N1$ should be corrected by roughly 0.27%/wt%, in order to maintain equal FN for varying ambient humidity conditions. Without correction a thrust decrease of roughly 0.6%/wt% is found, thereby accounting up to a decrease in FN of almost 2% in very humid conditions.

It must be noted that the applicability of the results for other control systems may not directly apply to engines with other control configurations since their physical characteristics will also be different. For example, the IEPR control as implemented by Rolls Royce is found on a three-spool turbofan engine while the simulation results regard a two-spool turbofan engine. The geometry of the components, and therefore the components maps, will most certainly differ, inherently affecting the engines new equilibrium and sensitivity to humidity regarding power setting. Nonetheless, even with other engine turbofan control configurations, from inlet to nozzle, the general component structure (e.g. inlet, compressor, combustor, turbine, nozzle) will be almost identical. It is therefore believed that the simulations, give a representative indication of the effects of humidity.

9.3. Historical Data, Simulation results and Test-cell corrections

The historical data indeed showed that higher reported EGTM were found for larger ambient humidity values. Indicating that the, due to ambient humidity, lower EGT results in an increase of EGTM since no correction is applied on-wing. The average regression slope of the CF6-80C2 matched the test-cell and simulation results really well. Referring to the research of Röell [62], the same can be concluded about the CF6-80E1 after properly correcting the data. It was found that the scatter present in the reported EGTM is of greater magnitude than the effect of humidity itself.

9.3.1. CF6-80C2

Especially the older CF6-80C2 is subjected to significant scatter. The average standard deviation of the $EGTM_{DIV}$ is $\sigma = 6.4K$. With an average $EGT \approx 1100K$ it follows that $0.35\%EGT/wt \approx 3.8K/wt\%$. The average standard deviation of humidity is $\sigma_\psi = 0.41wt\%$ and can be loosely converted to a humidity induced standard deviation of $3.8K/wt\% * 0.41wt\% = 1.56K$. Calculating the standard deviation of the $EGTM_{DIV}$ according to equation 7.4 assuming all uncertainty of humidity has been removed leads to $\sigma_{EGTM_{DIV}} = 6.24K$, which is a theoretical reduction of only 3%. Since much departure station information was missing this affects the moving average due to gaps in the data as also presented in Figure F.1, consequently affecting the $EGTM_{DIV}$. It is therefore no surprise that the supposed marginal decrease in standard deviation is not found after correcting the EGTM for the CF6-80C2. The generic and hybrid corrections however seem to reduce the regression slope significantly. With the scatter heavily influencing the linear regression it is also not in the line of expectation that the regression coefficients have not reached a slope of 0.

9.3.2. CF6-80E1

For the CF6-80E1 the standard deviation with respect to $EGTM_{DIV}$ is already significantly less without correction. Also, the engines seem to encounter humid areas more often compared to the CF6-80C2, since the mean encountered absolute humidity is higher as well as the standard deviation ($\sigma_\psi = 0.55wt\%$). Using the same approach as in the previous paragraph this leads to a standard

deviation on the $EGTM_{DIV}$ imposed by humidity in terms of $2.09K$. This would result in an average standard deviation of $\sigma_{EGTM_{DIV}} = 3.17K$, assuming all uncertainty due to humidity has been removed, indicating an average theoretical reduction of 16.5%. A scatter reduction was found for both the generic and the hybrid correction as presented in Table 8.1, being more pronounced for the hybrid correction (10% reduction) than for the generic correction. A lot more data were available for the CF6-80E1, thereby ensuring more representable rolling averages and thus more representable $EGTM_{DIV}$, which is also visible in Figure F.2. Due to reasons explained in section 8.2.2 both the generic and hybrid approach overestimate the problem, also affecting the scatter and thereby possibly not resulting in the expected standard deviation reduction.

9.3.3. Explanation of EGTM-Humidity linear regression slope variation

The deviation in correction slope can partly be explained by engine to engine differences resulting from deterioration. However, this effect is assumed to be small. According to simulation results of Röell [62], this assumption is justified as will be explained shortly. Röell performed a small study in GSP on the effects of deterioration on the sensitivity to humidity. The study was performed using the same model as used in this research and consisted of investigating the effects of several deterioration cases. Differences of sensitivity of minimally $-0.6\text{ }^{\circ}C$ to maximally $+0.5\text{ }^{\circ}C$ for significant ambient humidities ($\approx 2.75wt\%$) were found. Taking the average EGT $\approx 1150K$ of the dataset for the CF6-80E1 and using the approach of $0.35\%EGT/wt\%$, results for the aforementioned absolute humidity in an overall EGT variation induced by humidity of $11.1K$. With the found discrepancy due to deterioration as found by Röell, e.g. $10.5 - 12K$, this can be translated back to a variation of roughly $0.33 - 0.37\%/wt\%$, indicating possible discrepancies of maximally 5%. With the effect of humidity being small on itself, the impact of deterioration on the effect of humidity may be deemed sufficiently small to be negligible in an operational context.

Apart from engine to engine differences, it was found from simulations in section 6.1.2, that customer bleed can also affect the sensitivity to humidity. Since customer bleed changes the (corrected) mass flow in the engine, a different operating point is attained, possibly moving to a region of lower or higher sensitivity. The changes in sensitivity, as found in Table 6.1, account for approximately the same variation as found for deterioration and were assumed not to affect the sensitivity significantly. However, influence the of both the previous mentioned effects combined alter the sensitivity sufficiently to be notable.

Another possibility explaining the variations in regression slope next to customer bleed and engine to engine differences, is the average power setting of the specific turbofan in question. Both the test-cell corrections as well as the simulation results indicate that the overall effect on EGT slightly increases for higher power settings. Engines on average operating on a higher power setting may therefore be subjected to slightly steeper regression slopes than others and vice versa.

Furthermore, with the absolute humidity being highly variable for increasing altitude, the proposed correction to correct humidity for altitude also introduces uncertainty. However, with most of the snapshots found to be captured close to the METAR altitude and the correction on itself being small, it can easily be stated that the uncertainty originating from this correction is close to negligible.

It is believed that the main cause of the variation found in linear regression slopes is the scatter present in the reported EGTM, originating from other effects than humidity. With the linear regression being extremely sensitive to outliers it is in the line of expectation to find a large variation on the regression slopes, especially for the CF6-80C2. As mentioned before, confidence can be retrieved from the average regression slope of the historical data agreeing well with both the test-cell corrections and the simulation results.

9.4. Assessment of Operational Effects

Starting with the OEM, notable performance changes due to humidity were observed. Especially the thrust reduction when ambient humidity increases may be a point of interest. Since absolute humidity will only affect the performance of the engine at lower altitudes, changes in the derate procedure to account for ambient absolute humidity possibly enhance take-off performance. Referring to Table 6.4, the simulations indicate that whilst maintaining equal thrust, the temperatures in the turbines will still be lower in humid air than in dry air. Indicating that, for a N1-controlled engine, the fan speed can be increased to account for humidity to maintain equal thrust, without violating the red-line EGT. In other

words, humidity moves the corner point temperature slightly higher, giving more room to increase N1. Augmenting the current derate procedure for ambient absolute humidity will ensure that take-off field length does not increase due to humidity, by choosing an appropriate N1-speed producing exactly the desired amount of thrust.

Naturally, the derate procedure is eventually also corrected with a safety margin to ensure the aircraft do not surpass runway length. However, the effect of humidity will thus reduce this margin. Also, two downsides of increasing N1 are that the deterioration pace will also increase as well as that the fuel flow. Since there are no reports of aircraft violating the run-way length due to humidity related causes, one can argue not to change the derate procedure since it will mainly result in an increase in deterioration pace and increased fuel economy. What the overall benefits and downsides are should be investigated in future research. Nonetheless it can be concluded that there is room for improvement.

For the MRO industry, the main goal for investigating humidity effects on turbofan performance is twofold. First, it sheds a light on the impact of humidity on the reported EGTM and secondly, if the impact is not negligible, corrections may be applicable in order to more accurately trend the EGTM over time. With humidity induced EGT(M) deviations of maximally 12K, it can be concluded that the effect is most certainly not negligible and that correctional actions will have impact on the accuracy of the EGTM. For the CF6-80C2 the general scatter present is of such magnitude that even with a perfect correction for humidity effects, the impact on the overall scatter of the EGTM will only be slightly. For the CF6-80E1 a reduction of scatter of 10% for the hybrid correction was found. However, the effect of humidity was masked due to inaccurate temperature correction as discussed by Röell [62]. Possibly resulting in an average decrease of scatter of 16.5%, if the data is also appropriately corrected for T_{t2} .

Most of the CF6-80C2 turbofan engines will be phased out as of 2022 and the CEO of AFKLM recently announced the A330, powered by the CF6-80E1 turbofan, will be phased out as well in the coming years. Taking into account the timespan it will take from starting the discussion with the OEM to regulations to be adjusted and approved, implementing corrections for the CF6-80C2 engines will currently not be of added value for the industry. However, with the trend of engines reporting the EGTM more accurately, the effect of humidity will become relatively more pronounced. If the EGTM is more accurately calculated due to the incorporation of a humidity correction, this will provide a more accurate indication of engine condition as well as when exceedances will start to occur. This will in turn provide for improved maintenance planning, finally leading to a reduction of cost and safer operation.

Conclusions & Recommendations

This chapter finalizes the report, answering the main research question and summarizing the conclusions found throughout the report. This chapter concludes with recommendations for the MRO and OEM in terms of operational purposes, as well as recommendations for further research.

10.1. Conclusions

The main objective of this report is to research the effect of humidity on turbofan performance, in order to provide corrections for the reported EGT_M for ambient humidity variation regarding the General Electric CF6 turbofan engines. To research the effect of humidity on turbofan performance test-cell relations, simulation results and historical data were investigated and compared.

- It was found that, on average, the test-cell corrections and GSP simulation results were in good agreement, indicating a decrease in EGT of 3.8K per *wt%* of absolute humidity. Globally, the ambient absolute humidity generally varies from 0 to 3.1*wt%*. Indicating that the EGT, under identical take-off conditions, N1-setting and hardware condition, decreases by as much of 12K due to ambient absolute humidity. Since the EGT_M is currently not corrected for ambient humidity, it is overestimated with a maximum of 12K. Therefore, wrongfully indicating that engine performance has increased without any physical condition difference.
- The effect of humidity on turbofan performance was found to be severely influenced by the control configuration of the engine. In terms of changes in thrust, IEPR- and N1_c-control configurations show the lowest sensitivity to humidity. In the simulations, N1-control was found to have a decrease of thrust of roughly 0.6% per *wt%* absolute humidity. This translates to a thrust decrease of almost 2% for very humid circumstances, thereby increasing take-off field length. With the test-cell corrections indicating a higher sensitivity to humidity, the actual effect may possibly be slightly larger. To compensate the effect of humidity on thrust, simulation results indicated a required fan speed increase of 0.27% per *wt%*.
- Next to performance deviations, humidity may also interfere with GPA capabilities. If the measured pressure and temperature ratio are assumed to correspond to dry conditions, the result is an overestimation of compressor isentropic efficiency of roughly 1% and an underestimation of turbine isentropic efficiency with the same magnitude for very humid circumstances of 3.1*wt%*. For more moderate values of ambient humidity, such as 2*wt%*, still notable errors ($\approx 0.6\%$) will occur. Therefore, when calculating the isentropic efficiency using the pressure and temperature ratios, humidity may obscure the effects of deterioration for compressors or falsely indicate deterioration for turbines.
- Monte Carlo analysis displayed the possible flight to flight variation of the reported EGT_(M) whilst performing the exact same take-off under identical ambient conditions except for humidity variation. Whilst the results are extremely location and season dependent, the results displayed significant variations. For example, case study showed that during winter a flight from Amsterdam to Jakarta will experience on average a humidity induced EGT_(M) error of 6K.

- The scatter present on the reported EGTM was found to be far greater than the effect of humidity could possibly cause. Despite the severe scatter present on the reported EGTM for the CF6-80C2, it was found that the average linear regression slope between EGTM and absolute humidity displayed the expected correlation, as found from the test-cell corrections and simulation results, very accurately. Related research found a close to identical average linear regression slope for the CF6-80E1, after also correcting for inaccurately performed temperature corrections by the OEM. This proves that the test-cell corrections, simulation results and historical data provide very similar results on how humidity affects the EGT(M).
- For the CF6-80C2, the generic and hybrid corrections do not seem to reduce the scatter of the reported EGTM, but effectively decrease the average linear regression slope. With severe scatter present on the reported EGTM and the effect of humidity being a small part of that, a reduction in scatter was also not expected. For the CF6-80E1, the results for the generic and the hybrid approach overestimated the correction. The origin of the overestimation was found by related research as mentioned in the previous paragraph. For the hybrid correction, a decrease of standard deviation of 10% was found. With the average impact of humidity on the scatter expected to be roughly 16%, the result already indicates a relatively significant improvement.
- With the test-cell corrections, simulation results and historical data indicating very comparable results for both engines, it may be stated that the effect of humidity on the GE CF6 turbofan engines is clear. Deviation on the reported EGTM up to 12K can be expected due to ambient absolute humidity variations, as where a thrust decrease of up to 2% is also possible.
- The main conclusion, answering the research question, is that engine diagnostics can indeed be augmented by correcting on-wing reported EGTM for ambient humidity variations. However, since the reported EGTM is severely affected by scatter aside from the effect of humidity, currently no significant scatter reduction was achieved by accounting for humidity effects. Nonetheless, with the trend of newer engine types reporting the EGTM more accurately, the relative contribution of humidity to on-wing EGTM scatter increases. This is already visible for the CF6-80E1 displaying less scatter. It is therefore concluded that correcting the EGTM is of secondary interest at the moment, but with the trend of increasing reported EGTM accuracy, ambient humidity is expected to play a more prominent role in the near future.

10.2. Recommendations

Several recommendation follow from this research. Either for the MRO industry or the OEM, as well as for further research. The recommendations are listed below.

- Since the EGTM inaccuracy due to humidity is generally small compared to the total inaccuracy, KLM ES may want to start an investigation on the root causes for the inaccuracy to decide whether correctional actions for effects other than humidity can be applied.
- Humidity effects for other N1-controlled two-spool engines, such as the GE90 and the GENx, are expected to follow the same trends as found in this research due to similar overall architecture. However, further investigation is needed to validate this claim.
- It is left to KLM ES to decide whether to start a discussion with the OEM, with use of this research, on correcting the EGTM for ambient humidity on future engines, or to incorporate corrections on engines such as the GE-90 or GENx-1B to improve engine diagnostic capabilities.
- When performing GPA using on-wing data, it is advised not to use on-wing data concerning areas where high ambient humidity values are encountered. Since the dry air assumption may falsely indicate deterioration for turbines or obscure the effects of deterioration for compressors.
- For KLM ES, it is advised to be cautious when interpreting the results from the CF6-80C2 model when simulated power settings are higher than N1=105% (e.g. 3450 RPM), since the simulations were found to indicate non-physical results.
- It is recommended to the OEM to investigate possible alterations of their control configuration to incorporate humidity corrections on their future engines. Since humidity is only of interest during

take-off, there are possibilities excluding the need of installing a humidity sensor on the engine, but rather using the absolute humidity reported by the airport.

- Additional research can be performed on the prediction of condensation in the inlet. A possible approach is using the temperature sensor just below the cockpit of the aircraft, as well as the temperature sensor in the fan to indicate if temperature increase due to condensation has occurred.
- The absolute effect of humidity on the EGTM is related to the overall temperature and pressure ratios of the gas turbine, as well as the control configuration. Research can be performed investigating possible development of scaling factors to indicate humidity effects for any kind of turbofan engine and control system.
- To further investigate the effect of humidity on GPA capability, a study can be performed both including as well as excluding humidity measurements when performing GPA using the AM component of GSP, in order to identify the impact of humidity on GPA.
- To provide more accurate results in this research, the data can be cleaned more intensively such that the effect of water washes and overhaul are neutralized. Only points with close proximity to each other with respect to time should be selected. Also, it may prove useful to discard engines which are at the end of their lifetime since they indicate an increase in scatter. After more intensively cleaning the data, it will be possible to present a more representable $EGTM_{\text{rolling}}$, consequently positively affecting the $EGTM_{\text{DIV}}$. It is however important to critically reflect on the amount of data which is left after the cleaning process to assess if the database is large enough, such that statistical analysis is credible.

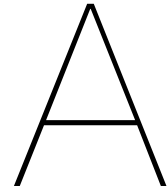
Bibliography

- [1] A.J. Volponi. Gas turbine engine health management: past, present, and future trends. *Journal of Engineering for Gas Turbines and Power*, 136(5):051201, 2014.
- [2] L. Marinai, D. Probert, and R. Singh. Prospects for aero gas-turbine diagnostics: a review. *Applied Energy*, 79(1):109–126, 2004.
- [3] R. Kurz and K. Brun. Degradation in gas turbine systems. *Journal of Engineering for Gas Turbines and Power*, 123(1):70–77, 2001.
- [4] Airbus. Global market forecast 2018-2037, 2018. Presentation by Eric Schulz, Chief Commercial Officer, last accessed: 5 april 2019: <https://www.airbus.com/aircraft/market/global-market-forecast.html>.
- [5] J.C. Samuels and B.M. Gale. Technical note 2119: Effect of humidity on performance of turbojet engines. Technical report, National Advisory Committee for Aeronautics, 1950.
- [6] J. Bird and W. Grabe. Humidity effects on gas turbine performance. In *ASME 1991 International Gas Turbine and Aeroengine Congress and Exposition*, pages V002T02A025–V002T02A025. American Society of Mechanical Engineers, 1991.
- [7] K.R. Garwood et al. Recommended practices for the assessment of the effects of atmospheric water ingestion on the performance and operability of gas turbine engines. Technical report, Advisory Group for Aerospace Research and Development, 1995.
- [8] K. Mathioudakis and T. Tsalavoutas. Uncertainty reduction in gas turbine performance diagnostics by accounting for humidity effects. *Journal of Engineering for Gas Turbines and Power(Transactions of the ASME)*, 124(4):801–808, 2002.
- [9] H. Hanachi, J. Liu, A. Banerjee, and Y. Chen. Effects of the intake air humidity on the gas turbine performance monitoring. In *ASME Turbo Expo 2015: Turbine Technical Conference and Exposition*, pages V006T05A018–V006T05A018. American Society of Mechanical Engineers, 2015.
- [10] S. Liu, J. Dong, and B. Zhang. Impact analysis of intake air humidity on turbofan engine performance. In *International Conference on Electronic, Control, Automation and Mechanical Engineering (ECAME)*, 2017. ISBN: 978-1-60595-523-0.
- [11] A.K. Shukla and O. Singh. Effect of compressor inlet temperature & relative humidity on gas turbine cycle performance. *International Journal of Scientific & Engineering Research*, 5(5):664–670, 2014.
- [12] A. Derber. Aircraft OEMs racing to catch up with health-monitoring solutions, 2019. Last accessed 16 April 2019: <https://www.mro-network.com/engineering-design/aircraft-oems-racing-catch-health-monitoring-solutions>.
- [13] Aviator. Rolls-Royce Intelligent engine Vision Makes Rapid Progress, 2019. Last accessed 16 April 2019: <https://newsroom.aviator.aero/rolls-royce-intelligentengine-vision-makes-rapid-progress/>.
- [14] P.A. Beishuizen. Improving compressor maps of the GE CF6-80C2 engine. Master’s thesis, Delft University of Technology, 2008.
- [15] D.M. den Haan. GSP GPA on CF6-80 engines at KLM Engine Services. Master’s thesis, Delft University of Technology, 2010.

- [16] M.P.R. van Moorselaar. Gas path analysis on GENx-1B at klm engine services. Master's thesis, Delft University of Technology, 2018.
- [17] R. Kurz, C. Meher-Homji, and K. Brun. Gas turbine degradation. In *Proceedings of the 43rd Turbomachinery & 30th Pump Users Symposia*, pages 23–25, Houston, TX, USA, 2014.
- [18] M.L. Verbist, W.P.J. Visser, and J.P. van Buijtenen. Experience with gas path analysis for on wing turbofan condition monitoring. *Journal of Engineering for Gas Turbines and Power*, 136, 2014.
- [19] M.L. Verbist. *Gas path analysis for enhanced aero-engine condition monitoring and maintenance*. PhD thesis, Delft University of Technology, 2017.
- [20] H.I.H. Saravanamuttoo, G.F.C. Rogers, and H. Cohen. *Gas Turbine Theory*. Pearson Education Limited, 2009.
- [21] C.C. Tonino. Analysis of post-overhaul engine performance at KLM Engine Services. Master's thesis, Delft University of Technology, 2013.
- [22] L.A. Urban. *Gas Turbine Engine Parameter Interrelationships*. Hamilton Standard Division of United Aircraft Corporation, 1969.
- [23] Y.G. Li. Performance-analysis-based gas turbine diagnostics: A review. *Proceedings of the Institution of Mechanical Engineers, Part A: Journal of Power and Energy*, 216(5):363–377, 2002.
- [24] M. Zedda. *Gas Turbine Engine and Sensor Fault Diagnosis*. PhD thesis, Cranfield University, 1999.
- [25] R. Capata. An artificial neural network-based diagnostic methodology for gas turbine path analysis, part i: introduction. *Energy, Ecology and Environment*, 1(6):343–350, 2016.
- [26] H.R. DePold and F.D. Gass. The application of expert systems and neural networks to gas turbine prognostics and diagnostics. In *ASME 1998 international gas turbine and aeroengine congress and exhibition*, pages V005T15A009–V005T15A009. American Society of Mechanical Engineers, 1998.
- [27] S.O.T. Ogaji, L. Marinai, S. Sampath, R. Singh, and S.D. Prober. Gas-turbine fault diagnostics: a fuzzy-logic approach. *Applied Energy*, 82(1):81–89, 2005.
- [28] G.D. Clow, C.P. McKay, G.M. Simmons Jr, and R.A. Wharton Jr. Climatological observations and predicted sublimation rates at lake hoare, antarctica. *Journal of Climate*, 1(7):715–728, 1988.
- [29] A.L. Buck. New equations for computing vapor pressure and enhancement factor. *Journal of applied meteorology*, 20(12):1527–1532, 1981.
- [30] H. Hanachi, J. Liu, A. Banerjee, and Y. Chen. Effects of humidity condensation on the trend of gas turbine performance deterioration. *Journal of Engineering for Gas Turbines and Power*, 137(12): 122604, 2015.
- [31] J.H. Spencer and D.C. Archer. The effect of condensation within an aircraft inlet duct on installed turbofan engine performance. Technical report, United States Navy, 1971.
- [32] J. Blake. Effects of condensation in the JT9D turbofan engine bellmouth inlet. In *11th Propulsion Conference*, page 1325, 1975.
- [33] T. Nikolaidis and P. Pilidis. The effect of water ingestion on an axial flow compressor performance. *Proceedings of the Institution of Mechanical Engineers, Part G: Journal of Aerospace Engineering*, 228(3):411–423, 2014.
- [34] D.J. Blazey. F404 Engine ESN 376044-1A Test Cell Correlation Results from Lynn Cell 108 and NRC Ottawa, Canada, Test Cell. Technical report, General Electric, 1983.
- [35] W.P.J. Visser. *Generic Analysis Methods for Gas Turbine Engine Performance*. PhD thesis, Delft University of Technology, 2015.

- [36] P.P. Walsh and P. Fletcher. *Gas Turbine Performance, Second Edition*. Blackwell Science, 2004.
- [37] A.G. Rao. AE4238 Aero Engine Technology Lecture 2, 2019. Engine calculations. Lecture Slides Delft University of Technology.
- [38] B.D. Fishbeyn and N.V. Pervyshin. Determination of the effect of atmospheric humidity on the characteristics of a turbofan engine. Technical report, Foreign Technology Division Wright-Patterson AFB OH, 1970.
- [39] J. Kurzke. Model based gas turbine parameter corrections. In *ASME Turbo Expo 2003, collocated with the 2003 International Joint Power Generation Conference*, pages 91–99. American Society of Mechanical Engineers, 2003.
- [40] GSP team. Gas turbine simulation program, 2019. <https://www.gspteam.com>.
- [41] W.P.J. Visser and M.J. Broomhead. Gsp, a generic object-oriented gas turbine simulation environment. In *ASME Turbo Expo 2000: Power for Land, Sea, and Air*, pages V001T01A002–V001T01A002. American Society of Mechanical Engineers, 2000.
- [42] M.L. Verbist. Gsp modeling elements and numerical methods. Technical report, Technical University of Delft, Process & Energy Department, 2010. Reader.
- [43] J. Kurzke. How to get component maps for aircraft gas turbine performance calculations. In *ASME 1996 International Gas Turbine and Aeroengine Congress and Exhibition*, pages V005T16A001–V005T16A001. American Society of Mechanical Engineers, 1996.
- [44] M. Zwingenberg, F.K. Benra, and K. Werner. Improvement of performance prediction by automated assimilation of gas turbine component maps. In *ASME Turbo Expo 2008: Power for Land, Sea, and Air*, pages 1761–1770. American Society of Mechanical Engineers, 2008.
- [45] M.L. Verbist, W.P.J. Visser, R. Pecnik, and J.P. van Buijtenen. Component map tuning procedure using adaptive modeling. In *ASME Turbo Expo 2012: Turbine Technical Conference and Exposition*, pages 371–379. American Society of Mechanical Engineers, 2012.
- [46] E. Tsoutsanis, N. Meskin, M. Benammar, and K. Khorasani. A component map tuning method for performance prediction and diagnostics of gas turbine compressors. *Applied Energy*, 135: 572–585, 2014.
- [47] M.L. Verbist, W.P.J. Visser, J.P. van Buijtenen, and R. Duivis. Gas path analysis on KLM in-flight engine data. In *ASME 2011 Turbo Expo: Turbine Technical Conference and Exposition*, pages 149–157. American Society of Mechanical Engineers, 2011.
- [48] W.P.J. Visser and S.C.A. Kluiters. Modelling the effects of operating conditions and alternative fuels on gas turbine performance and emissions. Technical report, National Aerospace Laboratory NLR, 1998.
- [49] S. Gordon and B.J. McBride. Computer program for calculation of complex chemical equilibrium compositions and applications. part 1: Analysis. Technical report, NASA, 1994.
- [50] B. J. McBride and S. Gordon. *Computer Program for Calculation of Complex Chemical Equilibrium Compositions and Applications. Part II. Users Manual and Program Description*, 1996.
- [51] GSPManual. *GSP 11 User Manual*, 2014. version 11.4.4.0.
- [52] M. Oostveen. Development of GPA functionality in GSP. Master’s thesis, Delft University of Technology, 2004.
- [53] E. van Dorp. Development and implementation of a GSP gas path analysis tool for gas turbine diagnostics. Master’s thesis, Delft University of Technology, 2009.
- [54] General Electric Aviation. *CF6-80C2 ENGINE MANUAL*, 2018. restricted document.
- [55] General Electric Aviation. *CF6-80E1 ENGINE MANUAL*, 2013. restricted document.

- [56] G. Yamamoto. Average vertical distribution of water vapour in the atmosphere. *Journal of the Meteorological Society of Japan. Ser. II*, 27(9):277–282, 1949.
- [57] ITU-R P Series Recommendation. 835-6: Reference standard atmospheres. *ITU-R Recommendations, P Series Fascicle*, ITU, Geneva, Switzerland, 2017.
- [58] American Geophysical Union. Water vapor in the climate system, 1995. Last accessed 17 October 2019: <https://www.eso.org/gen-fac/pubs/astclim/espas/pwv/mockler.html>.
- [59] A.D. Culf, J.H.C. Gash, and M.V.K. Sivakumar. Daily patterns of dew-point temperature in a semi-arid climate. *Agricultural and Forest Meteorology*, 68(1-2):107–111, 1994.
- [60] A.D. Culf and J.H.C. Gash. Longwave radiation from clear skies in niger: a comparison of observations with simple formulas. *Journal of applied Meteorology*, 32(3):539–547, 1993.
- [61] W. Brutsaert. On a derivable formula for long-wave radiation from clear skies. *Water resources research*, 11(5):742–744, 1975.
- [62] B. Röell. Test-cell and On-wing Turbofan Performance Comparison at KLM Engines Services. Master’s thesis, Delft University of Technology, 2019.



Thesis Assignment

Humidity Effects on Engine Performance and Time On-wing

MSc Assignment

Propulsion & Power (FPP),

Faculty of Aerospace Engi-

neering

Introduction

KLM Engine Services (ES) is part of Air France Industries KLM Engineering & Maintenance Group, overhauling approximately 200 aircraft engines annually. The overhaul shop visit ends with a standardized performance test, to assess compliance to certification rules and customer contracts, before it is released for operation on-wing. At two different locations, the following turbofan engine types are tested:

- CFM56-7B KLM E&M Testcell / Schiphol-Oost
- CFM56-7B KLM E&M Testcell / Schiphol-Oost
- CF6-80E1 KLM E&M Testcell / Schiphol-Oost
- CF6-80C2 KLM E&M Testcell / Schiphol-Oost
- GEnx-1B Zephyr Testcell / Charles de Gaulle Airport, Paris
- CFMI LEAP-1A & -1B (in gradual introduction)

The main performance indicator of engine gas path condition is the Exhaust Gas Temperature Margin (EGTM). A low margin is an indicator of poor performance and a decision support indicator for performance-related engine removals. EGTM is subject to certification limits. It is generally known that the EGTM is affected by ambient conditions and corrected accordingly by the engine's control and reporting systems. However, ambient humidity is not measured by any sensor on the engine or the airframe and thus, EGTM is not corrected for humidity. As a result, the reported EGTM is affected by humidity to an unknown extent. As the physical degradation of an engine progresses slowly, it is assumed that a correction of the EGTM during take-off, based on real-time airport weather data, can improve the operational decision support and provide a more accurate indication of engine condition. This means in some cases, engine removal can be postponed while retaining the certification safety requirements, which implies substantial economic benefits.

Key objectives

- To develop GSP performance models of the most critical engines in terms of an EGTM related engine removal, including effects of inlet air humidity on EGTM at fixed power settings, primarily take-off thrust. This normally is a specific fan speed. In addition, effects on actual thrust may be evaluated.

- Develop a Proof of Concept for correction of EGTM for humidity effects which will reveal the possible benefits of such an approach.

Assignment

Your work will include the following elements:

1. A literature study on turbofan engine performance modelling and test analysis
2. Introduction to current KLM performance and EGTM condition monitoring practice and relation to the maintenance concept.
3. Introduction to GSP (test analysis and gas path analysis models) as applied to KLM engines.
4. Development of models for analysis of humidity effects causing performance differences (on-wing and test cell) for the most EGTM critical engine type.
5. Selection of a number of airports, for which a weather dataset (including relative humidity or dew point, ambient temperature and pressure) will be requested and delivered by KLM's Operations.
6. Analysis of correlations between humidity and simulated performance (i.e. EGTM) and assessment of estimated EGTM degradation rate (including statistical analysis).
7. Assessment of the feasibility of delayed removal based on humidity effect correction of EGTM.
8. Identification of the required transition and next steps for application in existing engine performance monitoring systems (if concept feasible).

Report

Results of the work must be reported in English, with a copy of this assignment and an executive summary.

Coaching

The work will be performed in close collaboration with KLM Engine Services (Asteris Apostolidis, Rob Duivis)

Date 30 November 2018

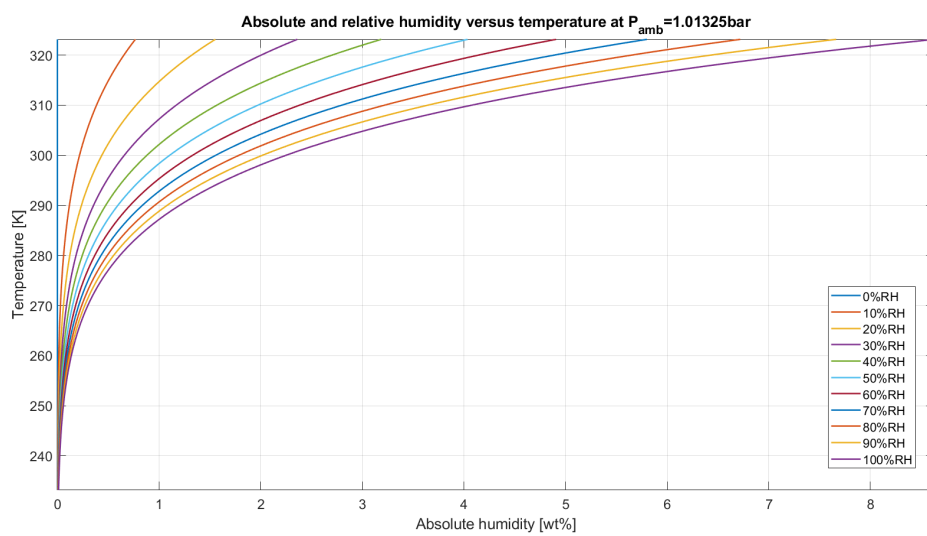
Professor,
Prof. dr. ir. P. Colonna
Duiuis

Delft University tutor,
Dr. ir. W.P.J. Visser

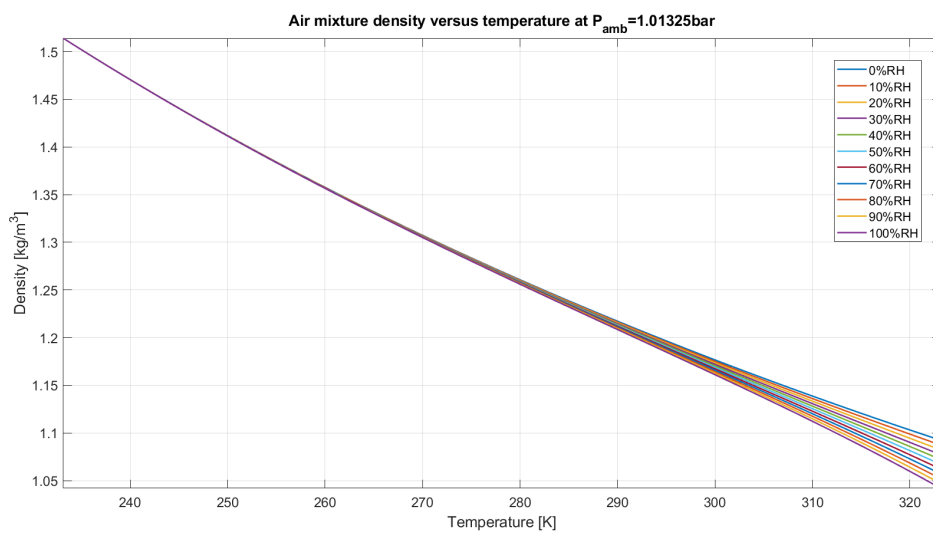
Supervisor at KLM
Asteris Apostolidis, Rob

B

Gas Properties versus Humidity



(a) A typical Mollier Diagram



(b) The density of the humid air mixture ρ_{mix}

Figure B.1: Mollier diagram and density for different ambient humidity levels

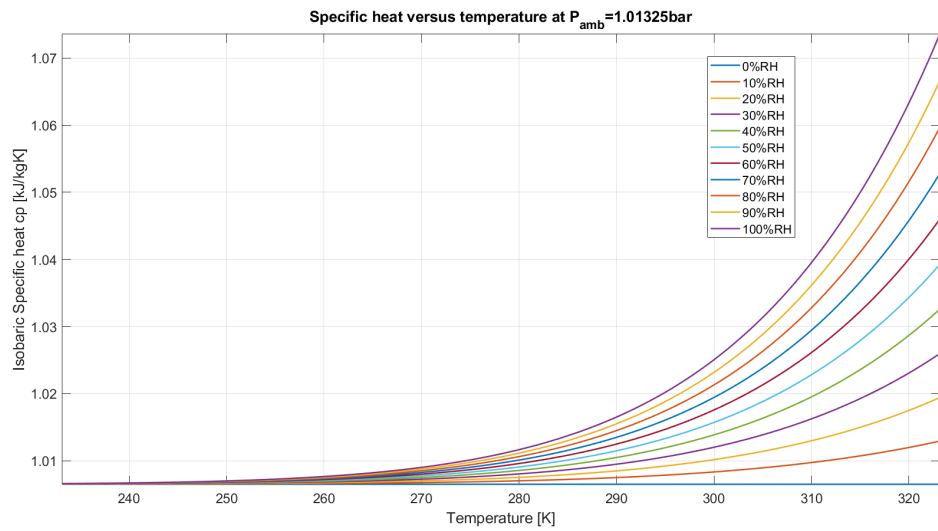
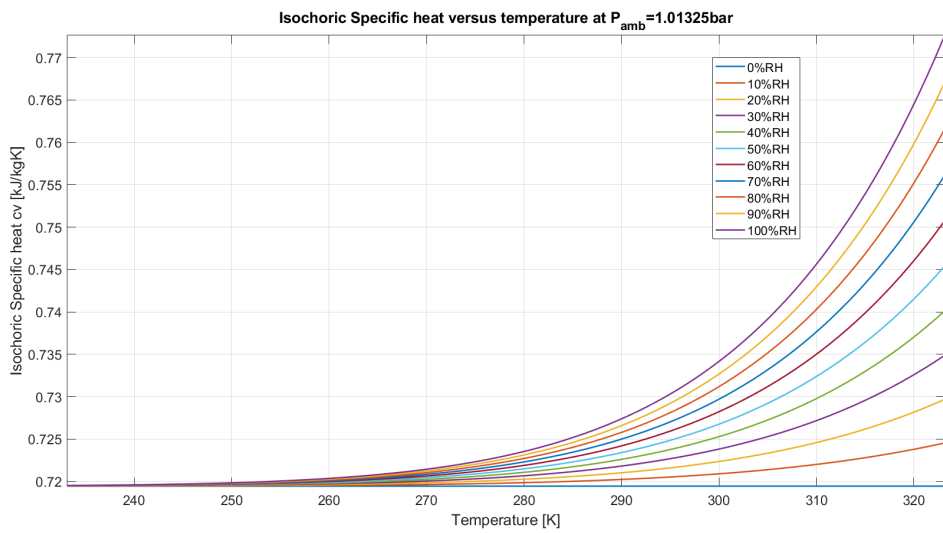
(a) The isobaric specific heat c_p (b) The isochoric specific heat c_v

Figure B.2: Specific heats for different ambient humidity levels

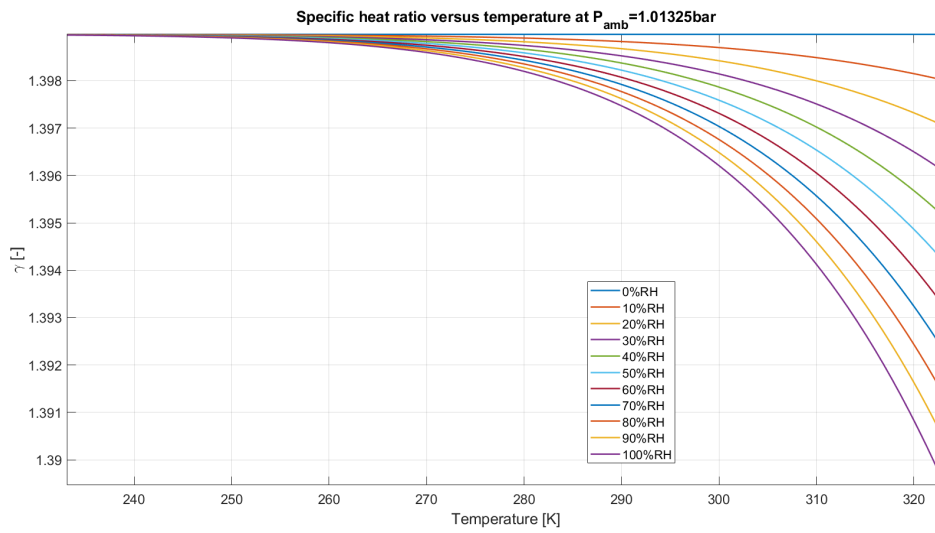
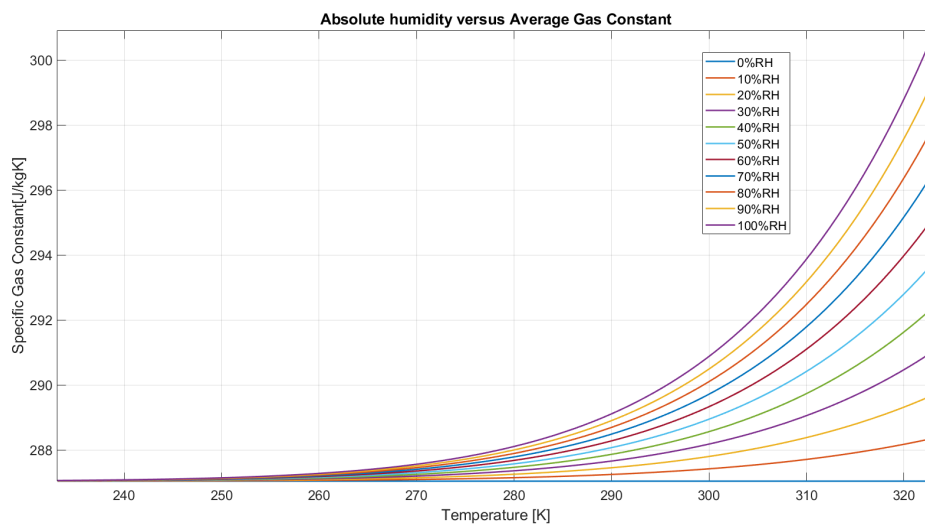
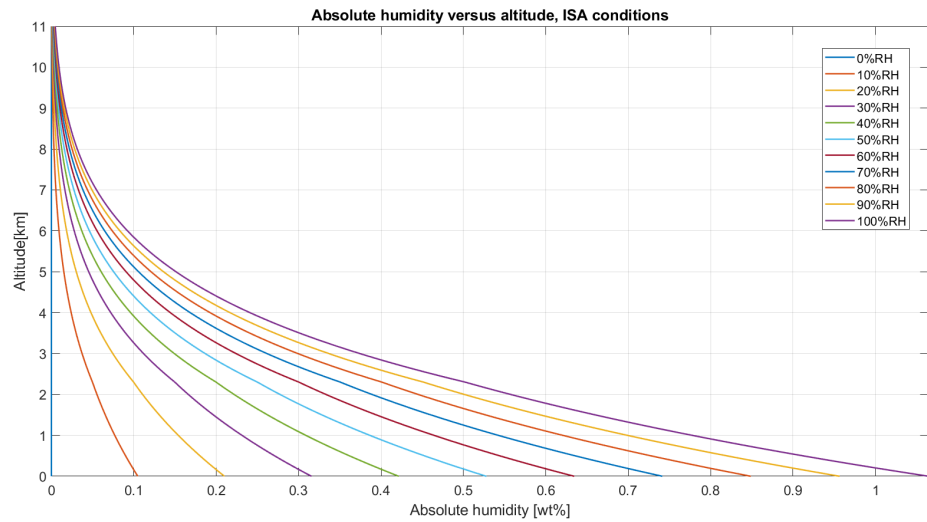
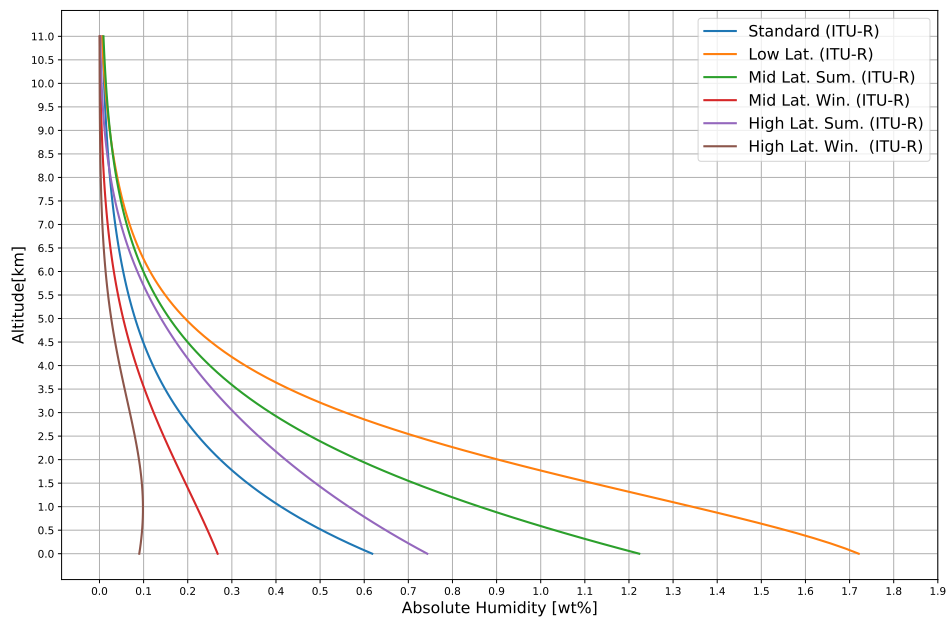
(a) Specific heat ratio γ (b) Gas constant \bar{R}_{mix}

Figure B.3: Specific heat ratio and Gas constant for different ambient humidity levels

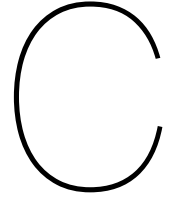


(a) Relative humidity w.r.t. altitude with ISA conditions



(b) Different absolute humidity profiles as proposed by ITU-R [57]

Figure B.4: Variation of relative and absolute humidity with altitude

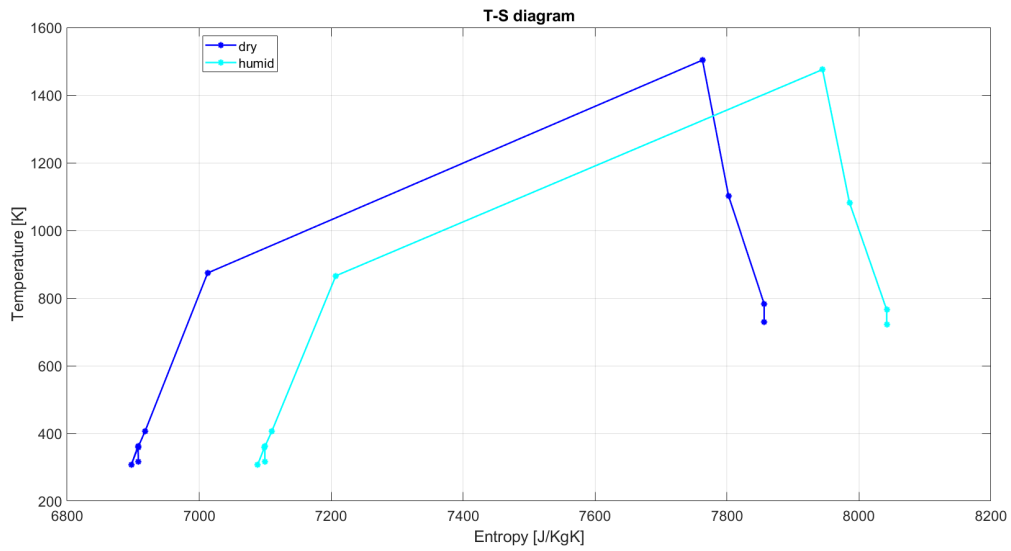


Effects of Humidity on Design Point Cycle Calculation

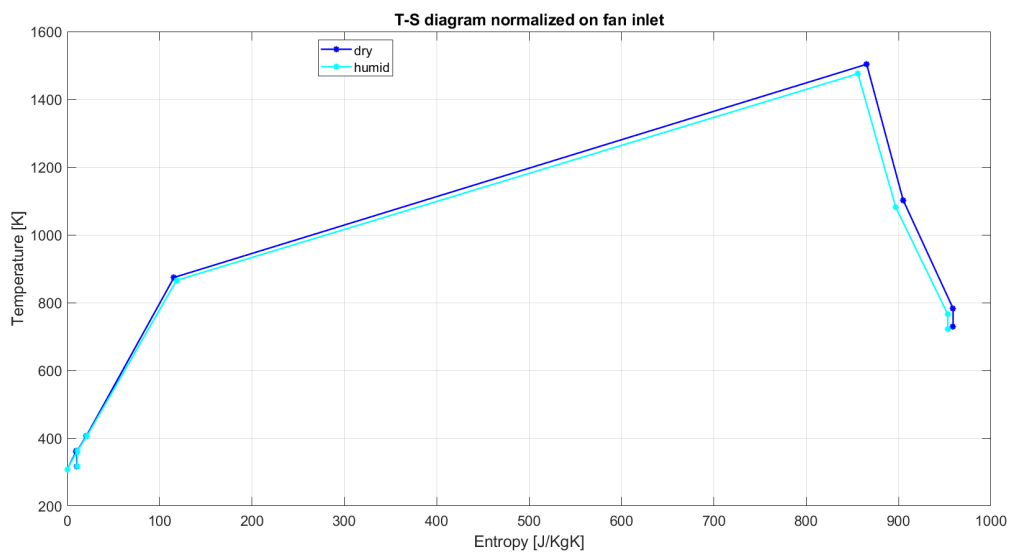
With the use of the sample project "BIGFAN.mxl" from GSP, a design point equation comparison is performed. The model in this project represents a typical twin spool turbofan engine. No changes were made in the model. The inlet conditions used represent extreme ambient humidity conditions in order to create significant changes in the performance and to be able to easily visualise these changes. The two design point equations are done for an ambient conditions of $T_{amb} = 308.15K$, $P_{amb} = 1.01325bar$, $M = 0$. For the first design point calculation the absolute humidity is set to zero. For the second design point equation the relative humidity is set to 100%, corresponding to an absolute humidity of $\approx 3.5[wt\%]$. No other settings were altered. The ducts in the "BIGFAN.mxl" example were not plotted in the figures since they add no interesting information other than a slight pressure loss and minor entropy increase.

Table C.1: Tabulated values of T, P, s and h

	S1	S2	S21	S25	S3	S4	S45	S5	S7	S9	S17	S18
$T_{dry}[K]$	308.15	308.15	358.9974297	406.6900494	674.2453463	1503.407292	1102.573507	783.0910111	783.0910111	728.6177468	362.2568258	316.3356102
$T_{humid}[K]$	308.15	308.15	358.5241465	405.7016195	665.8362945	1475.515301	1081.888277	765.1379611	765.1379611	721.313829	361.750593	316.2654229
$P_{dry}[bar]$	1.01325	1.01325	1.6718625	2.499434438	29.94322456	28.74549558	6.657959424	1.383068498	1.362322471	1.01325	1.722525	1.01325
$P_{humid}[bar]$	1.01325	1.01325	1.6718625	2.499434438	29.94322456	28.74549558	6.531418998	1.312857259	1.2931644	1.01325	1.722525	1.01325
$s_{dry}[J/kgK]$	0	6897.302768	6907.335553	6918.066604	7012.864771	7762.729941	7802.200618	7856.195771	7860.53378	7856.195771	6907.335553	6907.886851
$s_{humid}[J/kgK]$	0	7088.729067	7098.98341	7109.95016	7207.096613	7944.702675	7985.543612	8041.970306	8046.399586	8041.970306	7099.547293	7099.547293
$h_{dry}[kJ/kgK]$	5.715903908	5.715903908	56.91606735	105.156647	601.6355426	553.1570855	60.9041516	-310.5188918	-310.5188918	-310.5188918	60.20519419	60.20519419
$h_{humid}[kJ/kgK]$	-467.1631538	-467.1631538	-414.8985965	-365.714638	138.3260768	98.38232178	-401.3680523	-780.4427472	-780.4427472	-780.4427472	-411.5432562	-411.5432562

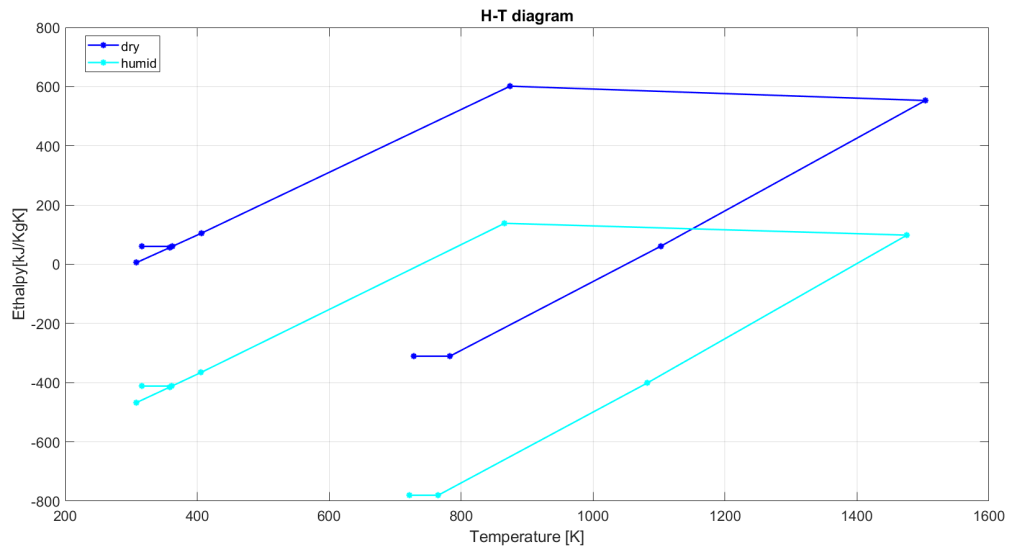


(a) T-S diagram for the "BIGFAN" Design Point calculation

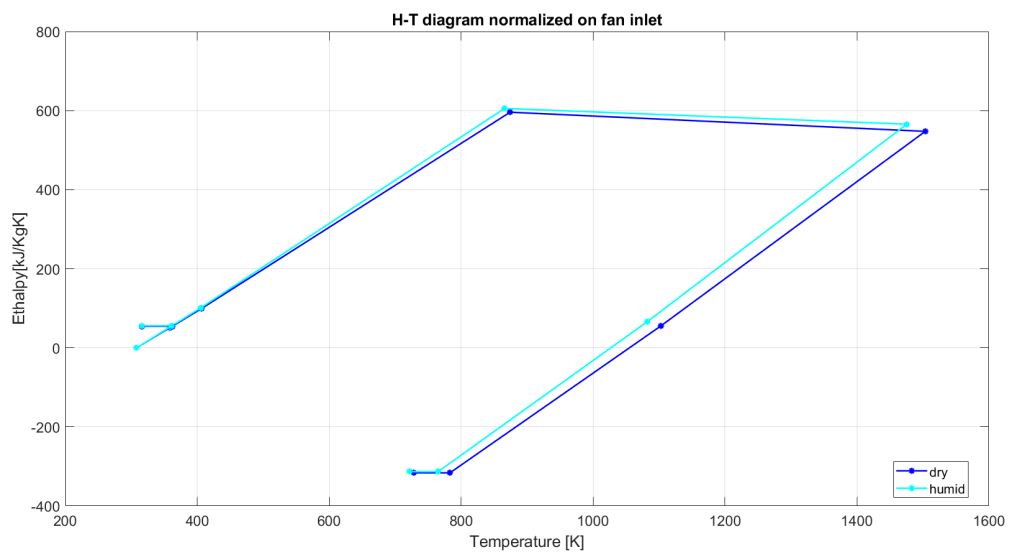


(b) T-S diagram for the "BIGFAN" Design Point calculation, normalised on Fan inlet

Figure C.1: T-S diagrams for the "BIGFAN" Design Point calculation



(a) H-T diagram for the "BIGFAN" Design Point calculation



(b) H-T diagram for the "BIGFAN" Design Point calculation, normalised on Fan inlet

Figure C.2: H-T diagrams for the "BIGFAN" Design Point calculation

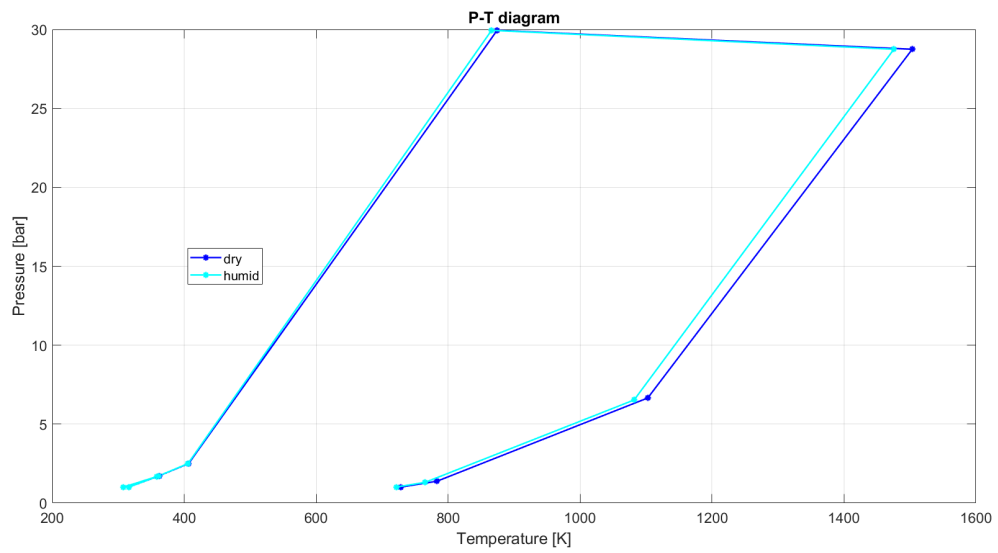
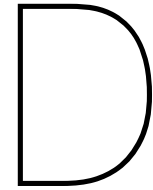


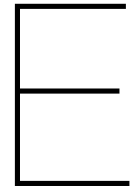
Figure C.3: P-T diagram of the "BIGFAN" Design Point calculation



CF6-80C2 and -80E1 Engine Specifications

Table D.1: CF6-80C2 and 80E1 specifications [15, 54, 55]

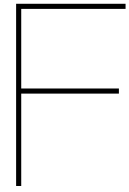
Component	CF6-80C2	CF6-80E1
LPC	1 Fan 4 primary booster stages	1 Fan 4 primary booster stages
HPC	14 primary stages 5 stages with variable stator vanes	14 primary stages 5 stages with variable stator vanes
HPT	2 primary stages	2 primary stages
LPT	5 primary stages	5 primary stages
Maximum diameter	approx. 2.69 [m]	approx. 2.896 [m]
Length	approx. 4.27 [m]	approx. 4.27 [m]
Overall pressure ratio	27.1 - 31.8	32.4-34.8
Bypass ratio	≈ 5.1	≈ 5.3
Maximum N1 speed	3854 [rpm] 117.5%	3835 [rpm] 115.5%
Maximum N2-speed	11055 [rpm] 112.5%	11105 [rpm] 113%
Max. EGT at TO	1233 K	1248K
Specific fuel consumption at maximum power	8.68 - 9.72 [g/(kN · s)]	9.40 - 9.77 [g/(kN · s)]
Maximum thrust at Sea Level	233.5 - 282.5 [kN]	300.3 - 320.3 [kN]



Simulated Bleed Flows

Table E.1: Bleed flows as defined in the CF6-80C2 model

Bleed flows				Cooling flows			
<i>Internal bleeds</i>							
Component	Location	Mass flow fraction [-]	dH fraction [-]		fraction for cooling [-]	frac. eff. T. flow [-]	Press. Frac [-]
HPC	Stage 7	0.0075	0.5	LPT (NGV)	1.0	0.95	-
HPC	Stage 11	0.01	0.786	HPT	1.0	0.95	0.9
HPC	Stage 14	0.1983	1.0	HPT (NGV)	0.5	0.9	-
				HPT	0.3	0.95	0.5
				HPT	0.2	0.25	0.5
HPC	CDP	0.005	1.0	LPT	1.0	1.0	0.95
<i>Customer bleed</i>							
HPC	Stage 8	0	0.571				



Corrected and Original EGTM Trend over Time

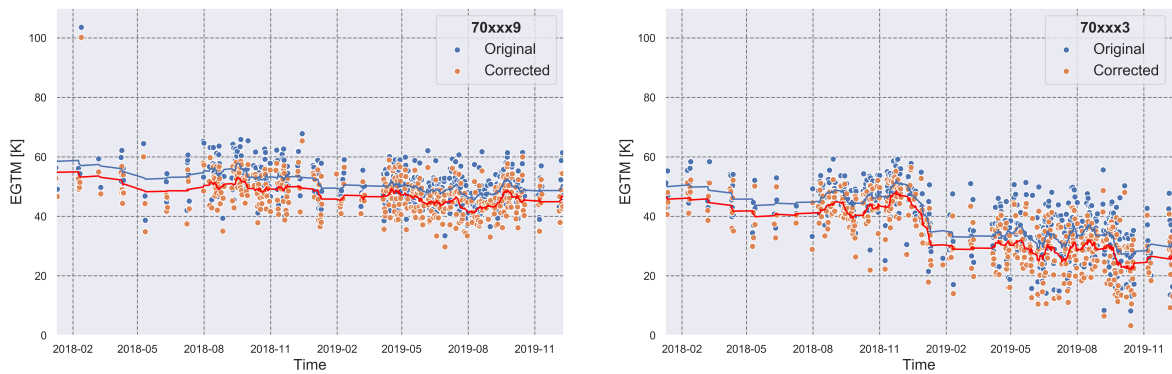


Figure F.1: CF6-80C2: Corrected and Original EGTM versus time

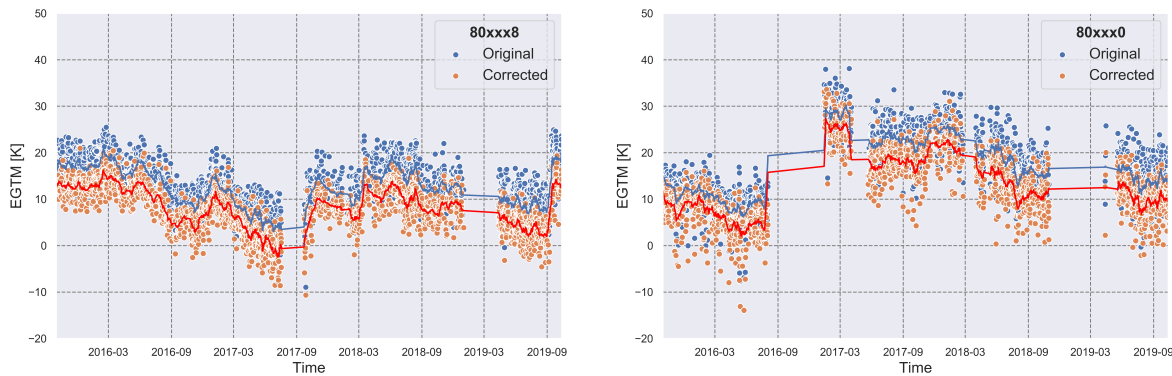


Figure F.2: CF6-80E1: Corrected and Original EGTM versus time